The Astronomical Journal, 140:1579–1622, 2010 December doi:10.1088/0004-6256/140/6/1579

THE PHASES DIFFERENTIAL ASTROMETRY DATA ARCHIVE. I. MEASUREMENTS AND DESCRIPTION

Matthew W. Muterspaugh[1,2], Benjamin F. Lane[3], S. R. Kulkarni[4], Maciej Konacki[5,6], Bernard F. Burke[7], M. M. Colavita[8], M. Shao[8], Sloane J. Wiktorowicz[9], and J. O'Connell[1]
[1] Department of Mathematics and Physics, College of Arts and Sciences, Tennessee State University, Boswell Science Hall, Nashville, TN 37209, USA; matthew1@coe.tsuniv.edu
[2] Center of Excellence in Information Systems, Tennessee State University, 3500 John A. Merritt Boulevard, Box No. 9501, Nashville, TN 37209-1561, USA
[3] Draper Laboratory, 555 Technology Square, Cambridge, MA 02139-3563, USA; blane@draper.com
[4] Division of Physics, Mathematics and Astronomy, 105-24, California Institute of Technology, Pasadena, CA 91125, USA
[5] Nicolaus Copernicus Astronomical Center, Polish Academy of Sciences, Rabianska 8, 87-100 Torun, Poland; maciej@ncac.torun.pl
[6] Astronomical Observatory, Adam Mickiewicz University, ul. Sloneczna 36, 60-286 Poznan, Poland
[7] MIT Kavli Institute for Astrophysics and Space Research, MIT Department of Physics, 70 Vassar Street, Cambridge, MA 02139, USA
[8] Jet Propulsion Laboratory, California Institute of Technology, 4800 Oak Grove Drive, Pasadena, CA 91109, USA
[9] Department of Astronomy, University of California, Mail Code 3411, Berkeley, CA 94720, USA
Received 2010 July 8; accepted 2010 September 4; published 2010 October 20

ABSTRACT

The Palomar High-precision Astrometric Search for Exoplanet Systems (PHASES) monitored 51 subarcsecond binary systems to determine precision binary orbits, study the geometries of triple and quadruple star systems, and discover previously unknown faint astrometric companions as small as giant planets. PHASES measurements made with the Palomar Testbed Interferometer (PTI) from 2002 until PTI ceased normal operations in late 2008 are presented. Infrared differential photometry of several PHASES targets were measured with Keck Adaptive Optics and are presented.

Key words: astrometry – binaries: close – binaries: visual – techniques: interferometric

Online-only material: color figure, machine-readable and VO tables

1. INTRODUCTION

A technique has been developed to obtain high-precision (35 μas) astrometry of close stellar pairs (separation less than 1 arcsec; Lane & Muterspaugh 2004) using long-baseline infrared interferometry at the Palomar Testbed Interferometer (PTI; Colavita et al. 1999). This technique was applied to 51 binary systems as the Palomar High-precision Astrometric Search for Exoplanet Systems (PHASES) program during 2002–2008. PHASES science results included precision binary orbits and component masses, studies of the geometries of and physical properties of stars in triple and quadruple star systems, and limits on the presence of giant planet companions to the binaries.

This paper is the first in a series analyzing the final results of the PHASES project as of its completion in late 2008. This paper describes the observing method, sources of measurement uncertainties, limits of observing precisions, derives empirical scaling rules to account for noise sources beyond those predicted by the standard reduction algorithms, and presents the full catalog of astrometric measurements from PHASES. The second paper combines PHASES astrometry, astrometric measurements made by other methods, and radial velocity observations (where available) to determine orbital solutions to several binaries' Keplerian motions, determining physical properties such as component masses and system distance when possible (Muterspaugh et al. 2010c). The third paper presents limits on the existence of substellar tertiary companions orbiting either the primary or secondary stars in those systems that are found to be consistent with being simple binaries (Muterspaugh et al. 2010a). Paper IV presents orbital solutions to a known triple star system (63 Gem A = HD 58728) and a newly discovered triple system (HR 2896 = HD 60318) (Muterspaugh et al. 2010b). Finally, Paper V presents candidate substellar companions to PHASES binaries as detected by astrometry (Muterspaugh et al. 2010d).

Astrometric measurements were made at PTI, which was located on Palomar Mountain near San Diego, CA. It was developed by the Jet Propulsion Laboratory, California Institute of Technology for NASA, as a testbed for interferometric techniques applicable to the Keck Interferometer and other missions such as the *Space Interferometry Mission* (*SIM*). It operated in the J (1.2 μm), H (1.6 μm), and K (2.2 μm) bands, and combined starlight from two out of three available 40 cm apertures. The apertures formed a triangle with one 110 and two 87 m baselines. PHASES observations began in 2002 and continued through 2008 November when PTI ceased routine operations.

2. OBSERVATIONS AND DATA PROCESSING

The initial PHASES observing method and data processing algorithm were presented by Lane & Muterspaugh (2004). Incremental improvements to these procedures were updated in papers from the PHASES science program. The final observing procedure and data processing algorithm is presented in complete form here. All astrometry measurements were reprocessed using the final algorithm presented here. Measurements taken with different instrumental configurations than the standard one presented here (for example, those lacking longitudinal dispersion compensation) are noted later in Table 4.

2.1. Astrometric Observation Method

2.1.1. Optical Interferometers

In an optical interferometer, light is collected at two or more apertures and brought to a central location where the beams are combined and a fringe pattern produced on a detector (at PTI, the detectors were NICMOS and HAWAII infrared arrays, of which only a few pixels were used). For a broadband source of central wavelength λ and optical bandwidth $\Delta\lambda$ (for PTI $\Delta\lambda = 0.4\ \mu$m),

the fringe pattern is limited in extent and appears only when the optical paths through the arms of the interferometer are equalized to within a coherence length ($\Lambda = \lambda^2/\Delta\lambda$). For a two-aperture interferometer, neglecting dispersion, the intensity measured at one of the combined beams is given by

$$I(x) = I_0 \left(1 + V \frac{\sin(\pi x/\Lambda)}{\pi x/\Lambda} \sin(2\pi x/\lambda)\right), \quad (1)$$

where V is the fringe contrast or "visibility," which can be related to the morphology of the source, and x is the optical path difference between arms of the interferometer. More detailed analysis of the operation of optical interferometers can be found in *Principles of Long Baseline Stellar Interferometry* (Lawson 2000).

2.1.2. Interferometric Astrometry

The location of the resulting interference fringes is related to the position of the target star and the observing geometry via

$$d = \vec{B} \cdot \vec{S} + \delta_a(\vec{S}, t) + c, \quad (2)$$

where d is the optical path length one must introduce between the two arms of the interferometer to find fringes. This quantity is often called the "delay." $\vec{B}$ is the baseline—the vector connecting the two apertures. $\vec{S}$ is the unit vector in the source direction, and c is a constant additional scalar delay introduced by the instrument. The term $\delta_a(\vec{S}, t)$ is related to the differential amount of path introduced by the atmosphere over each telescope due to variations in refractive index. For a 100 m baseline interferometer an astrometric precision of 10 μas corresponds to knowing d to 5 nm; while difficult, this is achievable for all terms except that related to the atmospheric delay. Atmospheric turbulence, which changes over distances of tens of centimeters and on millisecond timescales, forces one to use very short exposures (to maintain fringe contrast) and limits the sensitivity of the instrument. It also severely limits the astrometric accuracy of a simple interferometer, at least over large sky-angles.

However, in narrow-angle astrometry one is concerned with a close pair of stars, and the observable is a differential astrometric measurement, i.e., one is interested in knowing the angle between the two stars ($\vec{\Delta_s} = \vec{s_2} - \vec{s_1}$). The atmospheric turbulence is correlated over small angles. If the measurements of the two stars are simultaneous, or nearly so, the atmospheric term cancels out. Hence, it is still possible to obtain high-precision "narrow-angle" astrometry.

2.1.3. Subarcsecond Differential Astrometry

As illustrated in Figure 1 the light path of the PHASES astrometry program was as follows.

1. Light was collected by two of the three siderostats at PTI. The siderostats had diameter 50 cm and fed 40 cm beam compressing telescopes. These collimated the 40 cm input into a 7.5 cm beam.
2. At the siderostat enclosure, a fast steering mirror (FSM) provided tip–tilt correction for low-order adaptive optics improvement. The feedback sensor for the tip–tilt system was located in the beam combining facility (see step (9)), to include both atmospheric and instrumental sources of tip–tilt variations.
3. The collimated beams propagated through pipes to the central beam combining building. For the north and south siderostats, the pipes were held at vacuum; for the west siderostat, the pipe was filled with air.
4. Each collimated beam was directed to a long delay line (DL) which tracks the sidereal delay rate and receives feedback from the fringe-tracking beam combiner for removing some of the atmospheric turbulent delay variations. There were roughly ±38 m of optical delay available in the long DLs.
5. The collimated beams were recompressed to 2.5 cm collimated beams.
6. Each beam passed through a pair of matched prisms. In one arm, one prism was on a linear stage to vary the total glass thickness the starlight passed through. The positions of these prisms were calibrated using fringes from an internal light source to minimize the combined longitudinal dispersion of air path and glass. This calibration also determined the glass-to-air dispersion correction rate. The linear stage was operated in open-loop mode to minimize longitudinal dispersion even as the air path was varied by the long DLs. Some early measurements were made before this dispersion compensator was available, as marked in Table 4.
7. The 2.5 cm collimated beams were split ∼70/30 by plate beam splitters. The reflected ∼30% of the light was directed to the "secondary" beam combiner which made the astrometric science measurement. Red He–Ne LASER metrology signals were injected at these beam splitters and propagated through both beam combiners before being extracted just before the infrared array detectors to monitor path variations.
8. The ∼70% transmitted light from each beam was directed through a short DL. These were smaller versions of the long DLs with a few tens of centimeters of travel. The short DLs allowed one to set the delay offset between the fringe tracking and the science beam combiners such that both are near zero optical delay simultaneously. It also introduced the 50–100 Hz sawtooth modulation required for sampling fringes in the fringe tracker, without being in the science camera's optical path.
9. After the short DL, the ∼70% of the original light to be used for fringe tracking was directed to the "primary" beam combiner. *I*-band light was extracted using a dichroic beamsplitter and focused onto quad-cell avalanche photo diodes. The signal was used as feedback to the fast tip–tilt mirrors in step 2.
10. The longer-wavelength light was combined using a plate beam splitter. Half the light was focused on a single pixel of the NICMOS infrared array for high-signal-to-noise ratio (S/N) phase tracking. The other half passed through a single-mode fiber to improve wavefront quality (and system visibility), then through a low-resolution prism to disperse the light onto ∼5 pixels for slower group-delay tracking. Phase- and group-delay signals were fed to the long DLs to reduce jitter from atmospheric piston motions. This beam combiner was the same as used for PTI's standard visibility mode observations.
11. The ∼30% of the light redirected to the "secondary" table was used for the astrometric science measurement. The secondary beam combiner was identical to the first with the following exceptions.
    (a) A piezo-driven scanning mirror added up to ±300 μm of optical delay to allow scanning within the arcsecond

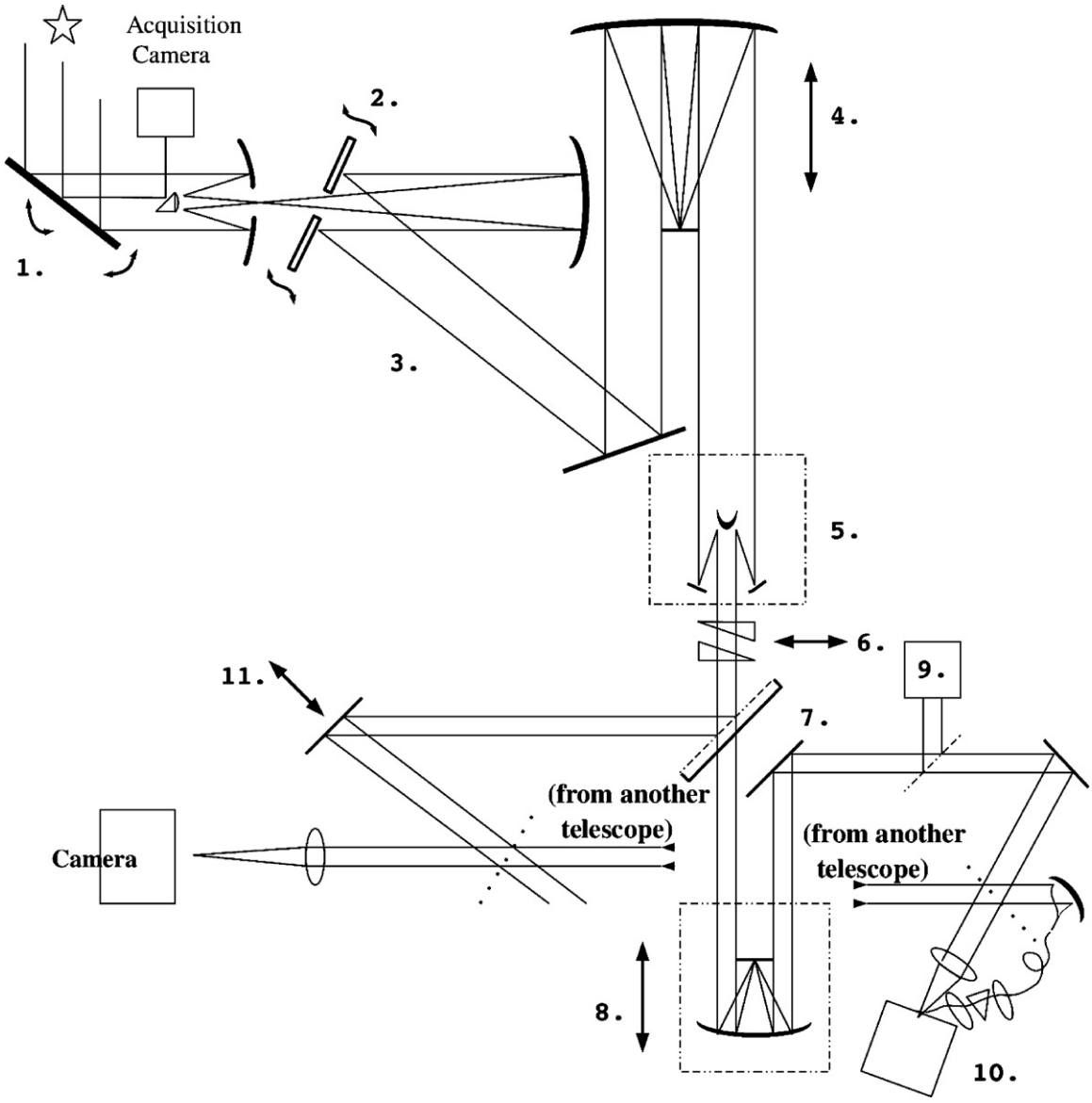

Figure 1. Configuration and light path used at PTI for the PHASES experiment is shown in schematic form; the corresponding description is described in Section 2.1.3. Note that the path for only one telescope is shown; light from the second telescope travels a similar path.

field of view. The scan was close-loop controlled using the LASER metrology signal.

(b) No single-mode fiber was used for spatial filtering.

(c) A HAWAII array was used instead of NICMOS.

The entire optical system was realigned at the beginning of the night and usually updated in the middle of the night, once per night. Alignment drifts from one night to the next were small. Standard detector calibrations (gain, bias and background) were acquired at the beginning of the night for both infrared array detectors; background levels were re-measured with each star acquisition.

The operating sequence began by acquiring the stars and locking star trackers for tip–tilt corrections on both telescopes. The 50–100 Hz fringe-tracking modulation was applied to the long DLs, which were moved until fringes were found with the "primary" beam combiner. Once fringe lock was made, the long and short DLs were moved simultaneously to maintain primary fringes until fringes were detected on the "secondary" beam combiner. Once fringes were found simultaneously on both beam combiners, (1) the zero-point offset for the short DLs was recorded, (2) the 50–100 Hz fringe-tracking modulation was moved from the long to short DLs so that only the "primary" beam combiner was affected by the modulation, (3) the "secondary" detector's read-out pattern was adjusted from one optimized for fringe tracking to a faster and more evenly spaced one that was better for scanning between fringe packets, and (4) the scanning mirror in the "secondary" beam combiner initiated its ∼Hz, ∼100 μm triangle modulation. The speed and amplitude of the triangle pattern were user-settable according to the predicted projected binary separation. Conservative values were used with larger amplitudes than predicted to ensure good coverage of the fringe packets. Observing a binary when its baseline projected separation ($\vec{B} \cdot \vec{\Delta S}$) was of order the interferometric coherence length ($\Lambda = \lambda^2/\Delta\lambda \approx 20\,\mu$m) or less was avoided due to potential biases associated with an imperfect template fringe packet.

This setup resulted in a special astrometry mode designed to work on pairs of stars separated by no more than ∼1 arcsec, the diffraction limit of the 40 cm apertures at $\lambda = 2.2\,\mu$m. In this mode, the small separation of the binary resulted in both binary

components being in the field of view of a single interferometric beam combiner. The fringe positions were measured by modulating the instrumental delay with an amplitude large enough to record both fringe packets. This eliminated the need for a complex internal metrology system to measure the entire optical path of the interferometer, and dramatically reduced the effect of systematic error sources such as uncertainty in the baseline vector (error sources which scale with the binary separation). The same instrumental configuration could be used for double Fourier spectroscopy.

However, since the fringe position measurement of the two stars was no longer truly simultaneous it was possible for the atmosphere to introduce path-length changes (and hence positional error) in the time between measurements of the separate fringes. To reduce this effect a fraction of the incoming starlight was redirected to a separate beam combiner, as described above. This beam combiner was used in a "fringe-tracking" mode (Shao & Staelin 1980; Colavita et al. 1999) where it rapidly (10–20 ms) measured the phase of one of the starlight fringes and adjusted the internal delay to keep that phase constant. The fringe-tracking data were used both in real time (operating in a feedback servo, after which a small—but measurable—residual phase error remained) and in post-processing (the measured residual error was applied to the data as a feed-forward servo). This technique—known as phase referencing—had the effect of stabilizing the fringe measured by the astrometric beam combiner. For this observing mode, LASER metrology was only required between the two beam combiners through the location of the light split (which occurred after the optical delay has been introduced), rather than throughout the entire array. This greatly reduced system complexity and increased the percentage of time on-sky. Extra efforts in system reliability and automation allowed most PHASES measurements to be acquired by a single night assistant with high (>90%, not counting weather) on-sky efficiency.

In making an astrometric measurement the optical delay was modulated in a triangle-wave pattern around the stabilized fringe position, while measuring the intensity of the combined starlight beams. The range of the delay sweep was set to include both fringe packets; typically, this required a scan amplitude on the order of 150 μm. Typically one such "scan" was obtained every second, consisting of up to 1000 intensity samples (the scan rate was limited by the source brightness and the requirement that >2 samples are made per fringe modulation period). A double fringe packet based on Equation (1) was then fit to the data, and the differential optical path between fringe packets was measured.

2.2. Astrometric Data Reduction Algorithm

The intensity versus delay position measurements produced by the interferometer were processed into astrometric measurements as follows.

1. Detector calibrations (gain, bias, and background) were applied to the intensity measurements.
2. The residual phase errors from the primary fringe tracker were converted to delay and applied to the data. Note that while the intensity measurements were spaced regularly in time, and the delay scanned linearly in time, the variable amount of delay correction applied from the fringe tracker resulted in the intensity measurements being unevenly spaced in delay. This somewhat complicated the downstream processing, in that FFT-based algorithms could not be used.
3. The data were broken up into "scans" either when the delay sweep changed direction or when the fringe tracker lost lock. Only scans for which at least 90% of the scan was continuously recorded (without fringe lock loss) were used in processing.
4. For each scan, a power spectrum was calculated using a Lomb–Scargle algorithm (Scargle 1982; Press et al. 1992). This spectrum provided an S/N estimate based on the ratio of the power in and out of the instrument bandpass. Only the scans with an S/N greater than unity were kept.
5. For a range of values of differential optical delays between fringe packets, a model of a double-fringe packet was calculated and compared to the observed scan to derive a χ^2 value versus differential delay.
6. A two-dimensional grid in differential R.A. and decl. over which to search was constructed (in ICRS 2000.0 coordinates). For each point in the search grid the expected differential delay was calculated based on the interferometer location, baseline geometry, and time of observation for each scan. These conversions were simplified using the routines from the Naval Observatory Vector Astrometry Subroutines C Language Version 2.0 (NOVAS-C; see Kaplan et al. 1989). The value of χ^2 for the grid point's differential delay as determined by the previous step was co-added to an R.A./decl. χ^2 grid.
7. After co-adding the R.A./decl. χ^2 over all the scans in one night, all resulting values of χ^2 within 4σ of the minimum point were used to fit a two-dimensional quadratic function to interpolate the location of the best minimum χ^2 value as the final astrometric solution, and the widths of the quadratics determined the formal uncertainties as discussed in detail below. The final product was a measurement of the apparent vector between the stars and associated uncertainty ellipse. Because the data were obtained with a single-baseline instrument, the resulting error contours are very elliptical, with aspect ratios at times $\geqslant$10.

Sample illustrations of several of these stages are plotted in Figure 2.

In previous data reductions, the scans were optionally digitally bandpass filtered before being processed for astrometry. This resulted in astrometric measurements that differed from those derived without filtering by much less than the measurement uncertainties. In this final analysis, the scans were not bandpass filtered.

2.2.1. Probability Distribution Function Sidelobes

One potential complication with fitting a fringe to the data was that there were many local minima spaced at multiples of the operating wavelength. If one were to fit a fringe model to each scan separately and average (or fit an astrometric model to) the resulting delays, one would be severely limited by this fringe ambiguity (for a 110 m baseline interferometer operating at 2.2 μm, the resulting positional ambiguity is ~4.1 mas). However, by using the χ^2-surface approach, and co-adding the probabilities associated with all possible delays for each scan, the ambiguity disappeared. This was due to two things, the first being that co-adding simply improved the S/N. Second, since the observations usually lasted for an hour or even longer, the associated baseline change due to Earth rotation also had the effect of "smearing" out all but the true global minimum.

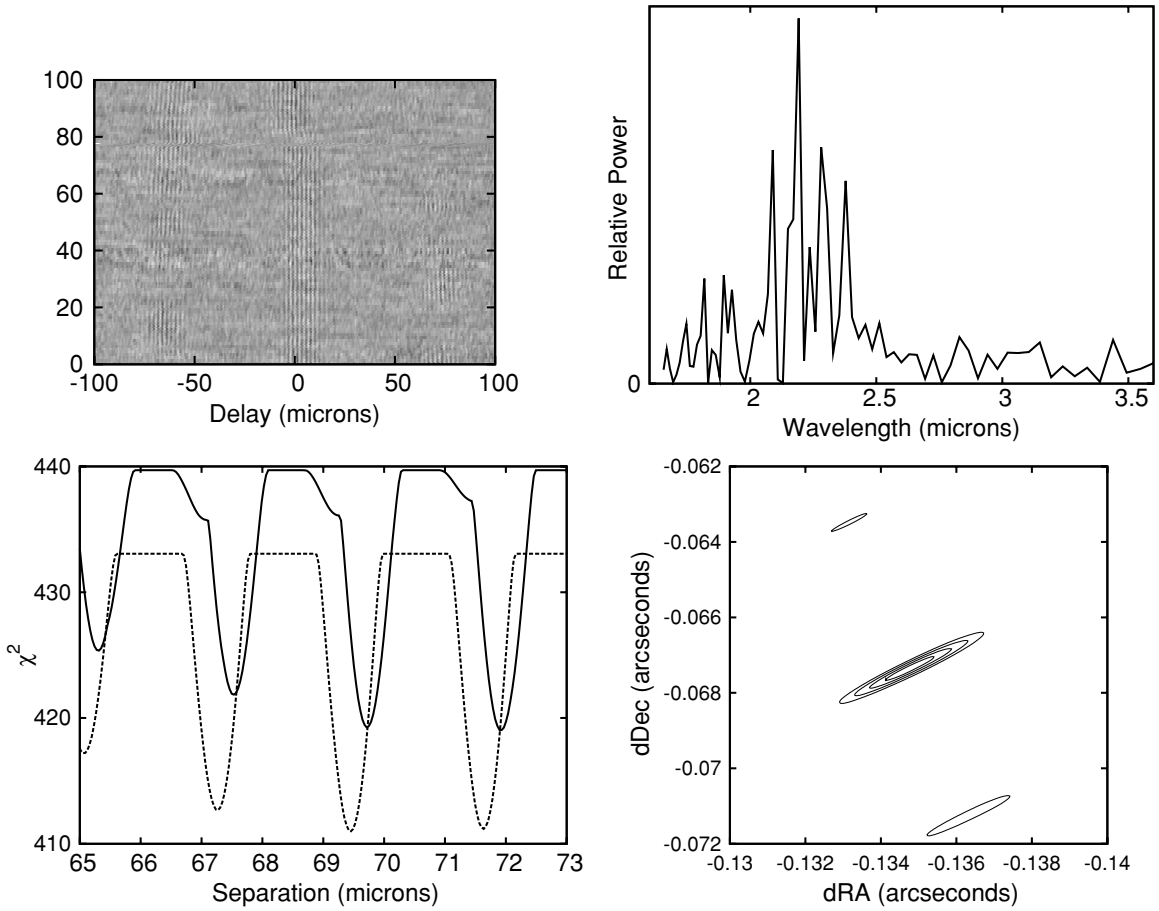

Figure 2. Several steps of the data processing pipeline are shown for an observation of HD 13872 (21 Ari) from MJD 54,385.33270. Upper left: raw interferograms show two distinct fringe packets, one from each star in the over-resolved binary. One star was found near zero delay, the other at $\sim \pm 70\,\mu$m. The flipping from side-to-side was a result of the fringe tracker first tracking on one star for some scans, then the other. Upper right: the periodogram of one scan used to evaluate the fringe S/N within the optical passband used (K-band, 2.0–2.4 μm). The power in the passband is not flat, but rather oscillates, a result of the object being a binary star (visibility changes with wavelength). Lower left: the likelihood metric χ^2 as a function of delay separation of the binaries for two scans. Note there are multiple minima separated by the fringe modulation period, and the noise is large enough to prevent high confidence identification of the correct local minimum. Lower right: the co-added χ^2 surface in differential R.A./decl., with contours corresponding to 1σ, 2σ, 3σ, and 4-σ confidence regions. Note that in this case sidelobes appeared at the 4σ confidence level, so the measurement was rejected as ambiguous.

The final χ^2-surfaces did have dips separated by $\sim$4.1 mas from the true location, but any data sets for which these showed up at the 4σ level were rejected. The 4σ region is that for which the properly normalized χ^2 function has a value less than the number of degrees of freedom plus 19.33, the latter being the value appropriate for two-dimensional χ^2 distributions. The final astrometry measurement and related uncertainties were derived by fitting only the 4σ region of the surface.

2.2.2. Residual Unmonitored Phase Noise

Unmonitored system phase noise can affect the χ^2 surface in two ways. First, components of the phase noise that operated at frequencies faster than the scan rate caused the two fringe packets to be smeared an extra amount, and to first order this appeared as extra noise in the intensity measurements. This affected the width of the χ^2 fit for each individual scan (which is designated as σ_m, the "measurement" noise), and thus appeared directly in the co-added χ^2 contour.

If instead the instrumental noise was much slower than an individual scan, it was essentially "frozen into" the scan—for the duration of that scan, the stars really did appear to have a different separation than their true separation. The χ^2 surface for the fit to an individual scan takes the form

$$f(d - d_j) = \frac{(d - d_j)^2}{\sigma_m^2} + n, \tag{3}$$

where d_j is the value of the star separation that minimizes $f = \chi^2$, and n is the number of degrees of freedom of the fit (typical values for n are 400–1000; for this derivation, it suffices to assume a one-dimensional χ^2 surface as it has no curvature in the direction perpendicular to the sky-projected baseline—only Earth-rotation synthesis lifts this degeneracy). The low-frequency components of the phase noise cause d_j to vary from d_o, the true star separation, by more than one expects from measurement noise alone. By taking many such scans, one can determine this instrumental scatter (which is designated as σ_i, the "instrument" noise for an individual scan) and add (in quadrature) the instrumental noise to the measurement noise as

$$F(d - d_o) = \frac{(d - d_o)^2}{\left(\sigma_m^2 + \sigma_i^2\right)/N} + nN, \tag{4}$$

where N is the number of scans (N was typically hundreds to thousands).

Consider a function $f(d-d_{o_j})$ with position of the minimum at d_{o_j}; this centroid position is distributed with probability

$$P\left(d_{o_j}\right) = \frac{e^{-(d_o-d_{o_j})^2/2\sigma_i^2}}{\sqrt{2\pi}\sigma_i}. \quad (5)$$

One may naively hope that summing several instances of this function with variable d_{o_j} together would properly add the instrumental and measurement noises in quadrature. However, the summation results in

$$\sum_{j=0}^{N} f\left(d-d_{o_j}\right) = N\int_{-\infty}^{\infty} f\left(d-x\right)P\left(x\right)dx \quad (6)$$

$$= \frac{(d-d_o)^2}{\left(\sigma_m^2\right)/N} + nN + N\frac{\sigma_i^2}{\sigma_m^2} \quad (7)$$

$$\neq \frac{(d-d_o)^2}{\left(\sigma_m^2+\sigma_i^2\right)/N} + nN. \quad (8)$$

Even if one renormalizes so that the additive term equals nN (i.e., multiply by $n/(n+\sigma_i^2/\sigma_m^2)$), this is still:

$$\sum_{j=0}^{N} f\left(d-d_{o_j}\right) = \frac{(d-d_o)^2}{\left(\sigma_m^2+\sigma_i^2/n\right)/N} + nN. \quad (9)$$

Note the extra factor of n dividing σ_i^2; this effectively underestimates the scan-to-scan instrumental noise by a very large amount—roughly 20 times for typical PHASES data.

Instead, the appropriate way to determine the scan-to-scan fit is by noticing that the minimum value of the co-added χ^2 surface is greater than the total number of degrees of freedom nN by the amount:

$$N\frac{\sigma_i^2}{\sigma_m^2}. \quad (10)$$

The quantity σ_m was measured directly from the shape of the surface, which remained unchanged, and the number of scans N was known. Thus, one could derive σ_i and apply it to the formal uncertainties. For all observations the average value of σ_i^2/σ_m^2 was 1.29; values ranged from 0.0042 (for bright sources and good weather conditions) to 7.2.

Phase referencing was used to decrease the amount of unmonitored phase noise during narrow-angle astrometry observations (see Section 3.1), but some residual phase noise remained, so the correction outlined here had to be applied to the astrometric data. Synthetic data were constructed both with and without unmonitored phase noise of the actual spectrum observed, and the data reduction algorithm determined measurement uncertainties consistent with the actual scatters in the measurements between multiple synthetic data sets. Without the additional phase-noise correction outlined here, the formal uncertainties significantly underestimated the scatter in the results.

3. EXPECTED PERFORMANCE

The expected astrometric performance of the PHASES observing mode was determined by several factors contributing measurement uncertainties and biases. These can be subdivided into three broad categories:

1. observational noise terms, which are fundamental to atmospheric turbulence and finite source brightness;
2. instrumental noise terms, which result from the design of the interferometer and the method in which the measurements were obtained; and
3. astrophysical noise terms, which result from the astrometric stability of the stars themselves.

Table 1
Astrometric Noise Sources

Source	Section	Typical Magnitude (μas)
Temporal decoherence	3.1.1	~5
Anisoplanatism	3.1.2	0.2
Photon noise	3.1.3	3
Differential dispersion	3.2.1	~30
Baseline errors	3.2.2	<10
Fringe template	3.2.3	1
Scan rate	3.2.4	1
Beam walk	3.2.5	1
Global astrometry	3.2.6	≪1
Star spots	3.3.1	<8
Stellar granulation	3.3.2	<3

Notes. Sources of astrometric noise vary in magnitude from tens of microarcseconds to submicroarcsecond levels. Differential dispersion depends on color difference between binary components; for many targets, this is nearly zero, but for extreme color differences, this can be hundreds of microarcseconds. This is not the case for any of the PHASES targets. Photometric variability accompanies star spots, of a magnitude that is easily detected for astrometric signatures of 8 μas or larger.

The size of each noise source is summarized in Table 1. The details of a few of these terms were described by Lane & Muterspaugh (2004); here, a more complete summary of the PHASES error budget is presented.

3.1. Astrometric Observational Noise

In calculating the expected astrometric performance three major sources of error were taken into account: errors caused by fringe motion during the delay sweep between fringes (loss of coherence with time), errors caused by differential atmospheric turbulence (loss of coherence with sky angle, i.e., anisoplanatism), and measurement noise in the fringe position. Each is quantified in turn below, and the expected measurement precision is the root-sum-squared of the terms.

3.1.1. Loss of Temporal Coherence

The power spectral density of the fringe phase of a source observed through the atmosphere has a power-law dependence on frequency; at high frequencies typically

$$A(f) \propto f^{-\alpha}, \quad (11)$$

where α is usually in the range 2.5–2.7. The effect of phase referencing is to high-pass filter this atmospheric phase noise. For PHASES, the servo was an integrating servo with finite processing delays and integration times, with the residual phase error "fed forward" to the second beam combiner (Lane & Colavita 2003). The response of this system to an input atmospheric noise can be written in terms of frequency as

$$H(f) = \frac{1-2\mathrm{sinc}(\pi f T_s)\cos(2\pi f T_d)+\mathrm{sinc}^2(\pi f T_s)}{1-2\frac{f_c}{f}\mathrm{sinc}(\pi f T_s)\sin(2\pi f T_d)+\left(\frac{f_c}{f}\right)^2\mathrm{sinc}^2(\pi f T_s)}, \quad (12)$$

where $\mathrm{sinc}(x) = \sin(x)/x$, f_c is the closed-loop bandwidth of the fringe-tracker servo (for PHASES $f_c = 10$ Hz or 5 Hz), T_s is the integration time of the phase sample (in standard mode, 6.75 ms), and T_d is the delay between measurement and correction (done in post-processing, effectively 5 ms). The phase noise superimposed on the double fringe measured by the astrometric beam combiner has a spectrum given by $A(f)H(f)$.

The sampling of the double fringe packet took a finite amount of time, first sampling one fringe, then the other. In the time domain, the sampling function can be represented as a "top-hat" function convolved with a pair of delta functions (one positive, one negative). The width of the top-hat is equal to the time taken to sweep through a single fringe, while the separation between the delta functions is equal to the time to sweep between fringes. In the frequency domain, this sampling function becomes

$$S(f) = \sin^2(2\pi f \tau_p)\mathrm{sinc}^2(\pi f \tau_*), \tag{13}$$

where τ_p is the time taken to move the delay between stars, $\Delta d/v_s$, and τ_* is the time to sweep through a single stellar fringe, Λ/v_s. v_s is the delay sweep rate.

The resulting error in the astrometric measurement, given in radians by σ_{tc}, can be found from

$$\sigma_{\mathrm{tc}}^2 = \left(\frac{\lambda}{2\pi \mathrm{B}}\right)^2 \frac{1}{N}\int_0^\infty A(f)H(f)S(f)df, \tag{14}$$

where N is the number of measurements. It is worth noting that if phase referencing was not used to stabilize the fringe, i.e., $H(f) = 1$, the atmospheric noise contribution increases by a factor of $\approx 10^2$–10^3. For ~Hz scanning, the corresponding error is less than 10 μas.

3.1.2. Anisoplanatism

The performance of a simultaneous narrow-angle astrometric measurement has been thoroughly analyzed by Shao & Colavita (1992). Here the primary result for the case of typical seeing at a site such as Palomar Mountain is restated, with the astrometric error in arcseconds due to anisoplanatism (σ_a) is given by

$$\sigma_a = 540 B^{-2/3}\theta t^{-1/2}, \tag{15}$$

where B is the baseline (in meters), θ is the angular separation of the stars (in radians), and t is the integration time in seconds. This assumes a standard (Lindegren 1980) atmospheric turbulence profile; it is likely that particularly good sites will have somewhat (a factor of two) better performance. For $\theta = 5 \times 10^{-7} \sim 100$ mas, and 1 hr of integration, this term is roughly a fifth of a microarcsecond.

3.1.3. Photon Noise

The astrometric error due to photon noise (σ_p) is given in radians as

$$\sigma_p = \frac{\lambda}{2\pi \mathrm{B}}\frac{1}{\sqrt{N}}\frac{1}{\mathrm{S/N}}, \tag{16}$$

where N is the number of fringe scans, and S/N is the signal-to-noise ratio of an individual fringe. For typical PHASES targets and PTI's throughput ($N \sim 2000$, S/N ~ 10), this was of order a few microarcsecond.

3.2. Astrometric Instrumental Noise

There were several effects internal to the instrument that could contribute noise terms or biases to the astrometric measurements. Some could potentially vary on night-to-night timescales as the optical alignments vary on roughly these timescales. Others resulted from properties of the measurement design.

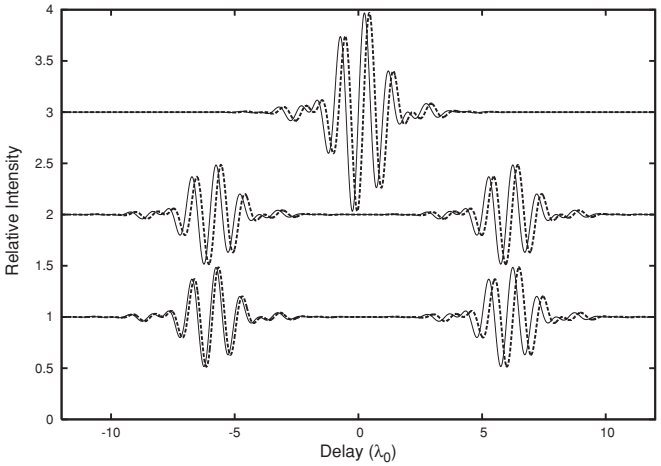

Figure 3. Schematic of the shift in fringe positions due to dispersion (the effect has been exaggerated for clarity). The vacuum (no dispersion) interferograms are plotted with solid lines; those dispersed by air with dotted lines. Top: dispersion shifts the point of zero optical path difference for a star, due to different amounts of air path in each arm of the interferometer (the effective optical path difference measured as if in vacuum). Middle: the dispersion shifts for stars of equal colors were equal and canceled; the measured separation is the same. Bottom: stars of unequal colors are shifted by slightly different amounts by dispersion, and the resulting measured separation is different. For very extreme color differences, the shift can be hundreds of microarcseconds. Not shown are the shape distortions to interferograms.

3.2.1. Differential Dispersion

The path compensation for the geometric delay at PTI was done with DLs in air. At near-infrared wavelengths, air introduces a wavelength-dependent index of refraction given by Cox (2000)

$$n = 1 + \left(\frac{pT_s}{p_s T}\right)\left(6.4328 \times 10^{-5} + \frac{0.029498}{146 - 1/\lambda^2} + \frac{2.554 \times 10^{-4}}{41 - 1/\lambda^2}\right) - 4.349 \times 10^{-5}(1\text{–}7.956 \times 10^{-3}/\lambda^2)\frac{p_w}{p_s}, \tag{17}$$

where λ is the vacuum wavelength in μm, p is the air pressure, p_w is the partial pressure of water vapor, $p_s = 1.01325 \times 10^5$ Pa, T is the temperature, and $T_s = 288.15$ K. The fringe packets of astrophysical sources were dispersed by an amount that depends on the difference in air paths between arms of the interferometer; this changed the shape and overall location of the fringe packets; see Figure 3. If two stars were in the same beam and identical in color, the change in location was common to both and canceled; similarly, the distortions of the fringe packets are common and canceled to first order in a differential measurement. Simulated data and reanalysis of real data with modified fringe templates showed that higher order terms in the fringe packet shape are negligible at the microarcsecond level.

If, however, the two stars were of differing colors, each would be dispersed by a slightly different amount, and their apparent separation would be biased. The shift in the apparent position of each star's fringes can be approximated by evaluating the dispersion at the effective average wavelength of the star in the passband. The effective average wavelength was calculated by multiplying the instrumental bandpass by the stellar spectrum. For an order-of-magnitude estimate of the effect of differential

Table 2
Differential Dispersion

Spectral Type	Effective Temperature (K)	Effective K-band Wavelength (μm)	$(n-1)$ $\times 10^4$	$(n-n_{\rm F5})$ $\times 10^9$	$(n-n_{\rm F5})$ $\times 38$ m (nm)	Error vs. F5 (μas)
O5	44500	2.1763	2.729232	0.93	35.4	73
B5	15400	2.1772	2.729229	0.66	25.0	51
A5	8200	2.1785	2.729225	0.25	9.7	20
F5	6440	2.1794	2.729223	0.00	0.0	0
G5	5770	2.1799	2.729221	−0.14	−5.4	11
K5	4350	2.1815	2.729217	−0.61	−23.3	48
M5	3240	2.1839	2.729210	−1.32	−50.3	103

Notes. Effect of color-dependent differential dispersion. Stellar temperatures are for dwarf stars, from Carroll & Ostlie (1996). All numbers are for zero water vapor pressure, $p_w = 0$. Increasing water vapor pressure to $p_w = p_s$ increases the astrometric effect by a factor of roughly 20%.

dispersion, one can model the instrumental bandpass as a top-hat function passing wavelengths 2–2.4 μm (nominal K-band) and the stellar spectra as blackbodies. The shifts in apparent positions for several spectral types over 40 m of differential air path (a maximum amount for PTI) are given in Table 2. Note that for G5–K5 binaries, the amount is 35.8 μas and for B5–A5 it is 30.6 μas. For much more extreme color ratios, the effect can be as large as 150.6 μas for B5–M5 binaries; the PHASES sample did not include such systems, as their high contrast ratios prevented observation.

Because the stars were often observed at the same hour angles from one night to the next (and thus the delay positions are relatively common between nights), this effect introduced a much smaller scatter than that listed in the table. However, it may have introduced biases in the stellar separations and introduced scatter between observations taken in multiple baselines (for which the delay positions differed). These biases and scatters were of order the amounts given in Table 2.

The binaries in the PHASES sample were generally of components with equal brightnesses and thus similar colors. No hour-angle-dependent biases significant on the level of the precision of the observations were observed. This effect is likely to be important for traditional narrow-angle astrometry methods at the Keck Interferometer or Very Large Telescope Interferometer, which aim to use field stars as astrometric references for nearby stars, and reference and target will often have very different colors. The effect is largely reduced if one uses a spectrometer to measure the group-delay positions of the fringes.

Starting in 2005, the longitudinal dispersion compensator addressed this potential systematic. The measurements acquired with this correction are flagged in Table 4.

3.2.2. Baseline Errors

The baseline vector used in the differential delay equation to determine astrometric quantities was derived by inversion of the delay equation from the fringe locations of point-like sources with known global astrometric positions. Uncertainties and variability of the baseline vector were sources of differential astrometry uncertainties via the differential delay equation. An incorrect baseline model would show up as an hour-angle-dependent error term that would potentially increase night-to-night scatter beyond that predicted by the formal uncertainties; this was tested by dividing data sets within single nights into multiple sets by hour-angle range and the results were self-consistent.

No evidence of hour-angle-dependent error terms was seen in the PHASES data, supporting evidence that the baseline models are correct. As shown in Figure 4, except for a few outliers (likely due to using point sources with poor global astrometry values or a night's observation only covering a small range of hour angles or declinations) the night-to-night drift in baseline model solutions were less than 1 mm in north–south and east–west directions for the two primary baselines used for PHASES observations (NS and SW). The up–down dimension was stable to a few millimeters in both cases; this scatter was likely due to limited measurement precision rather than actual baseline variability, implying that it could be improved by averaging several nights' values.

The amount by which a baseline error of $\overrightarrow{\sigma_B}$ affects a differential astrometry measurement $\overrightarrow{\Delta S}$ was determined as follows. To maintain the same observed differential delay between stars, the differential delay equation requires that

$$\overrightarrow{B} \cdot \overrightarrow{\Delta S} = (\overrightarrow{B} + \overrightarrow{\sigma_B}) \cdot (\overrightarrow{\Delta S} + \overrightarrow{\sigma_{\Delta S}}), \tag{18}$$

where $\overrightarrow{\sigma_{\Delta S}}$ is the astrometric error caused by baseline error $\overrightarrow{\sigma_B}$. Canceling like terms and assuming $\overrightarrow{\sigma_{\Delta S}} \cdot \overrightarrow{\sigma_B}$ is less than the other terms simplifies this to

$$\overrightarrow{\sigma_B} \cdot \overrightarrow{\Delta S} = -\overrightarrow{B} \cdot \overrightarrow{\sigma_{\Delta S}}. \tag{19}$$

The vector $\overrightarrow{\Delta S}$ was tangent to the celestial sphere; only that component which was not perpendicular to the baseline was actually measured (this measured component of the separation is referred to as δS) and only its uncertainty ($\sigma_{\delta S}$) was thus applicable. The angle between these measured components and the baseline vector is given by the target's zenith angle z; this was always kept to less than 45°. Of course, the baseline uncertainty vector $\overrightarrow{\sigma_B}$ need not be oriented with $\overrightarrow{B}$ itself; its components σ_{Bx} and σ_{By} tangent to and σ_{Bz} normal to the Earth (also referred to as the "U" or "Up" component) are introduced. Substituting into Equation (19) gives the relationship between baseline error and astrometric error as

$$\delta S((\sigma_{Bx}\cos\phi + \sigma_{By}\sin\phi)\cos z + \sigma_{Bz}\sin z) = -|B|\sigma_{\delta S}\cos z, \tag{20}$$

where ϕ is an angle determined by the hour angle and declination of the target. On rearranging terms, the fractional astrometric measurement uncertainty due to baseline uncertainties was

$$\frac{\sigma_{\delta S}}{\delta S} = -\frac{\sigma_{Bx}\cos\phi + \sigma_{By}\sin\phi + \sigma_{Bz}\tan z}{|B|}. \tag{21}$$

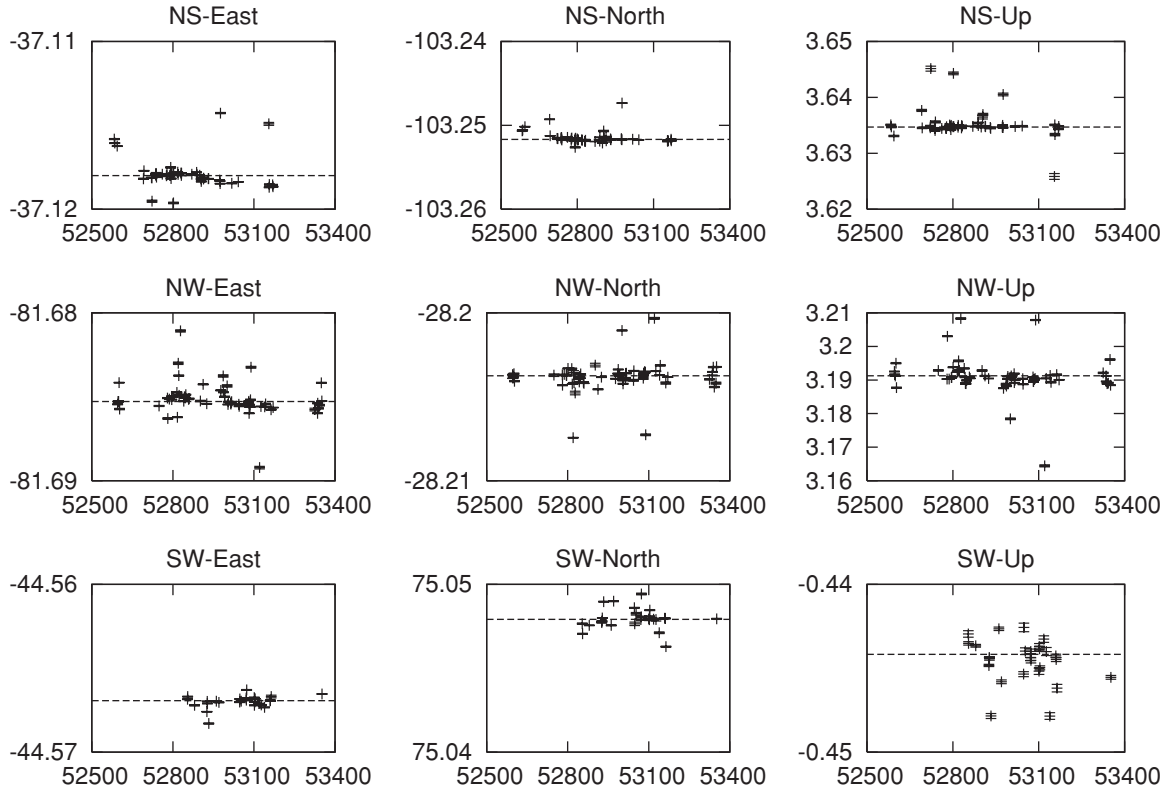

Figure 4. Solutions for the three PTI baseline vectors. The three baselines at PTI were named "NS," "NW," and "SW" due to their rough orientations. Each was a three-dimensional vector, which was given by components in the "East" (east–west), "North" (north–south), and "Up" (up–down) directions (the first two were tangent to the Earth, the last was perpendicular). Horizontal axes are time in modified Julian days (MJD), vertical axes are baseline length in meters. Lines represent average baseline fits used for data reduction presented in this paper; points with error bars represent a given night's baseline solution. The baseline solutions were derived from the observed delay positions of single-star sources with known global astrometric positions via inversion of Equation (2). The *y*-axis tick marks in each plot are all 10 mm. Note that the scatter in the "Up" dimension was much larger than the other dimensions; this was due to preferential observing of targets overhead, for which the "Up" component is highly covariant with the constant term in the delay equation. The baseline solution used for data analysis was a weighted average of the solutions plotted.

For $|B| = 100$ m and $z < 45°$, baseline uncertainties of 2 mm cause 10 μas errors in the astrometry for a binary with projected separation $\delta S = 0.5$ arcsec. Though the measured component of ΔS continually varies as the Earth rotates the baseline vector, the above derivation is true at any given instant. Earth rotation causes errors to appear in both astrometric dimensions.

A slightly more subtle baseline effect was that there can be differences between the wide-angle ("astrometric") and narrow-angle ("imaging") baselines. When determining the baseline vector via the delay positions for stars with known global astrometry solutions spread across the sky, the siderostats are repointed for each observation to place the target star on-axis. Thus, one was measuring the vector between the pivot points of the siderostats, about which the siderostats were repointed for each target. When measuring the separations between two stars in a single field with a single pointing of the telescopes, at least one of the stars would be off-axis; one instead desired to know the separations between the corresponding points on the surfaces of the two siderostats to get the proper delay scale. Through careful optical design, PTI was built to minimize differences between the astrometric and imaging baselines in order that the original narrow-angle astrometry mode would function at the 100 μas level for binaries with separations of tens of arcseconds. Because errors due to baseline uncertainty scale with binary separation, the effect was negligible at the level of a few microarcseconds for subarcsecond binaries in the PHASES sample.

3.2.3. Fringe Template

Because the astrometric measurements were differential between two stars, they were relatively insensitive to the model fringe template. The fringe model used in the astrometric analysis was determined by observing interferograms of single stars. An effective bandpass was constructed from an incoherent averaging of the periodograms of many such interferograms, and used to recompute a standard interferogram template, to be applied to the data. This effective bandpass was only an approximation for most stars, as there were variations in source temperature and spectra. However, reanalysis with several different fringe models showed variations only at the single microarcsecond level.

3.2.4. Scan Rate and Earth Rotation

Earth rotation caused variable projection of the binary separation on the interferometer baseline vector. The details of the variability depend of the observatory location, sky position of the target binary, and the orientation of the baseline vector, but for order-of-magnitude estimations, can be approximated as a sinusoid with period of 1 day and amplitude equal to the total binary separation a:

$$\Delta s \approx a \times \cos(2\pi t/\mathrm{day}). \quad (22)$$

The differential delay rate was given by the first derivative of this equation with respect to time, converted from sky angle to delay

length by the interferometer's resolution. For $a \sim 500$ mas, this differential delay rate is about 20 nm s^{-1}, or 5 nm (10 μas) in the (typically) 250 ms required to scan between the fringe packets. Roughly an equal number of scans were obtained in each scan direction (to within 10%), and this effect canceled to first order (to the same level, 10% or 1 μas). However, curvature in the differential delay motion does not cancel; it is given by the second time derivative of the projected separation and was roughly 1.4×10^{-3} nm s^{-2} (less than 3 nanoarcseconds s^{-2}). Thus, the differential delay rate was small enough, and the measurement rate fast enough, that the finite measurement rate did not contribute significant uncertainties.

3.2.5. Beam Walk

The interferometer telescopes imaged a sky field and then recollimated the light. Through this process, light from two stars separated on the sky by angle α was partially sheared with respect to each other and proceeded to illuminate slightly different parts of the optics that guide the light to the detector. Starlight in a recollimated beam that originated from different sky positions also developed relative shear equal to the path traveled multiplied by their angular separation (see Figure 5). To the extent that the optics were imperfect (had rough surfaces), the light from each star traveled slightly different path lengths from telescope to detector. This process is known as beam walk.

Colavita (2009) determined the extent to which beam walk introduces astrometric errors. That approximate stochastic analysis yielded an rms pathlength error ϵ given by

$$\epsilon \sim w \left(\frac{\delta}{q}\right)\left(\frac{q}{z}\right)^{1/4}, \quad \delta \ll q,$$

where w is the rms wavefront error over an optic of diameter z, q is the diameter of the starlight footprint, and δ is the linear beamwalk. For optics with a surface quality of $\lambda/20$ peak-to-valley (like those used at PTI), the wavefront rms is $w \simeq \lambda/40$. The actual error is $\sim\sqrt{2}$ larger than this due to the presence of two telescopes in the interferometer.

The first place where beam walk could occur was within the telescope itself. The beam was collimated at the telescope primary, focused by the primary, and recollimated to a $q = 0.075$ m beam by a $z = 0.1$ m diameter mirror to be fed to the "Fast Steering Mirror" (FSM; this mirror corrected for tip–tilt wavefront errors across the telescope, providing low-order adaptive optics). The distance from primary mirror to this mirror was the sum of their focal lengths 4.75 m. The beam walk over 0.1 arcsec (4.8×10^{-7} rad) was thus $\delta = 2.3\,\mu$m. Beam walk on the FSM thus contributed an astrometric error of 0.001 μas and was negligible.

The relative angles of starlight in the recollimated beam were increased by a factor of the ratio of the primary mirror and FSM focal lengths (5.33), thus light from sky locations separated by 0.1 arcsec had a differential angle of 0.533 arcsec (2.6×10^{-6} rad). This recollimated beam from the FSM traveled through light pipes to the beam combining laboratory, where movable mirrors added a variable amount of delay. This total travel is of order 50 m; the mirrors are typically $z = 0.1$ m diameter. The beam walk over 0.533 arcsec was $\delta = 130\,\mu$m, which contributed an astrometric error of 0.07 μas. There were a few mirrors along this path, and the total astrometric error would be determined by considering the optical qualities of all optics and adding the effects in quadrature. Because this beam walk was so small, the sum total of these remained negligible.

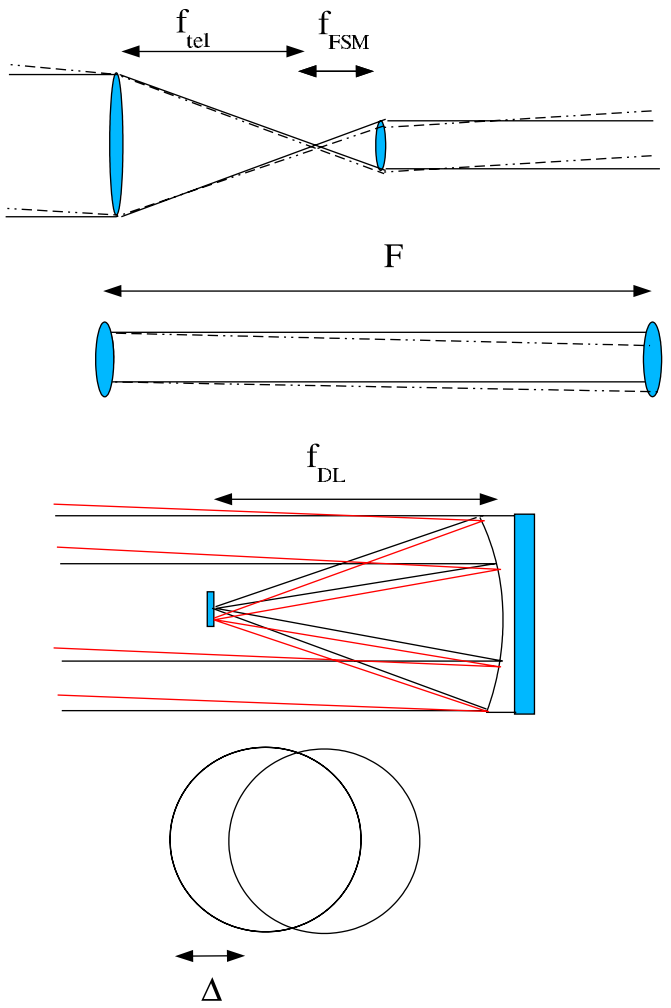

Figure 5. Three instances where beam walk could occur, causing stars at slightly different sky angles to illuminate different parts of optical elements. Top: shear introduced at the telescope by focusing and recollimating the beam. "FSM" stands for the "Fast Steering Mirror," which provided tip–tilt corrections (first-order adaptive optics) and recollimated the light after the telescope. Second from top: shear within a collimated beam over large optical paths. Second from bottom: shear at focus of delay line optics (DL; the movable mirrors that provide optical delays). Bottom: the shear of two beams by amount Δ causing only partial overlap.

(A color version of this figure is available in the online journal.)

The movable mirrors were comprised of a parabolic mirror of focal length 1.07 m and a small ($z \approx 0.01$ m) flat mirror located near its focus. Collimated light was directed to one side of the parabola, focused onto the flat mirror, then recollimated by the parabola's other side. On the flat mirror, the (diffraction-limited) beam diameter was only $q \sim \lambda f/d = 31\,\mu$m where λ is the operating wavelength of light, f is the parabola's focal length and d is the collimated beam diameter (0.075 m). The beam walk was 2.8 μm. The flat mirrors contributed an astrometric error of 0.9 μas from beam walk. It is concluded that beam walk did not contribute significant measurement errors.

3.2.6. Global Astrometry Errors

Uncertainty in the global position of a target binary on the celestial sphere was coupled into the differential astrometric measurement. Errors in right ascension were equivalent to measurement timing errors; declination uncertainties had similar

effects. The order of magnitude of this effect can be derived as follows: the fractional error in global astrometry (error in arcseconds divided by total number of arcseconds around a quarter circle) is roughly equal to the fractional error in differential astrometry separation vector (astrometric error divided by binary separation). A 1 arcsec global astrometry error caused differential astrometric errors of less than 3 μas for binaries of separation1 arcsec or less. Typical uncertainties in global astrometry were much less than an arcsecond, with 10 mas being a much more common value. Effects such as stellar aberration (20 arcsec) were accounted for in the PHASES data reduction software; if ignored, these could cause significant differential astrometry uncertainties.

3.3. Astrometric Astrophysical Noise

There were potential sources of apparent astrometric motion in the target stars due to processes within the stars themselves. These included star spots and stellar granulation.

3.3.1. Star Spots

As previously presented by Muterspaugh et al. (2006), the maximum shift in the center-of-light of a star caused by star spots can be evaluated with a model comprised of a uniform stellar disk (radius R) except for a zero-temperature (non-emitting) circular region of radius r tangent to the edge of the stellar disk (i.e., centered at $x = R - r$, $y = 0$). The center-of-light is displaced by

$$\frac{x_c}{R} = \frac{\int_{-R}^{R}\int_{-\sqrt{R^2-x^2}}^{\sqrt{R^2-x^2}} x\,dy\,dx - \int_{R-2r}^{R}\int_{-\sqrt{r^2-(x-R+r)^2}}^{\sqrt{r^2-(x-R+r)^2}} x\,dy\,dx}{R\pi(R^2-r^2)} = -\frac{r^2/R^2}{1+r/R}. \quad (23)$$

The presence of star spots can be confirmed through photometric measurements simultaneous with astrometric observations. The non-emitting spots in this model would cause photometric variations proportional to the fractional area of the stellar disk covered:

$$\frac{F}{F_o} = 1 - \frac{r^2}{R^2}, \quad (24)$$

where F_o is the star's flux when no spots are present. Equations (23) and (24) provide a relationship between the apparent astrometric and photometric shifts caused by star spots.

The largest possible astrometric shift by a star spot is given by evaluating a slightly different model. In this case, the star spot fills the (non-circular) area from the star's edge to a chord at distance x_o from the star's true center. The astrometric shift is

$$\frac{x_c}{R} = \frac{\int_{-R}^{x_o}\int_{-\sqrt{R^2-x^2}}^{\sqrt{R^2-x^2}} x\,dy\,dx}{R\int_{-R}^{x_o}\int_{-\sqrt{R^2-x^2}}^{\sqrt{R^2-x^2}} dy\,dx} = -\frac{2\left(1-\frac{x_o^2}{R^2}\right)^{3/2}}{3\left(\frac{\pi}{2}+\arcsin\frac{x_o}{R}+\frac{x_o}{R}\left(1-\frac{x_o^2}{R^2}\right)^{1/2}\right)} \quad (25)$$

with corresponding photometric variations of

$$\frac{F}{F_o} = \frac{1}{\pi}\left(\frac{\pi}{2}+\arcsin\frac{x_o}{R}+\frac{x_o}{R}\left(1-\frac{x_o^2}{R^2}\right)^{1/2}\right). \quad (26)$$

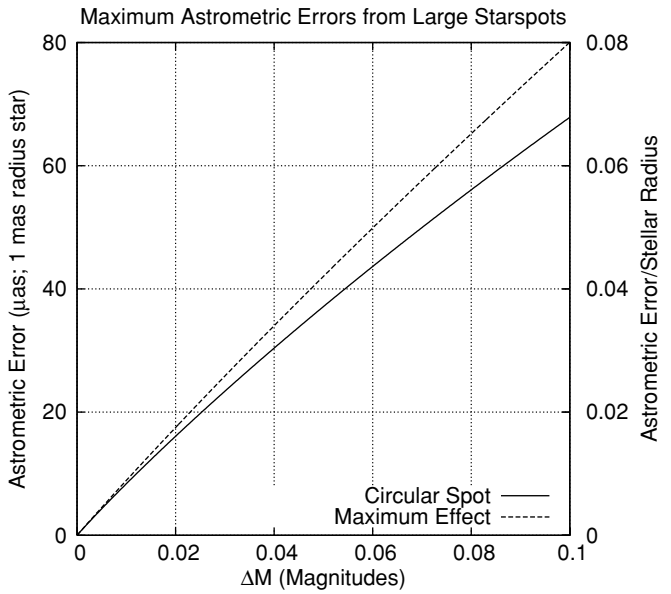

Figure 6. Maximum effect of star spots on astrometric measurements vs. the photometric variations they cause.

For stars of typical radius 1 mas, the simplified model gives a roughly linear relationship of 0.8 μas of astrometric shift per milli-magnitude of photometric variability, see Figure 6. Only stars with diameters smaller than PTI's resolution of ~4 mas were observed by PHASES. Photometric variations of these scales can be monitored by small ground-based telescopes. The timescale of these variations is on order the rotation rate of a star (days to weeks). Lanza et al. (2008) re-evaluated the effects of spots with a model that includes stellar limb darkening and lower spot contrast ("warm" spots rather than the completely non-emitting spots assumed above) and found this reduces the astrometric effect by ~40%.

3.3.2. Stellar Granulation

Stellar granulation causes photometric variability of subsections of a star's surface. Averaged over the whole of the stars surface, these photometric variations can cancel to large extent and the intrinsic variability of the star remains small, though with a large astrometric uncertainty. Svensson & Ludwig (2004) showed that the effects of stellar granulation are independent of a star's radius but are strongly correlated with surface gravity and provide values for the astrometric effects in white light.

For stars with very low surface gravities (i.e., red giants), astrometric perturbations can be quite large—as much as 300 μas/D (pc). Red giants within 100 pc were overresolved by PTI and could not be observed, thus even for these stars this effect was negligible. For main-sequence stars, the effect was closer to 0.1 μas/D (pc).

4. EMPIRICAL ERROR BAR SCALING RULES

The formal uncertainty ellipses derived with the procedure outlined in Section 2.2 were found to underestimate the actual scatter of the measurements to an orbital model. Two reasonable approaches to correct this are to find a multiplicative scale factor by which to increase the formal uncertainties, or a noise floor to be added-in-quadrature to the formal uncertainties. Unfortunately, no single multiplicative factor nor noise floor was found that could bring the measurement uncertainties and fit residuals

into satisfactory agreement for a majority of the stars. The instrumental changes made in 2005 to introduce a longitudinal dispersion compensator (discussed in Section 3.2.1) and an automated alignment system further complicate this effort. However, upon dividing the measurements into two subsets according to whether or not the instrumental changes were implemented (the subset without the upgrades will be referred to as subset 1, that with the upgrades will be referred to as subset 2), and allowing for different scaling or noise floor factors in each subset, again no single solution was obtained.

Recognizing that both multiplicative factors and noise floors might be present, and could affect the major and minor axes of the uncertainty ellipses in different ways, a solution was sought to incorporate parameters for both types of terms, allowing for different values in the two axes and in the two subsets. This finally produced a single satisfactory solution. The procedure used to find the solution and the final values obtained were as follows.

Of the 51 star systems observed by PHASES, 33 had 10 or more measurements. Six of those 33 had been previously discovered to be triple or quadruple star systems, and a seventh (HR 2896 = HD 60318) was discovered by PHASES to be a triple system; for simplicity of analysis, the effort to derive the uncertainty scaling rules was limited to binaries. Three more systems had too few measurements in one of or both subsets 1 and 2, and were not included in the analysis. Of the remaining 23 binaries, 15 ($\sim$2/3) were selected for evaluation; the other $\sim$1/3 of the systems were not included allowing for the possibility that their increased levels of scatter were the result of astrophysical phenomena; however, the empirical scaling rules have been found to work satisfactorily on many of these as well, as a check of the rules' validities.

The size of the major and minor axes of each measurement was resized by the formula

$$\sigma^2_{(i,j),c} = f^2_{(i,j)}\sigma^2_{(i,j),\mathrm{raw}} + \sigma^2_{(i,j),q},$$

where $i = 1, 2$ indicates the subset number, $j = 1, 2$ indicates whether it is the uncertainty ellipse major (1) or minor (2) axis, $\sigma_{(i,j),c}$ is the "corrected" 1σ uncertainty, $f_{(i,j)}$ is a multiplicative scaling factor, $\sigma_{(i,j),\mathrm{raw}}$ is the formal 1σ uncertainty, and $\sigma_{(i,j),q}$ is a noise floor added in quadrature.

An iterative procedure was used to optimize the values of the eight parameters $f_{(i,j)}$ and $\sigma_{(i,j),q}$ in order to produce the most statistically reasonable set of uncertainty ellipses to represent the observed scatter about Keplerian models for the 15 stars. The constraints for optimizing those eight parameters were: (1) within each subset, for each axis, the χ^2_r goodness-of-fit statistics computed along that axis should have minimal variance among the binaries (i.e., all the binaries being evaluated should have similarly good fits in a given axis), (2) averaged over all the binaries, the χ^2_r statistic computed within each subset/axis combinations should be equal to the other subset/axis (and unity; i.e., fit residuals should equally distributed among the various subsets and axes), and (3) the fits for as many binaries as possible should have χ^2_r as close to unity as possible.

The eight parameters $f_{(i,j)}$ and $\sigma_{(i,j),q}$ were given nominal values, and the 15 binaries' PHASES measurements were fit to Keplerian models using the replacement uncertainty ellipses. The correction parameters were varied one at a time, each step recalculating the Keplerian models, until the variance of the χ^2_r among the binaries on the affected subset/axis was minimized (criterion 1). This was repeated over the eight parameters, after which the average χ^2_r was calculated in each of the four subset/axis combinations, and the parameters affecting each subset/axis combination were renormalized to force the average $\chi^2_r = 1$ for that combination (criterion 2). This procedure was then iterated, varying the parameters individually to minimize χ^2_r variance followed by renormalizing to $\chi^2_r = 1$ for each axis, until the parameter values converged.

The final parameter values that produced the best universal uncertainty scaling rules were found to be

1. $f_{(1,1)} = 1.3$ (original instrument configuration, major axis);
2. $f_{(1,2)} = 3.8$ (original instrument configuration, minor axis);
3. $f_{(2,1)} = 1.3$ (revised instrument configuration, major axis);
4. $f_{(2,2)} = 1.0$ (revised instrument configuration, minor axis);
5. $\sigma_{(1,1),q} = 140$ μas (original instrument configuration, major axis);
6. $\sigma_{(1,2),q} = 35$ μas (original instrument configuration, minor axis);
7. $\sigma_{(2,1),q} = 140$ μas (revised instrument configuration, major axis);
8. $\sigma_{(2,2),q} = 35$ μas (revised instrument configuration, minor axis).

Only four non-trivial parameters end up being needed to correct the measurement uncertainties: a single multiplicative factor of 1.3 for the major axis (independent of subset), a multiplicative factor of 3.8 for the minor axis of data that lacked the dispersion compensator and/or automatic alignment system ($f_{(2,2)} = 1$ is a trivial value representing no correction is needed), and noise floors of 140 and 35 μas to be added in quadrature to the major and minor axes, respectively (independent of subset). These values are not entirely surprising: a large multiplicative factor for the minor axis before the instrument revisions disappeared as those changes made the instrument more stable and increased path monitoring. A noise floor of 35 μas in the minor axis, regardless of subset, is reasonably expected from the many noise sources described in Section 3. The root-sum-square of the errors in Table 1 is 15 μas. Given that some of the simple arguments presented were designed to provide error estimates at only the factor of two level, the resulting 35 μas noise floor is not unreasonable. In addition, it is possible some differential dispersion persisted even with the dispersion compensator in place, though it certainly reduced the amount. Because the major axis represents a direction perpendicular to that at which the interferometer baseline was oriented at the average measurement time, the measurement along that axis is slow to build via Earth-rotation synthesis, and it is not surprising to find a small multiplicative factor and larger noise floor in that direction.

After applying these corrections to the measurement uncertainties, the χ^2_r statistic was calculated for Keplerian fits to the data of all 26 binaries having more than 10 observations. Fourteen of the 26 (54%) evaluate to $0.5 < \chi^2_r < 1.5$, and an additional two just miss the cutoff (with values of 0.44 and 0.46; including these would bring the total to 62%). Furthermore, four of the systems with too-large values of χ^2_r are much better modeled by a double Keplerian model, indicating an additional component may be present; see Paper V. The 26 binaries, number of observations, the fits' χ^2_r metrics, and which binaries were used to evaluate the scaling rules are listed in Table 3.

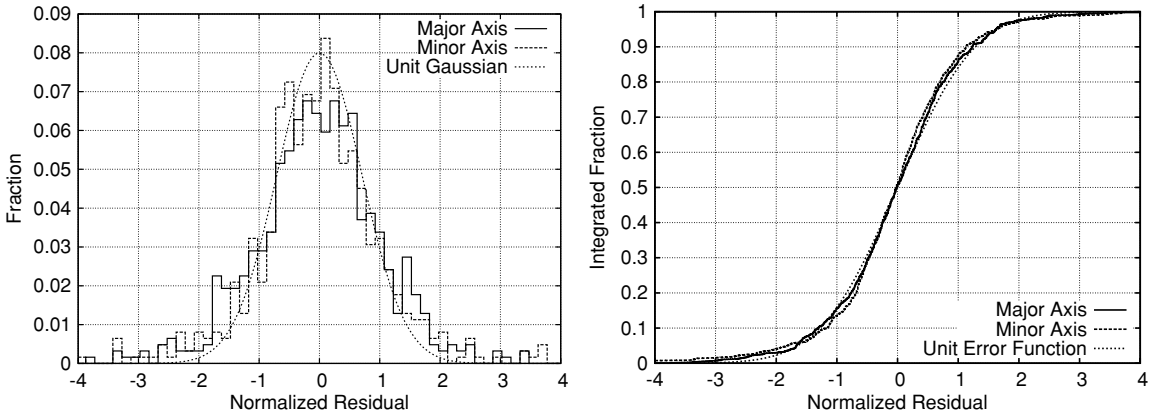

Figure 7. Distributions of normalized residuals for two-body Keplerian fits to 20 binaries, in major and minor axes. On the left is the histogram of the residuals and unit-width Gaussian for comparison, while on the right is the continuous distribution function, with the theoretical distribution for Gaussian noise (the error function).

Table 3
Binaries Evaluated Using Empirical Uncertainty Ellipse Scaling Laws

HD Number	Nights Observed	χ_r^2	
17904	46	0.53	*
26690	20	0.75	
44926	23	0.62	*
76943	16	1.10	
114378	24	1.24	*
137107	51	1.22	*
137391	23	0.59	*
137909	73	0.85	*
140159	15	1.15	*
171779	54	1.04	*
187362	10	0.97	
202275	69	0.91	*
207652	50	0.58	*
214850	53	0.87	*
5286	18	4.71	
6811	20	2.16	
13872	89	0.46	*
77327	47	0.44	*
81858	12	2.27	
129246	17	1.86	*
140436	43	1.82	*
155103	10	0.21	
176051	66	4.43	
196524	73	2.68	
202444	39	3.52	
221673	99	8.01	

Notes. Column 1 is the star's HD Catalog Number, Column 2 is the total number of nights the star was observed, and Column 3 is the value of χ_r^2 calculated for a Keplerian model. An asterisk appears in the fourth column of stars used to evaluate the uncertainty ellipse scaling rules.

5. DISTRIBUTION OF FIT RESIDUALS

To use the PHASES measurements for orbit fitting and companion searches, it was important to establish the statistical properties of the measurement residuals to determine whether they are Gaussian. Using uncertainties derived from the process outlined in Section 4, Keplerian orbits were fit for 19 of the 20 binaries presented in Paper II (HD 202444 has been omitted, since there is some evidence to suggest it hosts a substellar companion; see Paper V), as well as δ Equ (HD 202275), which has previously been studied at length (Muterspaugh et al. 2005, 2008). The fits included all the non-PHASES and radial velocity measurements as listed in Paper II, rather than just the PHASES measurements, to ensure the residuals represented the best known binary motions. The PHASES measurement residuals along the minor axes of the error ellipses for these 20 binaries were normalized by their minor axis measurement uncertainties and combined into a joint residual distribution; a similar distribution was made for the major axis residuals. Histograms and continuous distribution functions (the latter being the integral of the histogram, which has the advantage of avoiding misinterpretation of the statistics caused by the granularity of bin size used in the histograms, though at the expense of being a less-familiar distribution) of the minor- and major-axis residuals are presented in Figure 7, along with the theoretical distributions one would obtain from unit-deviation distribution (a Gaussian and an error function, respectively). The distributions agree quite well with the theoretical distributions, though there might be a slight excess number in the distribution wings. However, any excess is small, and Gaussian statistics are a reasonable approximation for orbit-fitting and companion search applications.

6. SUMMARY OF PHASES MEASUREMENTS

The 1332 PHASES measurements are presented in Table 4. All have been processed with the standard pipeline described in Section 2.2. In total, 51 binaries were observed on 443 nights. An average of 1983 scans was used for each measurement, and the average formal minor-axis uncertainty is 13 μas. After the scaling laws from Section 4 were applied, the average minor- and major-axis uncertainties were 53 μas and 486 μas, respectively.

7. SUPPORTING MEASUREMENTS

Infrared differential photometry between the primary and secondary components of several PHASES targets were obtained using Keck Adaptive Optics on MJD 53,227. The differential photometries were measured in the K_p filter for faint systems, and a narrowband H_2 2–1 filter centered at 2.2622 μm for brighter binaries. Six systems of moderate brightness were measured with both filters. Differential magnitudes for the 20 binaries observed with Keck AO are presented in Table 5.

Table 4
PHASES Astrometry Measurements

HD Number	HJD 2400000.5	δR.A. (mas)	δDecl. (mas)	σ_{min} (μas)	σ_{maj} (μas)	ϕ_e (deg)	$\sigma_{R.A.}$ (μas)	$\sigma_{Decl.}$ (μas)	$\frac{\sigma^2_{R.A.,decl.}}{\sigma_{R.A.}\sigma_{decl.}}$	$\sigma_{min,c}$ (μas)	$\sigma_{maj,c}$ (μas)	$\sigma_{R.A.,c}$ (μas)	$\sigma_{Decl.,c}$ (μas)	$\frac{\sigma^2_{R.A.,decl.,c}}{\sigma_{R.A.,c}\sigma_{decl.,c}}$	N	LDC	Align	Rate (Hz)	Outlier
4934	54004.36328	−57.0674	−179.9978	27.8	416.4	161.61	395.3	134.0	−0.97578	44.7	559.1	530.8	181.4	−0.96573	345	1	1	50	0
5286	52894.31345	−681.5589	665.6299	17.8	1360.0	146.08	1128.5	759.1	−0.99960	76.2	1773.5	1472.3	991.7	−0.99571	648	0	0	100	0
5286	52896.29389	−681.5838	665.5458	19.6	549.6	144.35	446.7	320.8	−0.99717	82.3	728.1	593.6	429.6	−0.97200	241	0	0	100	0
5286	52897.28803	−681.9351	665.8532	16.4	382.3	144.32	310.7	223.4	−0.99590	71.5	516.3	421.5	306.7	−0.95838	566	0	0	100	0
5286	53198.45485	−676.2609	690.8888	3.9	213.7	143.53	171.9	127.1	−0.99928	38.0	311.1	251.2	187.4	−0.96795	3129	0	0	100	0
5286	53215.43340	−675.9374	692.1281	7.2	273.5	146.42	227.9	151.4	−0.99838	44.4	382.1	319.3	214.6	−0.96882	2038	0	0	100	0
5286	53222.39706	−676.3939	693.0688	4.1	217.5	144.05	176.1	127.7	−0.99921	38.3	315.5	256.4	187.8	−0.96798	2583	0	0	100	0
5286	53229.40966	−674.7178	692.6724	17.9	1669.5	148.35	1421.2	876.3	−0.99971	76.5	2174.9	1851.8	1143.1	−0.99691	400	0	0	100	0
5286	53235.41932	−675.2293	693.4864	6.3	197.6	152.60	175.4	91.1	−0.99699	42.4	292.6	260.5	139.8	−0.94017	967	0	0	100	0
5286	53250.34592	−675.1408	694.9482	13.0	133.2	148.22	113.4	71.0	−0.97667	60.5	222.7	192.0	128.1	−0.83623	790	0	0	100	0
5286	53578.49345	−667.5496	720.3887	10.6	239.7	155.25	217.7	100.8	−0.99324	53.4	341.6	311.0	151.0	−0.92161	520	0	0	100	0
5286	53585.41899	−667.3132	720.7603	21.9	1887.5	146.03	1565.4	1054.8	−0.99969	90.3	2457.7	2038.9	1375.3	−0.99686	167	0	0	100	0
5286	53600.39059	−667.0935	721.9211	20.9	273.1	148.09	232.1	145.4	−0.98558	86.8	381.6	327.2	214.8	−0.88194	318	0	0	100	0
5286	53632.29638	−666.8551	724.8877	14.2	150.3	146.28	125.3	84.3	−0.97936	64.3	240.4	203.1	143.8	−0.84831	965	0	0	100	0
5286	53636.28795	−667.6554	725.7109	9.6	98.1	147.56	82.9	53.2	−0.97721	50.6	189.4	162.1	110.2	−0.84421	924	0	0	100	0
5286	53691.15757	−666.0233	729.6058	7.5	85.8	150.80	75.0	42.3	−0.97949	45.1	179.0	157.8	95.8	−0.84521	1175	0	0	100	0
5286	53957.40057	−659.8107	749.8176	5.1	57.2	147.73	48.5	30.9	−0.98055	35.4	158.5	135.4	89.8	−0.88717	3777	1	1	50	0
5286	53970.37137	−659.5338	750.6116	3.8	44.9	147.90	38.1	24.1	−0.98252	35.2	151.7	129.8	85.9	−0.87808	4330	1	1	50	0
5286	53971.35704	−660.2025	751.1008	6.9	97.3	145.40	80.2	55.5	−0.98873	35.7	188.7	156.6	111.1	−0.92215	2282	1	1	50	0
6811	52894.40088	422.2735	−280.2728	25.9	811.8	159.74	761.6	282.1	−0.99521	104.5	1064.6	999.4	381.4	−0.95651	936	0	0	100	0
6811	52895.40411	422.3082	−280.3050	19.6	376.1	160.62	354.8	126.1	−0.98635	82.3	508.6	480.5	185.8	−0.88327	735	0	0	100	0
6811	52896.40601	411.4655	−275.8378	30.4	395.5	158.80	368.9	145.8	−0.97461	120.7	532.9	498.7	223.2	−0.81607	454	0	0	100	2
6811	52897.38891	422.7105	−280.3014	26.7	998.1	158.42	928.2	367.9	−0.99694	107.3	1305.1	1214.2	490.3	−0.97192	686	0	0	100	0
6811	53222.50651	426.1493	−277.4293	5.2	118.3	161.03	111.9	38.8	−0.98974	40.2	208.0	197.1	77.6	−0.83727	4905	0	0	100	0
6811	53228.48820	424.8371	−276.7571	16.5	621.1	160.37	585.1	209.3	−0.99647	71.8	819.5	772.2	283.5	−0.96320	1593	0	0	100	0
6811	53263.39025	426.2968	−276.7695	9.9	263.6	159.41	246.7	93.1	−0.99351	51.4	370.2	347.0	138.8	−0.91870	2099	0	0	100	0
6811	53271.37223	426.4827	−276.6943	10.1	126.2	160.62	119.1	42.9	−0.96867	51.9	215.7	204.2	86.7	−0.77450	2816	0	0	100	0
6811	53313.25700	427.3890	−276.3916	22.3	270.8	160.25	255.0	93.9	−0.96777	91.7	378.9	357.9	154.4	−0.77773	794	0	0	100	0
6811	53636.36731	430.7551	−273.1652	15.8	592.3	158.72	551.9	215.5	−0.99690	69.5	782.6	729.7	291.3	−0.96671	1356	0	0	100	0
6811	53663.36469	424.8200	−272.0314	26.9	1466.0	175.11	1460.7	127.9	−0.97740	108.0	1910.9	1904.0	195.3	−0.83160	580	0	0	100	0
6811	53687.19475	431.4921	−272.0317	27.4	230.6	22.43	213.4	91.5	0.94638	109.8	330.9	308.7	162.0	0.68692	878	0	0	100	0
6811	53972.46365	433.3682	−269.1288	16.5	400.9	163.19	383.8	117.0	−0.98914	38.7	539.6	516.7	160.4	−0.96774	2134	1	1	50	0
6811	54003.36229	434.3438	−269.0321	12.5	556.2	158.67	518.1	202.6	−0.99782	37.2	736.5	686.2	270.1	−0.98904	2559	1	1	50	0
6811	54006.35815	433.6679	−268.6007	24.4	414.3	159.97	389.4	143.8	−0.98361	42.7	556.5	523.0	194.8	−0.97246	1260	1	1	50	0
6811	54008.35403	433.9942	−268.7999	8.5	110.9	159.82	104.1	39.1	−0.97295	36.0	201.0	189.0	77.1	−0.86807	3740	1	1	50	0
6811	54341.44154	437.0441	−264.9185	17.3	361.7	160.07	340.1	124.4	−0.98896	74.5	490.6	461.9	181.3	−0.89980	1879	0	1	50	0
6811	54350.42520	437.1835	−264.9587	8.6	124.5	161.89	118.4	39.5	−0.97365	47.9	214.0	203.9	80.6	−0.78190	5096	0	1	50	0
6811	54357.40553	437.5387	−264.8896	18.4	314.6	161.36	298.2	102.0	−0.98180	78.2	432.3	410.4	156.8	−0.85087	2348	0	1	50	0
6811	54769.28217	441.7437	−260.4480	35.0	1055.9	162.13	1005.0	325.8	−0.99359	49.5	1379.8	1313.3	426.0	−0.99252	580	1	1	50	0
11636	53638.46558	24.8811	−10.4154	10.6	313.6	39.98	240.4	201.7	0.99764	53.4	431.0	332.1	280.0	0.96891	3263	0	0	100	0
13872	52868.45994	−134.4324	4.9165	19.5	2025.3	149.53	1745.7	1027.0	−0.99976	82.0	2636.6	2272.9	1338.9	−0.99748	280	0	0	100	0
13872	53215.50012	−144.8076	−14.6601	28.0	1083.3	148.43	923.1	567.7	−0.99832	112.0	1415.2	1207.2	747.1	−0.98443	199	0	0	100	0
13872	53222.46534	−143.9341	−15.6965	5.5	212.2	145.90	175.8	119.1	−0.99845	40.8	309.4	257.2	176.7	−0.96072	1792	0	0	100	0
13872	53234.45075	−144.5008	−16.2052	16.8	179.2	149.25	154.2	92.7	−0.97750	72.8	271.8	236.5	152.4	−0.83586	361	0	0	100	0
13872	53249.46019	−144.8697	−17.0067	6.2	49.3	157.43	45.6	19.8	−0.93981	42.2	154.0	143.1	70.8	−0.76725	1350	0	0	100	0

Table 4
(Continued)

HD Number	HJD 2400000.5	δR.A. (mas)	δDecl. (mas)	σ_{min} (μas)	σ_{maj} (μas)	ϕ_e (deg)	$\sigma_{R.A.}$ (μas)	$\sigma_{Decl.}$ (μas)	$\frac{\sigma^2_{R.A.,decl.}}{\sigma_{R.A.}\sigma_{decl.}}$	$\sigma_{min,c}$ (μas)	$\sigma_{maj,c}$ (μas)	$\sigma_{R.A.,c}$ (μas)	$\sigma_{Decl.,c}$ (μas)	$\frac{\sigma^2_{R.A.,decl.,c}}{\sigma_{R.A.,c}\sigma_{decl.,c}}$	N	LDC	Align	Rate (Hz)	Outlier
13872	53250.46337	−144.6809	−17.1576	31.6	488.9	159.08	456.8	177.1	−0.98155	125.1	650.8	609.5	260.1	−0.85813	113	0	0	100	0
13872	53263.40075	−145.2831	−17.7597	6.3	51.7	153.42	46.4	23.8	−0.95598	42.4	155.3	140.2	79.2	−0.80486	1574	0	0	100	0
13872	53271.38426	−145.3640	−18.2781	5.5	45.8	154.32	41.4	20.5	−0.95411	40.8	152.1	138.2	75.5	−0.80416	2510	0	0	100	0
13872	53312.30383	−146.5058	−20.3929	2.7	31.5	160.49	29.7	10.8	−0.96334	36.5	145.9	138.0	59.6	−0.76296	5214	0	0	100	0
13872	53313.28343	−147.1579	−20.1609	10.7	417.5	156.00	381.4	170.1	−0.99761	53.6	560.5	512.5	233.2	−0.96783	905	0	0	100	0
13872	53333.23983	−146.8661	−21.5534	8.8	231.2	158.14	214.6	86.5	−0.99400	48.4	331.6	308.3	131.4	−0.91811	935	0	0	100	0
13872	53334.25787	−148.3531	−21.1557	18.4	1427.2	162.48	1361.0	430.0	−0.99899	78.2	1860.6	1774.5	565.1	−0.98942	327	0	0	100	0
13872	53340.19672	−147.4399	−21.7883	20.1	960.2	153.66	860.5	426.5	−0.99862	84.0	1256.1	1126.3	562.4	−0.98602	289	0	0	100	0
13872	53341.24624	−147.7720	−21.7435	25.5	1154.0	164.19	1110.4	315.4	−0.99646	103.0	1506.7	1450.0	422.3	−0.96733	242	0	0	100	0
13872	53584.47779	−151.6375	−34.5213	21.7	690.1	146.43	575.1	382.0	−0.99768	89.6	908.0	758.2	507.6	−0.97741	430	0	0	100	0
13872	53586.47768	−151.4689	−34.7058	9.9	121.5	147.59	102.7	65.7	−0.98387	51.4	211.1	180.3	121.2	−0.86806	780	0	0	100	0
13872	53599.45344	−152.3887	−34.8899	19.7	979.5	148.68	836.8	509.4	−0.99898	82.6	1281.0	1095.2	669.6	−0.98953	294	0	0	100	0
13872	53606.44225	−151.5573	−35.8371	9.0	275.7	150.03	238.8	137.9	−0.99716	48.9	384.8	334.2	196.8	−0.95817	909	0	0	100	0
13872	53607.43452	−151.2101	−36.0727	12.4	422.4	149.08	362.4	217.3	−0.99778	58.7	566.7	487.1	295.5	−0.97293	677	0	0	100	0
13872	53613.41692	−151.9164	−35.9521	23.1	826.9	148.91	708.2	427.5	−0.99800	94.5	1084.0	929.6	565.6	−0.98084	200	0	0	100	0
13872	53614.41517	−151.7623	−36.2031	26.2	1064.2	148.83	910.6	551.3	−0.99846	105.5	1390.5	1191.0	725.3	−0.98547	182	0	0	100	0
13872	53639.35205	−151.7435	−37.6653	20.2	1070.3	149.46	921.8	544.2	−0.99907	84.4	1398.4	1205.2	714.3	−0.99057	661	0	0	100	0
13872	53670.28242	−151.3679	−39.3993	38.5	1039.2	151.85	916.5	491.4	−0.99605	150.4	1358.2	1199.6	654.4	−0.96554	268	0	0	100	0
13872	53691.18919	−152.6309	−39.7322	14.6	118.9	148.36	101.5	63.6	−0.96314	65.6	208.5	180.9	122.8	−0.78788	847	0	0	100	0
13872	53718.18737	−152.6133	−41.2864	16.0	274.5	159.62	257.4	96.8	−0.98433	70.2	383.3	360.2	148.8	−0.86501	690	0	0	100	0
13872	53726.15532	−152.5621	−41.7723	16.0	185.2	156.69	170.2	74.7	−0.97261	70.2	278.5	257.3	127.7	−0.80380	509	0	0	100	0
13872	53732.15251	−152.6477	−42.0269	11.0	112.7	159.93	105.9	40.0	−0.95623	54.5	202.6	191.3	86.4	−0.74338	599	0	0	100	0
13872	53739.16051	−152.1406	−42.5017	23.3	313.4	165.31	303.3	82.6	−0.95660	95.2	430.8	417.4	142.9	−0.72602	125	0	0	100	0
13872	53746.13612	−152.4635	−42.7666	4.6	57.0	164.45	54.9	15.9	−0.95335	39.1	158.4	153.0	56.8	−0.70062	2806	0	0	100	0
13872	53748.13687	−152.4947	−42.8582	13.6	171.7	165.49	166.3	45.0	−0.95031	62.4	263.5	255.6	89.5	−0.69495	580	0	0	100	0
13872	53753.13686	−152.2448	−43.1148	12.3	234.1	169.46	230.2	44.5	−0.95959	58.4	335.0	329.5	84.0	−0.70723	567	0	0	100	0
13872	53929.49251	−153.9562	−49.6856	30.3	1547.8	141.53	1212.0	963.2	−0.99919	46.3	2017.0	1579.4	1255.3	−0.99889	335	1	1	50	0
13872	53930.49739	−151.9120	−51.3218	6.8	347.4	142.44	275.4	211.8	−0.99917	43.5	472.8	375.8	290.3	−0.98206	2478	0	1	50	0
13872	53935.47952	−151.9327	−51.4370	21.3	896.2	141.49	701.4	558.2	−0.99881	41.0	1173.4	918.6	731.3	−0.99744	621	1	1	50	0
13872	53936.48606	−151.7695	−51.6402	7.1	195.4	142.94	156.0	117.9	−0.99718	35.7	290.0	232.5	177.1	−0.96783	2387	1	1	50	0
13872	53937.48724	−151.9168	−51.5570	4.4	116.0	143.48	93.2	69.1	−0.99684	38.8	205.8	167.0	126.4	−0.92568	4028	0	1	50	0
13872	53951.44870	−151.7068	−52.1619	15.7	351.3	143.26	281.7	210.5	−0.99565	38.4	477.7	383.5	287.4	−0.98608	998	1	1	50	0
13872	53956.48858	−151.5248	−52.5074	4.3	48.8	152.38	43.3	23.0	−0.97759	35.3	153.7	137.2	77.8	−0.86144	6979	1	1	50	0
13872	53957.44792	−151.3560	−52.6303	7.2	125.5	145.75	103.8	70.9	−0.99248	35.7	215.0	178.8	124.5	−0.93864	2481	1	1	50	0
13872	53958.48472	−151.5132	−52.5578	8.8	72.8	152.17	64.5	34.9	−0.95903	36.1	169.0	150.4	85.1	−0.87917	1998	1	1	50	0
13872	53963.46233	−151.5164	−52.7090	30.3	292.0	150.43	254.4	146.5	−0.97146	46.3	404.6	352.6	203.7	−0.96540	439	1	1	100	0
13872	53965.50072	−151.5046	−52.8522	4.9	59.3	158.31	55.2	22.4	−0.97196	35.3	159.8	149.1	67.6	−0.82807	4409	1	1	50	0
13872	53970.40460	−151.2200	−53.1663	6.6	114.1	143.60	91.9	67.9	−0.99263	35.6	204.0	165.5	124.4	−0.93568	2412	1	1	50	0
13872	53971.49071	−150.9509	−53.2562	15.3	84.3	157.82	78.3	34.9	−0.88075	38.2	177.8	165.3	75.9	−0.84062	1125	1	1	50	0
13872	53972.40215	−150.9837	−53.4119	10.3	152.6	144.73	124.7	88.5	−0.98973	36.5	242.8	199.4	143.3	−0.95073	1832	1	1	50	0
13872	53977.40389	−150.9146	−53.6256	8.1	233.8	146.35	194.7	129.7	−0.99716	35.9	334.6	279.3	187.8	−0.97338	2089	1	1	50	0
13872	53978.44990	−151.3107	−53.4354	7.2	45.9	154.75	41.6	20.6	−0.92351	35.7	152.2	138.5	72.5	−0.84071	2307	1	1	50	0
13872	53979.48348	−151.3883	−53.4012	18.7	362.6	161.35	343.6	117.3	−0.98576	39.7	491.7	466.1	161.7	−0.96589	624	1	1	50	0
13872	53985.43797	−151.6481	−53.5143	9.6	239.1	155.73	218.0	98.6	−0.99429	36.3	340.9	311.1	144.0	−0.96110	1797	1	1	50	0
13872	53986.38174	−150.7794	−53.9608	26.9	451.2	147.18	379.5	245.6	−0.99149	44.1	603.0	507.3	328.9	−0.98720	320	1	1	50	0

Table 4
(Continued)

HD Number	HJD 2400000.5	δR.A. (mas)	δDecl. (mas)	σ_{min} (μas)	σ_{maj} (μas)	ϕ_e (deg)	$\sigma_{R.A.}$ (μas)	$\sigma_{Decl.}$ (μas)	$\frac{\sigma^2_{R.A.,decl.}}{\sigma_{R.A.}\sigma_{decl.}}$	$\sigma_{min,c}$ (μas)	$\sigma_{maj,c}$ (μas)	$\sigma_{R.A.,c}$ (μas)	$\sigma_{Decl.,c}$ (μas)	$\frac{\sigma^2_{R.A.,decl.,c}}{\sigma_{R.A.,c}\sigma_{decl.,c}}$	N	LDC	Align	Rate (Hz)	Outlier
13872	53996.32588	−151.1242	−54.0624	8.3	117.1	142.31	92.8	71.9	−0.98925	36.0	206.8	165.1	129.6	−0.93765	1463	1	1	50	0
13872	54003.37200	−150.7523	−54.5566	8.4	46.6	153.62	41.9	22.0	−0.90585	36.0	152.5	137.6	75.1	−0.84696	2820	1	1	50	0
13872	54004.32755	−150.7397	−54.5913	14.3	75.8	145.35	62.9	44.7	−0.92271	37.8	171.2	142.5	102.2	−0.89572	1047	1	1	50	0
13872	54005.38271	−150.9772	−54.4755	12.7	71.8	157.90	66.7	29.5	−0.88566	37.2	168.3	156.5	72.1	−0.83174	2289	1	1	50	0
13872	54006.38793	−150.5945	−54.7009	11.3	78.5	158.98	73.4	30.1	−0.91518	36.8	173.2	162.3	71.0	−0.83309	1407	1	1	50	0
13872	54007.40917	−150.4264	−54.8060	6.0	167.7	161.80	159.4	52.7	−0.99280	35.5	259.1	246.4	87.7	−0.90476	2562	1	1	50	0
13872	54008.36643	−150.7097	−54.7213	6.6	74.6	154.63	67.5	32.5	−0.97412	35.6	170.3	154.6	79.8	−0.87068	2491	1	1	50	0
13872	54009.33295	−150.6374	−54.7549	16.1	70.2	147.98	60.2	39.7	−0.88013	38.5	167.1	143.2	94.4	−0.87932	879	1	1	50	0
13872	54010.43151	−150.6045	−54.8265	37.0	249.7	168.10	244.5	62.9	−0.80000	50.9	353.5	346.1	88.3	−0.80801	431	1	1	50	0
13872	54029.25388	−150.1810	−55.6599	16.0	125.1	144.61	102.4	73.6	−0.96399	38.5	214.6	176.4	128.2	−0.93087	851	1	1	50	0
13872	54031.35220	−150.3564	−55.7080	27.5	296.3	162.81	283.2	91.4	−0.94929	44.5	409.8	391.8	128.4	−0.93189	494	1	1	50	0
13872	54032.28753	−150.1185	−55.8089	26.2	122.2	152.72	109.3	60.6	−0.87580	43.7	211.7	189.3	104.5	−0.88378	329	1	1	50	0
13872	54055.29473	−149.6837	−56.6572	10.5	75.3	168.50	73.8	18.2	−0.80786	36.5	170.8	167.6	49.4	−0.65703	1598	1	1	50	0
13872	54056.27674	−149.6402	−56.7221	9.8	84.1	161.60	79.9	28.1	−0.93069	36.3	177.6	168.9	65.8	−0.81422	1516	1	1	50	0
13872	54061.26736	−149.6525	−56.9097	23.2	214.0	161.51	203.1	71.4	−0.93932	42.0	311.4	295.7	106.5	−0.90967	787	1	1	50	0
13872	54075.19906	−149.2366	−57.4598	11.9	66.8	157.71	62.0	27.6	−0.88510	37.0	164.7	153.1	71.2	−0.82951	1114	1	1	50	0
13872	54083.18848	−148.7537	−57.8983	33.6	271.4	157.82	251.6	107.1	−0.94091	48.5	379.6	352.0	150.2	−0.93734	348	1	1	50	0
13872	54084.15457	−148.7872	−57.9119	28.1	237.5	153.46	212.8	109.0	−0.95781	44.9	339.0	303.9	156.7	−0.94760	343	1	1	50	0
13872	54306.50056	−140.2172	−65.2065	10.3	236.8	146.72	198.1	130.3	−0.99550	36.5	338.2	283.4	188.1	−0.97284	1193	1	1	50	0
13872	54320.50160	−139.5456	−65.4951	7.2	184.2	152.76	163.8	84.6	−0.99540	44.4	277.4	247.5	133.0	−0.92722	2199	0	1	50	0
13872	54321.48036	−140.1975	−65.0709	26.4	1400.9	149.35	1205.3	714.4	−0.99907	106.3	1826.5	1572.3	935.6	−0.99126	430	0	1	50	0
13872	54335.47793	−138.5053	−65.9154	10.1	106.6	155.70	97.2	44.8	−0.96914	51.9	197.0	180.8	93.9	−0.79786	1868	0	1	50	0
13872	54336.47475	−138.5287	−65.9115	7.1	87.3	155.45	79.5	36.8	−0.97763	44.2	180.2	165.0	85.0	−0.82295	2012	0	1	50	0
13872	54341.39967	−138.9760	−65.4734	22.5	865.2	145.33	711.7	492.5	−0.99846	92.4	1133.4	933.7	649.2	−0.98497	455	0	1	50	0
13872	54348.40089	−137.5612	−66.3738	15.2	312.9	148.94	268.1	162.0	−0.99400	67.5	430.2	370.2	229.4	−0.93963	991	0	1	50	0
13872	54350.42515	−137.4713	−66.3429	9.4	69.0	154.52	62.4	30.9	−0.94159	50.0	166.3	151.6	84.6	−0.76138	1782	0	1	50	0
13872	54356.42061	−137.2160	−66.4234	6.3	61.1	155.82	55.8	25.7	−0.96365	42.4	161.0	147.9	76.4	−0.79709	2500	0	1	50	0
13872	54357.35796	−136.6772	−66.6918	19.8	700.8	145.41	577.1	398.2	−0.99817	83.0	921.7	760.3	527.7	−0.98166	924	0	1	50	0
13872	54370.39212	−136.2901	−66.7839	7.7	89.3	157.78	82.7	34.5	−0.97087	45.6	181.9	169.2	80.7	−0.79439	2369	0	1	50	0
13872	54376.32513	−136.3925	−66.5157	30.9	920.9	148.30	783.7	484.6	−0.99719	122.5	1205.3	1027.5	641.9	−0.97461	392	0	1	50	0
13872	54377.39723	−135.9560	−66.7954	24.3	84.5	160.67	80.1	36.1	−0.70637	98.8	178.0	171.1	110.2	−0.36297	579	0	1	50	0
13872	54419.26390	−132.8213	−67.6774	10.5	131.4	158.73	122.5	48.6	−0.97272	53.1	220.9	206.7	94.2	−0.79829	1678	0	1	50	0
13872	54685.47397	−103.8655	−67.3995	10.8	145.4	148.45	124.0	76.6	−0.98619	36.6	235.2	201.4	127.0	−0.94151	1241	1	1	50	0
13872	54695.48895	−102.5878	−66.9776	18.7	283.4	155.34	257.7	119.5	−0.98513	39.7	394.1	358.6	168.3	−0.96585	465	1	1	50	0
13872	54713.46790	−99.9635	−66.4378	24.6	442.3	160.83	417.8	147.1	−0.98415	42.8	591.8	559.1	198.5	−0.97363	334	1	1	50	0
13872	54740.39294	−95.4755	−65.4747	15.9	90.1	160.30	85.0	33.9	−0.86767	38.4	182.5	172.3	71.4	−0.82139	937	1	1	50	0
13872	54763.34251	−91.4004	−64.5013	10.9	68.1	161.32	64.6	24.1	−0.87997	36.7	165.6	157.4	63.4	−0.79349	1099	1	1	50	0
13872	54769.34859	−90.4781	−64.1907	15.0	71.9	167.92	70.4	21.0	−0.68485	38.1	168.3	164.8	51.3	−0.65133	812	1	1	50	0
13872	54794.26958	−85.6181	−62.9320	19.3	80.1	162.77	76.7	30.0	−0.74244	40.0	174.5	167.1	64.3	−0.76024	892	1	1	50	0
16234	53242.45987	47.2253	−57.0737	21.9	147.4	22.05	136.8	58.9	0.91675	90.3	237.3	222.6	122.2	0.61615	376	0	0	100	0
16234	53272.50347	48.6455	−53.4479	12.4	303.0	176.11	302.3	24.0	−0.85551	58.7	418.0	417.1	65.1	−0.42725	594	0	0	100	0
16234	53284.34866	50.1017	−51.6841	26.4	269.7	22.53	249.4	106.2	0.96310	106.3	377.5	351.1	174.8	0.75684	205	0	0	100	0
16234	53986.48518	50.5112	−50.5456	12.6	133.1	161.93	126.6	43.0	−0.95139	37.2	222.6	211.9	77.6	−0.86388	1026	1	1	50	0
16234	54003.45071	50.2442	−47.4788	9.9	51.1	162.07	48.7	18.3	−0.82398	36.4	155.0	147.9	58.9	−0.76265	1660	1	1	50	0
16739	53243.52050	31.6286	−43.4840	15.8	332.3	33.41	277.5	183.4	0.99466	69.5	454.1	381.0	256.7	0.94650	880	0	0	100	0

Table 4
(Continued)

HD Number	HJD 2400000.5	δR.A. (mas)	δDecl. (mas)	σ_{min} (μas)	σ_{maj} (μas)	ϕ_e (deg)	$\sigma_{R.A.}$ (μas)	$\sigma_{Decl.}$ (μas)	$\frac{\sigma^2_{R.A.,decl.}}{\sigma_{R.A.}\sigma_{decl.}}$	$\sigma_{min,c}$ (μas)	$\sigma_{maj,c}$ (μas)	$\sigma_{R.A.,c}$ (μas)	$\sigma_{Decl.,c}$ (μas)	$\frac{\sigma^2_{R.A.,decl.,c}}{\sigma_{R.A.,c}\sigma_{decl.,c}}$	N	LDC	Align	Rate (Hz)	Outlier
16739	54447.20268	−19.2362	−37.7102	32.3	242.8	156.55	223.1	101.1	−0.93761	47.6	345.3	317.3	144.2	−0.93318	261	1	1	50	0
16739	54763.30273	−22.8473	−26.1662	4.3	133.5	150.40	116.1	66.0	−0.99721	35.3	223.0	194.7	114.3	−0.93550	3657	1	1	50	0
17904	52868.49771	−54.7748	193.1608	15.1	252.1	151.25	221.2	122.0	−0.98995	67.2	356.4	314.1	181.3	−0.90720	578	0	0	100	0
17904	52895.47559	−56.0072	192.9863	15.0	332.0	161.33	314.6	107.2	−0.98899	66.9	453.7	430.4	158.5	−0.89554	853	0	0	100	0
17904	52896.45244	−56.9743	193.4265	24.7	1125.4	156.97	1035.8	440.8	−0.99814	100.2	1469.7	1353.1	582.3	−0.98239	563	0	0	100	0
17904	52915.44772	−56.7591	192.9154	25.0	542.2	166.40	527.1	129.8	−0.98012	101.2	718.6	698.9	195.5	−0.84651	426	0	0	100	0
17904	52919.38659	−57.1669	192.9632	23.9	673.6	156.02	615.6	274.6	−0.99546	97.3	886.8	811.2	371.2	−0.95805	546	0	0	100	0
17904	52951.32546	−59.0320	192.9003	26.3	934.3	161.49	886.0	297.7	−0.99566	105.9	1222.6	1159.9	400.9	−0.96046	481	0	0	100	0
17904	52979.24870	−59.2207	192.5059	24.6	496.9	160.95	469.7	163.8	−0.98734	99.8	661.0	625.6	235.5	−0.89410	594	0	0	100	0
17904	53208.49209	−68.8063	191.1796	15.2	379.7	3.67	379.0	28.7	0.84635	67.5	513.1	512.0	75.0	0.43044	1336	0	0	100	0
17904	53221.50824	−70.2302	190.9742	16.1	470.4	16.08	452.0	131.2	0.99186	70.5	627.3	603.1	186.5	0.91948	1272	0	0	100	0
17904	53229.49625	−71.9627	191.9201	29.8	1340.7	148.93	1148.4	692.4	−0.99874	118.5	1748.5	1498.9	908.1	−0.98834	657	0	0	100	0
17904	53235.49051	−70.3854	190.7896	25.4	858.1	151.06	751.1	415.8	−0.99755	102.7	1124.3	985.1	551.4	−0.97716	821	0	0	100	0
17904	53242.51461	−71.0318	190.6123	22.2	242.3	29.33	211.5	120.3	0.97734	91.3	344.7	303.8	186.7	0.83181	837	0	0	100	0
17904	53249.49233	−71.2281	190.7635	5.4	37.3	159.12	34.9	14.2	−0.91328	40.6	148.2	139.2	65.0	−0.74737	3990	0	0	100	0
17904	53263.49057	−72.1259	190.7931	14.7	393.5	166.40	382.5	93.6	−0.98685	65.9	530.4	515.7	140.2	−0.87534	1076	0	0	100	0
17904	53284.42312	−72.7156	190.3493	16.4	145.5	33.77	121.3	82.0	0.97089	71.5	235.3	199.6	143.7	0.80995	1304	0	0	100	0
17904	53285.36332	−72.4170	190.4805	21.0	201.7	22.00	187.2	78.0	0.95683	87.1	297.2	277.5	137.6	0.73469	862	0	0	100	0
17904	53312.38452	−74.6204	190.2752	13.3	367.1	171.53	363.1	55.7	−0.97047	61.5	497.3	492.0	95.2	−0.75757	946	0	0	100	0
17904	53333.27871	−75.3351	190.1275	28.2	1597.9	160.94	1510.3	522.5	−0.99837	112.7	2082.0	1968.2	688.2	−0.98487	604	0	0	100	0
17904	53334.28896	−74.9998	189.9412	16.1	210.9	162.09	200.8	66.7	−0.96714	70.5	307.8	293.7	116.0	−0.77110	705	0	0	100	0
17904	53593.48089	−85.6820	186.4908	15.5	239.9	12.96	233.9	55.9	0.95883	68.5	341.9	333.5	101.7	0.72305	2115	0	0	100	0
17904	53599.50102	−85.7398	186.2555	13.2	247.3	152.42	219.3	115.1	−0.99157	61.2	350.7	312.1	171.2	−0.91586	1481	0	0	100	0
17904	53670.34114	−88.3975	185.1358	15.1	210.6	156.85	193.7	84.0	−0.98080	67.2	307.5	284.0	135.8	−0.84418	1603	0	0	100	0
17904	53676.29680	−88.0306	184.5033	26.4	863.3	152.18	763.6	403.5	−0.99726	106.3	1131.0	1001.5	536.1	−0.97463	1472	0	0	100	0
17904	53687.21628	−90.5435	184.9247	19.6	115.9	11.09	113.8	29.4	0.73496	82.3	205.7	202.5	89.9	0.36837	1580	0	0	100	2
17904	53705.23989	−90.1875	184.6091	30.9	261.5	158.62	243.8	99.6	−0.94297	122.5	367.6	345.3	176.0	−0.67120	667	0	0	100	0
17904	53746.19958	−91.0840	183.8636	24.5	432.5	172.21	428.6	63.5	−0.92075	99.5	579.4	574.2	126.0	−0.60471	368	0	0	100	0
17904	53957.50712	−100.2106	180.0509	5.9	129.9	150.03	112.5	65.1	−0.99459	35.5	219.4	190.9	113.8	−0.93355	6579	1	1	50	0
17904	53971.47164	−100.8707	179.7833	18.3	382.4	150.06	331.5	191.5	−0.99392	39.5	516.5	448.0	260.0	−0.98455	1625	1	1	50	0
17904	53977.45176	−101.1291	179.6746	9.7	248.0	149.59	214.0	125.8	−0.99600	36.3	351.5	303.7	180.7	−0.97255	3402	1	1	50	0
17904	53978.46943	−100.9825	179.5559	10.6	112.7	152.21	99.9	53.4	−0.97436	36.6	202.6	180.1	99.9	−0.91115	2252	1	1	50	0
17904	54003.41510	−101.8039	179.0073	12.4	70.4	154.36	63.7	32.4	−0.90678	37.1	167.3	151.6	79.7	−0.85803	2181	1	1	50	0
17904	54075.21871	−104.4772	177.4768	19.3	153.1	156.32	140.5	64.0	−0.94421	40.0	243.3	223.4	104.4	−0.90885	1138	1	1	50	0
17904	54321.51425	−113.3554	171.5662	9.5	282.9	150.83	247.1	138.1	−0.99690	50.3	393.5	344.5	196.8	−0.95644	3585	0	1	50	0
17904	54335.50232	−114.1699	171.3764	7.7	88.7	156.89	81.6	35.5	−0.97185	45.6	181.4	167.8	82.6	−0.80238	4434	0	1	50	0
17904	54336.49358	−114.0004	171.2792	6.5	63.1	154.18	56.9	28.1	−0.96614	42.8	162.3	147.2	80.5	−0.81006	5238	0	1	50	0
17904	54343.45469	−114.3753	171.1791	6.9	189.5	150.41	164.8	93.8	−0.99640	43.7	283.4	247.3	145.0	−0.93841	4717	0	1	50	0
17904	54349.44708	−114.4152	170.9166	8.3	89.3	151.16	78.3	43.7	−0.97633	47.1	181.9	160.9	97.0	−0.83568	4563	0	1	50	0
17904	54356.41519	−114.8098	170.8137	7.5	238.5	149.43	205.4	121.5	−0.99742	45.1	340.2	293.8	177.3	−0.95558	4406	0	1	50	0
17904	54370.41375	−115.3712	170.5431	7.4	43.1	155.51	39.3	19.1	−0.90458	44.9	150.8	138.5	74.7	−0.75594	3394	0	1	50	0
17904	54385.35724	−115.5743	170.0673	32.9	254.8	150.95	223.3	127.0	−0.95533	129.8	359.6	320.6	208.3	−0.71495	715	0	1	50	0
17904	54419.26027	−116.7572	169.0748	14.3	215.0	151.68	189.4	102.8	−0.98748	64.6	312.6	276.9	158.8	−0.88822	2224	0	1	50	0
17904	54713.47536	−126.7889	161.1280	21.0	173.5	157.37	160.4	69.5	−0.94508	40.8	265.5	245.5	108.9	−0.91416	1439	1	1	50	0
17904	54740.40809	−127.8307	160.4343	24.9	173.7	157.78	161.1	69.6	−0.92237	43.0	265.7	246.5	108.1	−0.90356	1056	1	1	50	0

Table 4
(Continued)

HD Number	HJD 2400000.5	δR.A. (mas)	δDecl. (mas)	σ_{min} (μas)	σ_{maj} (μas)	ϕ_e (deg)	$\sigma_{R.A.}$ (μas)	$\sigma_{Decl.}$ (μas)	$\frac{\sigma^2_{R.A.,decl.}}{\sigma_{R.A.}\sigma_{decl.}}$	$\sigma_{min,c}$ (μas)	$\sigma_{maj,c}$ (μas)	$\sigma_{R.A.,c}$ (μas)	$\sigma_{Decl.,c}$ (μas)	$\frac{\sigma^2_{R.A.,decl.,c}}{\sigma_{R.A.,c}\sigma_{decl.,c}}$	N	LDC	Align	Rate (Hz)	Outlier
17904	54763.34405	−129.1195	159.9749	22.3	300.2	156.05	274.5	123.6	−0.98026	41.5	414.6	379.3	172.5	−0.96481	1142	1	1	50	0
17904	54769.33578	−128.8847	159.5838	23.6	247.6	157.51	229.0	97.2	−0.96477	42.2	351.0	324.7	139.8	−0.94524	918	1	1	50	0
17904	54794.26290	−129.6028	158.8408	22.4	281.1	157.05	259.0	111.5	−0.97603	41.6	391.3	360.7	157.3	−0.95806	1364	1	1	50	0
19356	54468.24107	−33.3272	17.2516	14.2	148.6	172.17	147.2	24.6	−0.81447	37.8	238.6	236.4	49.6	−0.63918	6847	1	1	50	0
26690	52895.52618	−60.6904	111.7775	30.8	1059.7	158.16	983.7	395.2	−0.99647	122.2	1384.7	1286.1	527.5	−0.96841	153	0	0	100	0
26690	52896.49745	−61.1543	111.9381	29.2	1768.6	153.09	1577.1	800.9	−0.99916	116.3	2303.4	2054.7	1047.7	−0.99222	270	0	0	100	0
26690	52951.36244	−50.4678	105.9390	13.4	397.7	155.40	361.6	166.0	−0.99603	61.8	535.6	487.7	229.9	−0.95546	774	0	0	100	0
26690	53620.53066	57.4978	−81.3535	23.8	698.3	156.26	639.3	281.9	−0.99575	97.0	918.5	841.7	380.3	−0.96050	475	0	0	100	0
26690	53663.40922	53.3058	−87.0778	6.9	115.2	155.27	104.7	48.6	−0.98759	43.7	205.0	187.1	94.5	−0.86196	2857	0	0	100	0
26690	53676.35969	50.6665	−83.1246	24.6	833.9	152.41	739.1	386.8	−0.99742	99.8	1093.1	969.9	513.9	−0.97575	748	0	0	100	1
26690	53691.31987	50.0569	−89.9745	9.9	95.1	153.81	85.5	42.9	−0.96616	51.4	186.8	169.1	94.5	−0.79941	1896	0	0	100	0
26690	53732.22590	43.9410	−92.1914	13.9	248.4	155.52	226.1	103.7	−0.98914	63.4	352.0	321.4	156.8	−0.89680	763	0	0	100	0
26690	53977.50681	0.4743	−81.3542	9.2	270.6	148.49	230.8	141.7	−0.99710	36.2	378.6	323.3	200.3	−0.97736	2250	1	1	50	0
26690	53979.52302	−0.8235	−80.5741	24.8	950.6	151.80	837.8	449.7	−0.99804	42.9	1243.7	1096.3	588.9	−0.99658	542	1	1	50	0
26690	54003.41073	−5.8826	−77.3104	18.0	2195.5	145.06	1799.7	1257.5	−0.99985	39.4	2857.6	2342.6	1636.9	−0.99957	1248	1	1	50	0
26690	54075.26912	−18.5487	−68.1538	7.9	86.1	153.16	76.9	39.5	−0.97436	35.9	179.2	160.8	87.0	−0.88808	3072	1	1	50	0
26690	54342.51646	−64.3062	−21.2231	11.8	251.1	149.79	217.1	126.8	−0.99416	56.9	355.2	308.3	185.4	−0.93541	2658	0	1	50	0
26690	54343.50565	−64.2432	−21.1709	4.7	135.5	148.57	115.7	70.8	−0.99699	39.3	225.0	193.1	122.0	−0.92693	4237	0	1	50	0
26690	54348.52167	−64.6958	−20.2642	13.9	259.8	153.69	233.0	115.8	−0.99096	63.4	365.6	328.9	171.7	−0.91202	1447	0	1	50	0
26690	54356.47952	−66.1069	−18.6432	7.4	260.7	149.84	225.4	131.1	−0.99787	44.9	366.7	317.8	188.3	−0.96141	2794	0	1	50	0
26690	54369.45682	−67.8037	−16.2381	14.3	330.3	152.04	291.8	155.4	−0.99455	64.6	451.6	400.1	219.3	−0.94303	1464	0	1	50	0
26690	54370.45481	−68.7716	−15.5673	6.4	148.2	151.88	130.7	70.1	−0.99460	42.6	238.2	211.0	118.4	−0.91371	3606	0	1	50	0
26690	54376.43547	−69.5418	−14.5283	13.1	300.9	151.37	264.1	144.6	−0.99467	60.9	415.5	365.8	206.1	−0.94211	1640	0	1	50	0
26690	54425.27913	−76.2399	−5.0107	23.6	796.7	147.61	672.8	427.3	−0.99787	96.3	1045.1	884.0	565.7	−0.97956	875	0	1	50	0
28307	54468.21255	−28.9516	24.9986	15.7	147.4	152.73	131.2	68.9	−0.96662	38.4	237.3	211.7	114.0	−0.92605	6685	1	1	50	0
29140	52979.33952	−32.1749	−101.5914	8.3	191.2	163.71	183.5	54.2	−0.98733	47.1	285.3	274.1	91.9	−0.84586	2353	0	0	100	0
29140	53034.13427	−40.3178	−91.5427	5.6	124.7	152.78	111.0	57.3	−0.99394	41.0	214.2	191.4	104.5	−0.89870	2951	0	0	100	0
29140	53250.50243	−65.6824	−53.5439	16.1	710.2	147.24	597.3	384.5	−0.99876	70.5	933.8	786.2	508.8	−0.98637	1027	0	0	100	0
29140	53263.53075	−68.2378	−50.0532	5.0	119.6	158.10	111.0	44.9	−0.99268	39.8	209.2	194.7	86.3	−0.86852	4074	0	0	100	0
29140	53271.46792	−70.0370	−48.2688	6.6	267.9	150.15	232.4	133.5	−0.99836	43.1	375.4	326.3	190.5	−0.96561	4005	0	0	100	0
29140	53291.40263	−71.5816	−44.8765	35.3	703.7	148.37	599.5	370.3	−0.99371	138.6	925.5	791.3	499.5	−0.94586	408	0	0	100	0
29140	53294.47732	−71.0249	−44.6002	12.9	680.3	164.09	654.2	186.9	−0.99742	60.2	895.4	861.3	252.2	−0.96868	1355	0	0	100	0
29140	53312.38161	−74.1286	−40.9474	3.1	27.2	154.15	24.5	12.2	−0.95879	36.9	144.4	130.9	71.2	−0.82024	8150	0	0	100	0
29140	53320.33469	−74.5083	−39.6051	16.1	830.4	150.23	720.8	412.6	−0.99899	70.5	1088.6	945.5	543.9	−0.98881	1838	0	0	100	0
29140	53334.32195	−76.1005	−36.8198	8.5	333.3	154.46	300.8	143.9	−0.99785	47.6	455.3	411.4	201.0	−0.96498	2093	0	0	100	0
29140	53340.29375	−77.4849	−35.5086	7.3	86.1	152.98	76.7	39.6	−0.97862	44.7	179.2	161.0	90.6	−0.83600	3602	0	0	100	0
29140	53341.28189	−77.5106	−35.2744	6.9	220.6	150.70	192.4	108.1	−0.99734	43.7	319.1	279.1	160.8	−0.95041	3630	0	0	100	0
29140	53605.52839	−104.7430	15.6169	7.3	382.6	147.65	323.2	204.8	−0.99911	44.7	516.7	437.2	279.0	−0.98195	2855	0	0	100	0
29140	53606.51646	−106.5086	16.8979	6.3	389.0	146.14	323.0	216.8	−0.99939	42.4	524.7	436.4	294.5	−0.98489	3205	0	0	100	0
29140	53613.51062	−105.2544	17.0220	9.3	312.5	147.80	264.5	166.7	−0.99781	49.7	429.7	364.6	232.8	−0.96778	1614	0	0	100	0
29140	53614.50772	−105.6802	17.1894	10.2	309.4	147.94	262.3	164.4	−0.99734	52.2	425.9	362.0	230.4	−0.96377	1716	0	0	100	0
29140	53687.37896	−112.2999	31.2083	9.9	91.0	31.80	77.5	48.7	0.97114	51.4	183.3	158.1	106.0	0.82717	3260	0	0	100	0
29140	53711.29672	−114.6778	35.8973	32.3	352.2	29.41	307.2	175.2	0.97743	127.6	478.8	421.8	260.1	0.83045	833	0	0	100	0
29140	53712.28445	−114.0277	36.0766	16.5	130.5	27.87	115.6	62.7	0.95493	71.8	220.0	197.3	120.8	0.74914	2889	0	0	100	0
29140	53789.14494	−120.0513	51.3666	23.8	1243.5	40.17	950.3	802.3	0.99925	97.0	1622.6	1241.5	1049.3	0.99268	761	0	0	100	0

Table 4
(Continued)

HD Number	HJD 2400000.5	δR.A. (mas)	δDecl. (mas)	σ_{min} (μas)	σ_{maj} (μas)	ϕ_e (deg)	$\sigma_{R.A.}$ (μas)	$\sigma_{Decl.}$ (μas)	$\frac{\sigma^2_{R.A.,decl.}}{\sigma_{R.A.}\sigma_{decl.}}$	$\sigma_{min,c}$ (μas)	$\sigma_{maj,c}$ (μas)	$\sigma_{R.A.,c}$ (μas)	$\sigma_{Decl.,c}$ (μas)	$\frac{\sigma^2_{R.A.,decl.,c}}{\sigma_{R.A.,c}\sigma_{decl.,c}}$	N	LDC	Align	Rate (Hz)	Outlier
29140	53790.13845	−119.0497	52.0580	31.0	1065.5	39.39	823.6	676.6	0.99824	122.9	1392.2	1078.8	888.6	0.98394	624	0	0	100	0
29140	54030.46166	−135.6394	94.2528	20.2	605.8	163.75	581.7	170.6	−0.99240	40.4	799.9	768.0	227.2	−0.98269	1268	1	1	50	0
29140	54055.38704	−136.2414	98.5399	19.2	348.0	161.74	330.5	110.6	−0.98318	39.9	473.6	449.9	153.1	−0.96162	1679	1	1	50	0
29140	54061.37315	−136.6954	99.4920	6.5	120.8	163.08	115.6	35.7	−0.98164	35.6	210.4	201.5	70.1	−0.84776	4216	1	1	100	0
29140	54075.33237	−136.8559	101.6153	5.4	99.8	162.18	95.0	31.0	−0.98298	35.4	190.9	182.0	67.4	−0.83479	5902	1	1	50	0
29140	54083.30631	−137.8506	103.1454	12.6	275.5	161.39	261.1	88.7	−0.98863	37.2	384.5	364.6	127.7	−0.95163	3845	1	1	50	0
29140	54084.31264	−136.7974	103.1035	25.5	696.6	163.11	666.6	203.8	−0.99139	43.3	916.3	876.9	269.4	−0.98580	1182	1	1	50	0
29140	54103.25527	−137.6727	106.3288	17.1	404.7	162.34	385.7	123.8	−0.98949	39.0	544.4	518.9	169.3	−0.97042	743	1	1	100	0
29140	54138.15393	−139.3240	112.2447	11.4	183.2	161.39	173.6	59.5	−0.97917	36.8	276.3	262.1	94.8	−0.91242	3142	1	1	50	0
29140	54349.52640	−143.0809	143.4811	5.7	127.3	152.85	113.3	58.3	−0.99386	41.2	216.8	193.8	105.5	−0.89971	9473	0	1	50	0
29140	54384.45472	−142.3448	147.7776	14.6	453.7	156.65	416.6	180.4	−0.99612	65.6	606.2	557.2	247.7	−0.95759	1729	0	1	100	0
30090	54007.52586	−48.9471	51.9661	18.7	268.0	165.19	259.2	70.8	−0.96217	39.7	375.5	363.1	103.4	−0.91784	1515	1	1	50	0
30090	54008.52179	−48.2120	51.8597	13.1	228.3	164.52	220.1	62.2	−0.97575	37.4	328.2	316.4	94.7	−0.91241	3134	1	1	50	0
30090	54356.52411	−58.9350	79.8443	15.2	368.1	155.47	334.9	153.4	−0.99407	67.5	498.6	454.5	215.9	−0.93928	2396	0	1	50	0
40932	53271.50038	59.1469	105.9933	5.2	281.6	146.70	235.4	154.7	−0.99918	40.2	391.9	328.3	217.8	−0.97543	3092	0	0	100	0
40932	53285.47135	61.8963	110.1620	8.5	217.9	19.95	204.8	74.8	0.99273	47.6	316.0	297.5	116.7	0.90121	2503	0	0	100	0
40932	53290.47993	62.4497	112.0044	22.9	1175.7	151.07	1029.0	569.1	−0.99894	93.8	1534.8	1344.0	747.0	−0.98967	531	0	0	100	0
40932	53312.46235	66.0452	119.6805	3.0	62.6	158.79	58.3	22.8	−0.98982	36.8	161.9	151.6	67.9	−0.81512	6840	0	0	100	0
40932	53334.41285	69.4570	127.2486	6.7	136.0	160.77	128.4	45.2	−0.98775	43.3	225.5	213.4	84.8	−0.84199	2876	0	0	100	0
40932	53340.38026	70.2143	128.6950	8.7	95.5	157.63	88.4	37.2	−0.96792	48.1	187.1	174.0	84.0	−0.78739	2056	0	0	100	0
40932	53341.34797	70.4710	129.3401	7.7	84.7	153.15	75.7	38.9	−0.97538	45.6	178.1	160.2	90.2	−0.82684	3570	0	0	100	0
40932	53639.51369	104.4656	211.4485	9.4	131.0	149.61	113.1	66.8	−0.98653	50.0	220.5	191.8	119.6	−0.87694	1204	0	0	100	0
40932	53663.47710	106.2449	217.1611	6.0	70.2	153.87	63.0	31.4	−0.97702	41.8	167.1	151.2	82.6	−0.82913	1829	0	0	100	0
40932	53698.43976	110.2453	225.7801	27.1	516.9	37.76	409.0	317.2	0.99417	108.8	686.4	546.7	429.0	0.94800	827	0	0	100	0
40932	53705.34728	108.6099	226.3862	32.5	1039.0	151.29	911.5	499.9	−0.99724	128.4	1357.9	1192.6	662.0	−0.97532	574	0	0	100	0
40932	53732.29770	111.8056	231.4895	11.6	108.3	156.29	99.3	44.8	−0.95961	56.3	198.5	183.2	95.0	−0.76673	1103	0	0	100	0
40932	53753.23345	113.4811	235.7264	25.3	200.4	158.08	186.2	78.4	−0.93783	102.3	295.8	277.0	145.6	−0.66118	621	0	0	100	0
40932	53789.18175	117.7651	244.3028	27.4	1326.5	36.86	1061.4	796.1	0.99908	109.8	1730.1	1385.8	1041.5	0.99129	610	0	0	100	0
40932	54056.41997	131.6216	287.8565	20.5	161.6	159.05	151.1	60.9	−0.93262	40.6	252.5	236.2	97.9	−0.89660	699	1	1	50	0
40932	54061.42509	132.3700	288.4524	17.8	335.4	161.71	318.5	106.6	−0.98450	39.3	457.9	435.0	148.5	−0.96046	515	1	1	100	0
40932	54103.32274	134.6930	294.9206	25.9	616.3	163.89	592.2	172.8	−0.98779	43.5	813.3	781.5	229.5	−0.98032	182	1	1	100	0
40932	54376.53421	143.7491	326.7842	16.1	246.3	156.47	225.9	99.4	−0.98427	70.5	349.5	321.6	153.8	−0.86713	639	0	1	50	0
40932	54384.53862	144.3181	327.8358	19.1	398.7	161.42	378.0	128.3	−0.98766	80.6	536.9	509.5	187.3	−0.89142	558	0	1	100	0
40932	54391.50585	144.4388	328.8837	32.3	584.0	158.22	542.5	218.7	−0.98730	127.6	772.0	718.5	310.0	−0.89681	271	0	1	100	0
41116	52979.30446	−66.3021	−208.2956	26.8	1525.0	147.21	1282.2	826.1	−0.99926	107.7	1987.4	1671.8	1080.1	−0.99295	1107	0	0	100	0
41116	53294.53873	−88.2656	−155.7271	4.6	92.1	166.41	89.6	22.1	−0.97711	39.1	184.2	179.3	57.6	−0.71644	5367	0	0	100	0
41116	53333.48253	−89.7805	−148.6646	8.9	131.9	177.46	131.8	10.7	−0.54724	48.7	221.4	221.2	49.6	−0.18821	3951	0	0	100	0
41116	53340.45440	−90.9105	−146.6141	6.0	59.9	172.85	59.4	9.5	−0.77520	41.8	160.2	159.0	46.0	−0.40384	5359	0	0	100	0
41116	53341.40117	−91.1426	−146.4472	5.5	34.1	164.67	32.9	10.5	−0.83856	40.8	146.9	142.0	55.3	−0.64664	6204	0	0	100	0
41116	53446.17307	−95.9927	−125.5838	21.1	546.1	178.11	545.8	27.7	−0.64874	87.5	723.6	723.2	90.6	−0.25945	1559	0	0	100	0
41116	53632.51409	−101.1302	−86.5536	5.7	79.0	148.68	67.6	41.4	−0.98712	41.2	173.6	149.9	96.9	−0.87041	6802	0	0	100	0
41116	53637.49803	−101.6928	−84.5006	17.0	325.4	148.11	276.4	172.5	−0.99325	73.5	445.6	380.3	243.5	−0.93544	1869	0	0	100	0
41116	53639.48943	−101.3809	−84.4832	5.2	77.6	148.27	66.1	41.1	−0.98900	40.2	172.6	148.3	97.0	−0.87600	5352	0	0	100	0
41116	53648.46693	−102.0040	−82.1033	3.8	85.2	147.36	71.8	46.1	−0.99514	37.9	178.5	151.7	101.4	−0.89835	8580	0	0	100	0
41116	53676.48593	−102.6684	−75.5939	7.6	56.0	164.94	54.1	16.3	−0.87684	45.4	157.8	152.8	60.0	−0.62487	6904	0	0	100	0

Table 4
(Continued)

HD Number	HJD 2400000.5	δR.A. (mas)	δDecl. (mas)	σ_{min} (μas)	σ_{maj} (μas)	ϕ_e (deg)	$\sigma_{R.A.}$ (μas)	$\sigma_{Decl.}$ (μas)	$\frac{\sigma^2_{R.A.,decl.}}{\sigma_{R.A.}\sigma_{decl.}}$	$\sigma_{min,c}$ (μas)	$\sigma_{maj,c}$ (μas)	$\sigma_{R.A.,c}$ (μas)	$\sigma_{Decl.,c}$ (μas)	$\frac{\sigma^2_{R.A.,decl.,c}}{\sigma_{R.A.,c}\sigma_{decl.,c}}$	N	LDC	Align	Rate (Hz)	Outlier
41116	53690.37578	−101.8137	−73.7882	16.0	163.8	150.02	142.1	83.0	−0.97506	70.2	254.8	223.5	141.1	−0.82379	2926	0	0	100	0
41116	53725.40629	−103.4052	−64.3701	7.3	97.8	177.25	97.7	8.7	−0.53915	44.7	189.1	188.9	45.5	−0.18819	5423	0	0	100	0
41116	53747.28929	−102.5682	−60.3672	11.4	85.1	164.11	81.9	25.8	−0.88779	55.7	178.4	172.3	72.5	−0.60584	3985	0	0	100	0
41116	53753.26569	−103.5685	−57.7633	7.2	45.9	162.23	43.8	15.6	−0.87561	44.4	152.2	145.6	62.8	−0.67336	6523	0	0	100	0
41116	53760.26558	−102.6124	−57.0295	16.2	99.3	172.39	98.4	20.8	−0.61596	70.8	190.4	189.0	74.6	−0.29101	3342	0	0	100	0
41116	53992.52332	−101.7159	0.4800	6.2	174.8	147.52	147.5	94.0	−0.99692	35.5	266.9	226.0	146.4	−0.95801	4773	1	1	100	0
41116	53993.53718	−100.2397	−0.1331	23.6	1190.0	150.05	1031.2	594.4	−0.99895	42.2	1553.3	1346.1	776.3	−0.99803	915	1	1	50	0
41116	54005.50485	−100.2658	2.5738	3.8	43.1	150.77	37.7	21.3	−0.97876	35.2	150.8	132.7	79.8	−0.86524	12158	1	1	50	0
41116	54009.51223	−98.3076	2.6117	6.0	252.9	152.70	224.8	116.1	−0.99831	35.5	357.3	318.0	166.9	−0.97099	5461	1	1	50	0
41116	54029.41661	−96.2216	11.4119	28.7	593.7	146.39	494.7	329.5	−0.99454	45.3	784.4	653.8	435.8	−0.99221	1132	1	1	50	1
41116	54369.52002	−74.6987	86.9307	3.0	47.4	152.01	41.8	22.4	−0.98862	36.8	153.0	136.2	78.8	−0.85128	14346	0	1	50	0
41116	54376.47755	−76.0054	85.0768	6.6	321.9	147.82	272.4	171.5	−0.99897	43.1	441.3	374.2	237.8	−0.97694	5151	0	1	50	1
41116	54384.49380	−72.3091	89.5548	6.0	147.2	154.26	132.6	64.1	−0.99463	41.8	237.1	214.3	109.6	−0.90684	5792	0	1	100	0
41116	54391.44955	−71.4185	90.3825	9.5	192.7	150.78	168.3	94.4	−0.99329	50.3	287.0	251.7	146.8	−0.92057	6421	0	1	100	0
41116	54420.45604	−67.5093	95.7218	4.9	42.3	163.49	40.6	12.9	−0.91879	39.6	150.4	144.7	57.2	−0.69325	6067	0	1	50	0
41116	54425.41497	−68.4678	98.1220	6.2	54.9	159.19	51.3	20.3	−0.94612	42.2	157.1	147.7	68.4	−0.75396	6844	0	1	50	0
41116	54524.18054	−53.7486	112.9393	3.9	23.1	165.35	22.4	6.9	−0.81735	35.2	143.2	138.8	49.7	−0.68285	7182	1	1	50	0
41116	54769.46872	−10.4299	127.9161	7.5	125.2	157.83	116.0	47.8	−0.98567	35.8	214.7	199.3	87.5	−0.89772	8293	1	1	50	0
41116	54794.41053	−5.2193	125.9489	8.3	152.4	160.44	143.7	51.6	−0.98533	36.0	242.6	228.9	88.0	−0.90132	7367	1	1	50	0
44926	52979.39500	−35.2577	119.9384	7.8	330.6	160.82	312.3	108.9	−0.99709	45.9	452.0	427.2	154.7	−0.94952	1101	0	0	100	0
44926	53034.23459	−34.8746	119.6472	5.8	139.7	158.68	130.2	51.1	−0.99265	41.4	229.3	214.1	91.8	−0.87604	1788	0	0	100	0
44926	53250.53134	−32.0356	117.5082	25.0	2606.9	142.49	2067.8	1587.6	−0.99980	101.2	3391.9	2691.3	2066.9	−0.99809	296	0	0	100	0
44926	53271.53548	−33.7021	118.8737	4.8	167.3	150.71	146.0	82.0	−0.99778	39.5	258.7	226.4	131.1	−0.93904	2926	0	0	100	0
44926	53272.54422	−33.0730	118.5858	17.3	2086.3	152.61	1852.4	959.9	−0.99979	74.5	2715.8	2411.6	1251.1	−0.99775	458	0	0	100	0
44926	53284.49457	−33.8095	118.8309	13.8	138.0	18.94	130.6	46.7	0.95010	63.0	227.6	216.2	94.9	0.71511	692	0	0	100	0
44926	53312.51677	−33.8413	118.8095	2.7	66.5	168.42	65.2	13.6	−0.97877	36.5	164.5	161.4	48.7	−0.64479	5124	0	0	100	0
44926	53334.45165	−33.6514	118.7316	5.3	208.1	167.00	202.8	47.1	−0.99319	40.4	304.6	296.9	79.0	−0.85156	1838	0	0	100	0
44926	53340.45995	−33.9078	118.7351	7.2	265.4	172.71	263.3	34.4	−0.97730	44.4	372.3	369.4	64.6	−0.72080	1302	0	0	100	0
44926	53670.43724	−30.3885	116.3393	18.2	772.7	149.13	663.3	396.8	−0.99857	77.5	1014.2	871.4	524.6	−0.98510	807	0	0	100	0
44926	53727.30559	−31.4332	116.9579	14.5	171.8	152.53	152.6	80.3	−0.97902	65.3	263.6	235.8	134.7	−0.84051	575	0	0	100	0
44926	53732.32706	−31.2318	116.8380	5.2	30.7	159.29	28.8	11.9	−0.88278	40.2	145.6	136.9	63.7	−0.74199	2040	0	0	100	0
44926	53753.26329	−30.9670	116.6434	16.6	207.8	155.05	188.5	88.9	−0.97870	72.1	304.3	277.5	144.1	−0.83582	536	0	0	100	0
44926	53780.16231	−31.4738	116.7661	19.4	340.5	153.26	304.2	154.2	−0.99007	81.6	464.3	416.2	221.2	−0.91145	280	0	0	100	0
44926	54003.53291	−30.1816	115.6561	11.3	720.2	150.97	629.8	349.7	−0.99932	36.8	946.7	827.9	460.5	−0.99582	2220	1	1	50	0
44926	54006.51469	−29.8046	115.3735	9.0	215.1	149.25	184.9	110.2	−0.99545	36.1	312.7	269.4	162.9	−0.96626	2719	1	1	50	0
44926	54056.44638	−29.6302	115.1160	12.9	105.6	160.48	99.6	37.3	−0.93095	37.3	196.1	185.2	74.4	−0.84733	1148	1	1	50	0
44926	54075.40339	−29.4892	115.0714	6.5	120.3	162.27	114.6	37.2	−0.98294	35.6	209.9	200.2	72.4	−0.85674	2274	1	1	50	0
44926	54350.53105	−28.1189	113.5520	10.3	619.4	143.81	499.9	365.8	−0.99939	52.5	817.3	660.3	484.4	−0.99096	2054	0	1	50	0
44926	54483.24948	−26.6224	112.3288	21.5	180.3	156.77	165.9	73.8	−0.94874	41.1	273.0	251.4	114.1	−0.92043	837	1	1	50	0
44926	54524.16706	−26.8294	112.2227	5.2	78.0	160.66	73.7	26.3	−0.97785	35.4	172.9	163.5	66.3	−0.82550	2873	1	1	50	0
44926	54748.50946	−25.6082	110.7129	17.0	250.0	154.50	225.7	108.7	−0.98490	38.9	353.9	319.8	156.3	−0.96134	1382	1	1	50	0
44926	54762.44298	−25.9496	110.8420	17.9	358.2	149.17	307.7	184.2	−0.99358	39.3	486.3	418.0	251.5	−0.98333	771	1	1	50	0
58728	53034.27303	−21.7671	69.7307	10.8	343.2	157.37	316.8	132.4	−0.99611	53.9	467.6	432.1	186.7	−0.94987	2226	0	0	100	0
58728	53648.52545	−24.0983	102.0803	7.5	201.5	147.85	170.7	107.4	−0.99662	45.1	297.0	252.6	162.6	−0.94524	6540	0	0	100	0
58728	53663.52313	−23.5607	100.7802	5.9	64.3	154.41	58.0	28.3	−0.97280	41.6	163.1	148.2	79.8	−0.81929	6293	0	0	100	0

Table 4
(Continued)

HD Number	HJD 2400000.5	δR.A. (mas)	δDecl. (mas)	σ_{min} (μas)	σ_{maj} (μas)	ϕ_e (deg)	$\sigma_{R.A.}$ (μas)	$\sigma_{Decl.}$ (μas)	$\frac{\sigma^2_{R.A.,decl.}}{\sigma_{R.A.}\sigma_{decl.}}$	$\sigma_{min,c}$ (μas)	$\sigma_{maj,c}$ (μas)	$\sigma_{R.A.,c}$ (μas)	$\sigma_{Decl.,c}$ (μas)	$\frac{\sigma^2_{R.A.,decl.,c}}{\sigma_{R.A.,c}\sigma_{decl.,c}}$	N	LDC	Align	Rate (Hz)	Outlier
58728	53705.41371	−23.6320	94.8323	10.9	70.3	152.52	62.6	33.9	−0.93234	54.2	167.2	150.4	90.9	−0.74869	3183	0	0	100	0
58728	53727.33588	−21.9527	89.4581	25.8	1204.1	150.55	1048.6	592.4	−0.99875	104.1	1571.6	1369.5	778.0	−0.98814	1157	0	0	100	0
58728	53732.39012	−22.6217	88.7557	8.1	101.0	162.58	96.4	31.2	−0.96273	46.6	191.9	183.7	72.7	−0.74203	2692	0	0	100	0
58728	53739.31549	−22.1496	86.7264	12.2	326.7	152.77	290.5	149.9	−0.99580	58.1	447.2	398.5	211.0	−0.95110	2054	0	0	100	0
58728	53746.29719	−22.4211	85.1343	9.6	66.3	153.84	59.7	30.5	−0.93716	50.6	164.4	149.2	85.5	−0.75885	2658	0	0	100	0
58728	53747.35674	−22.3286	84.7353	21.7	406.3	165.65	393.7	102.9	−0.97597	89.6	546.4	529.8	160.9	−0.81861	910	0	0	100	0
58728	53779.20452	−20.3576	74.4071	21.2	132.5	150.45	115.7	67.9	−0.93377	87.8	222.0	197.9	133.5	−0.67483	1190	0	0	100	0
58728	53790.20966	−18.9168	70.5481	27.2	239.3	30.76	206.1	124.6	0.96737	109.1	341.1	298.4	198.1	0.77675	699	0	0	100	0
58728	54174.16806	−8.6169	42.2071	8.0	74.3	160.67	70.2	25.7	−0.94447	35.9	170.1	160.9	65.7	−0.81642	4377	1	1	50	0
58728	54370.52780	−23.7857	103.1992	8.0	277.9	144.91	227.4	159.9	−0.99814	46.4	387.4	318.1	225.9	−0.96828	6305	0	1	50	0
58728	54383.51155	−24.4379	103.4596	31.0	689.9	147.56	582.5	371.0	−0.99510	122.9	907.7	768.9	497.8	−0.95660	2204	0	1	50	0
58728	54420.47609	−24.1552	101.3020	8.4	84.6	157.90	78.4	32.7	−0.96108	47.4	178.0	165.9	80.1	−0.77272	6149	0	1	50	0
58728	54425.46497	−24.8721	101.1027	17.2	163.6	158.05	151.8	63.2	−0.95604	74.1	254.6	237.8	117.4	−0.73679	2941	0	1	50	0
58728	54483.33279	−23.4139	91.0054	18.0	123.0	164.37	118.5	37.4	−0.86616	39.4	212.5	204.9	68.7	−0.80419	1895	1	1	50	0
58728	54503.23719	−22.0842	85.5832	25.9	519.3	155.69	473.3	215.1	−0.99124	43.5	689.5	628.6	286.6	−0.98602	1769	1	1	50	0
58728	54524.19366	−21.4321	79.3948	9.0	174.0	157.34	160.6	67.6	−0.98945	36.1	266.0	245.9	107.8	−0.93188	3559	1	1	50	0
58728	54526.16985	−21.0047	78.5180	36.3	1269.6	154.42	1145.2	549.2	−0.99731	50.4	1656.4	1494.2	716.6	−0.99695	1163	1	1	50	0
58728	54529.16654	−17.9140	76.3879	16.1	898.3	155.39	816.8	374.3	−0.99888	38.5	1176.2	1069.4	491.0	−0.99627	2141	1	1	50	0
60318	52948.54661	50.6805	−59.5074	3.5	62.2	165.74	60.3	15.7	−0.97250	37.4	161.7	157.0	53.9	−0.69831	3366	0	0	100	0
60318	52952.49909	51.4400	−59.6509	7.6	203.3	157.89	188.4	76.9	−0.99427	45.4	299.1	277.6	120.2	−0.91351	1641	0	0	100	0
60318	52979.49138	51.1041	−58.3711	10.8	481.2	171.72	476.2	70.1	−0.98787	53.9	641.0	634.4	106.6	−0.85952	920	0	0	100	0
60318	53034.32232	49.0157	−55.6260	3.9	109.6	166.98	106.8	25.0	−0.98703	38.0	199.8	194.8	58.3	−0.74350	2908	0	0	100	0
60318	53284.53247	45.2897	−47.1859	3.4	40.7	17.46	38.9	12.7	0.95873	37.3	149.7	143.2	57.3	0.73276	4342	0	0	100	0
60318	53312.55639	45.0879	−46.9776	1.7	37.6	166.79	36.6	8.8	−0.97880	35.6	148.3	144.6	48.5	−0.65787	6209	0	0	100	0
60318	53333.53712	45.3627	−46.7988	7.6	258.7	175.88	258.0	20.1	−0.92495	45.4	364.3	363.4	52.3	−0.49281	1534	0	0	100	0
60318	53334.53365	45.7510	−46.7960	3.5	132.4	175.23	131.9	11.5	−0.95181	37.4	221.9	221.1	41.6	−0.43058	2536	0	0	100	0
60318	53340.52090	44.7072	−46.6276	3.0	66.0	175.72	65.8	5.7	−0.85574	36.8	164.2	163.8	38.7	−0.30071	3962	0	0	100	0
60318	53341.51946	44.5720	−46.6507	3.7	35.7	176.05	35.7	4.4	−0.54756	37.7	147.5	147.2	39.0	−0.24359	3679	0	0	100	0
60318	53466.17741	43.6811	−44.8996	5.0	53.1	176.16	53.0	6.1	−0.57727	39.8	156.1	155.8	41.1	−0.23783	1969	0	0	100	0
60318	53473.16554	43.3236	−44.7518	3.7	60.6	178.48	60.6	4.1	−0.39431	37.7	160.6	160.6	37.9	−0.10611	3671	0	0	100	0
60318	53687.49497	40.5353	−37.8723	4.4	47.0	29.60	40.9	23.5	0.97657	38.8	152.8	134.2	82.6	0.84533	3729	0	0	100	0
75470	54175.21628	264.5539	58.6260	9.8	83.5	159.86	78.4	30.2	−0.93862	36.3	177.2	166.8	69.9	−0.83362	1150	1	1	50	0
76943	54083.45907	−243.2769	491.0586	7.3	155.3	156.07	141.9	63.3	−0.99203	35.8	245.7	225.0	104.9	−0.92815	2841	1	1	50	0
76943	54084.47707	−243.4674	490.7196	9.4	111.8	161.34	105.9	36.8	−0.96344	36.2	201.8	191.5	73.1	−0.85288	1561	1	1	100	0
76943	54090.44605	−245.6274	488.8202	21.1	371.2	158.36	345.2	138.3	−0.98646	40.9	502.5	467.3	189.1	−0.97264	601	1	1	100	0
76943	54103.38879	−249.1727	484.6900	11.6	137.6	152.86	122.6	63.6	−0.97871	36.9	227.2	202.8	108.7	−0.92503	1087	1	1	100	0
76943	54138.28852	−259.1432	473.1842	29.0	462.9	152.45	410.6	215.7	−0.98842	45.5	617.8	548.2	288.6	−0.98412	530	1	1	50	0
76943	54174.18725	−268.1380	460.6022	11.1	299.7	152.26	265.3	139.8	−0.99598	36.7	414.0	366.8	195.4	−0.97726	2363	1	1	50	0
76943	54179.20791	−270.1570	459.0538	26.1	318.2	159.43	298.1	114.4	−0.97001	43.7	436.7	409.2	158.8	−0.95597	931	1	1	50	0
76943	54194.15600	−273.3613	453.6365	14.0	264.6	156.59	242.9	105.9	−0.98962	37.7	371.4	341.1	151.6	−0.96264	2072	1	1	50	0
76943	54420.54028	−329.5905	369.6534	14.2	437.5	158.11	406.0	163.6	−0.99561	64.3	585.7	544.0	226.4	−0.95207	1630	0	1	50	0
76943	54433.49036	−332.4642	364.4549	23.9	339.7	155.17	308.5	144.3	−0.98328	42.4	463.3	420.8	198.3	−0.97193	1902	1	1	50	0
76943	54483.34004	−344.5220	345.1646	19.1	806.1	151.75	710.2	381.9	−0.99838	39.9	1057.2	931.5	501.6	−0.99592	1912	1	1	50	0
76943	54526.29870	−353.8186	327.4686	33.6	1083.4	167.11	1056.1	243.9	−0.98994	48.5	1415.4	1379.7	319.3	−0.98777	674	1	1	50	0
76943	54529.34042	−354.0925	326.1132	22.5	147.0	178.82	147.0	22.7	−0.12997	41.6	236.9	236.8	41.9	−0.11288	957	1	1	50	0

Table 4
(Continued)

HD Number	HJD 2400000.5	δR.A. (mas)	δDecl. (mas)	σ_{min} (μas)	σ_{maj} (μas)	ϕ_e (deg)	$\sigma_{R.A.}$ (μas)	$\sigma_{Decl.}$ (μas)	$\frac{\sigma^2_{R.A.,decl.}}{\sigma_{R.A.}\sigma_{decl.}}$	$\sigma_{min,c}$ (μas)	$\sigma_{maj,c}$ (μas)	$\sigma_{R.A.,c}$ (μas)	$\sigma_{Decl.,c}$ (μas)	$\frac{\sigma^2_{R.A.,decl.,c}}{\sigma_{R.A.,c}\sigma_{decl.,c}}$	N	LDC	Align	Rate (Hz)	Outlier
76943	54530.24857	−353.8025	325.6138	24.9	165.4	158.46	154.2	65.0	−0.91158	43.0	256.6	239.2	102.3	−0.89287	1371	1	1	50	0
76943	54538.23460	−355.8054	322.5258	7.9	70.7	161.27	67.0	23.9	−0.93774	35.9	167.5	159.0	63.6	−0.80445	2556	1	1	50 & 100	0
76943	54544.24148	−357.0549	319.9628	12.4	92.5	164.91	89.4	26.9	−0.87857	37.1	184.6	178.5	59.9	−0.76789	1566	1	1	50	0
77327	52979.53035	−110.2675	85.2636	10.4	275.0	167.10	268.0	62.2	−0.98530	52.8	383.9	374.4	100.0	−0.84074	1079	0	0	100	0
77327	53033.37609	−114.2128	86.1745	12.4	401.5	164.98	387.8	104.8	−0.99248	58.7	540.4	522.2	151.1	−0.91561	616	0	0	100	0
77327	53034.38885	−114.5321	86.2387	4.0	36.5	167.91	35.7	8.6	−0.88040	38.2	147.8	144.8	48.5	−0.59512	3064	0	0	100	0
77327	53109.25209	−120.2164	87.6006	8.9	125.1	5.71	124.5	15.3	0.80954	48.7	214.6	213.6	52.9	0.38255	814	0	0	100	0
77327	53123.17148	−121.0349	87.8155	5.2	103.4	175.66	103.1	9.4	−0.83267	40.2	194.1	193.6	42.7	−0.32930	2139	0	0	100	0
77327	53285.53887	−132.4920	90.3807	4.8	120.0	3.60	119.7	8.9	0.84170	39.5	209.6	209.2	41.5	0.30565	2697	0	0	100	0
77327	53333.56349	−135.5142	90.8606	10.6	328.6	167.60	321.0	71.3	−0.98844	53.4	449.5	439.2	109.7	−0.86725	971	0	0	100	0
77327	53334.56941	−136.1269	90.9579	10.0	202.5	169.67	199.2	37.6	−0.96248	51.7	298.2	293.5	73.8	−0.70267	653	0	0	100	0
77327	53340.57025	−136.4403	91.0411	11.2	241.3	173.55	239.7	29.3	−0.92269	55.1	343.5	341.4	67.0	−0.56116	789	0	0	100	0
77327	53341.55502	−136.6624	91.1231	16.9	147.5	170.45	145.5	29.6	−0.81530	73.1	237.4	234.4	82.2	−0.43325	540	0	0	100	0
77327	53466.23066	−145.0282	92.6659	9.3	59.2	174.15	58.9	11.1	−0.53277	49.7	159.8	159.0	52.1	−0.28216	748	0	0	100	0
77327	53467.22246	−144.8811	92.5945	17.5	202.4	172.63	200.7	31.3	−0.82461	75.1	298.0	295.7	83.8	−0.42720	324	0	0	100	0
77327	53473.26739	−145.8576	92.6361	24.9	329.1	9.15	325.0	57.8	0.89955	100.9	450.2	444.7	122.7	0.55393	197	0	0	100	0
77327	53687.51884	−158.9633	94.9883	6.6	47.7	21.60	44.4	18.6	0.92521	43.1	153.1	143.2	69.1	0.74620	2283	0	0	100	0
77327	53698.44537	−159.9349	95.0992	15.6	99.7	10.95	97.9	24.4	0.75695	68.8	190.8	187.8	76.7	0.41002	916	0	0	100	0
77327	53699.46898	−159.9509	95.0570	19.4	109.3	16.29	105.1	35.9	0.82698	81.6	199.5	192.8	96.3	0.48054	750	0	0	100	0
77327	53718.56135	−161.1589	95.3146	12.2	119.7	179.01	119.7	12.4	−0.16542	58.1	209.3	209.3	58.2	−0.05736	612	0	0	100	0
77327	53726.52349	−161.4619	95.3770	11.1	183.4	175.11	182.7	19.1	−0.81294	54.8	276.5	275.5	59.5	−0.38062	455	0	0	100	0
77327	53732.49665	−161.8307	95.4057	4.5	45.1	172.21	44.7	7.5	−0.80147	39.0	151.8	150.5	43.7	−0.43914	1889	0	0	100	0
77327	53734.47257	−161.9759	95.4596	3.3	30.1	167.83	29.4	7.1	−0.88005	37.2	145.4	142.3	47.5	−0.60155	3500	0	0	100	0
77327	53746.46960	−162.8842	95.5801	8.0	94.0	174.54	93.6	12.0	−0.73969	46.4	185.8	185.0	49.4	−0.33542	731	0	0	100	0
77327	53753.43625	−162.8057	95.5909	20.8	813.3	171.92	805.2	116.1	−0.98349	86.4	1066.5	1056.0	172.6	−0.86267	1180	0	0	100	0
77327	53777.36184	−164.5512	95.8050	9.5	188.7	170.04	185.8	33.9	−0.95855	50.3	282.4	278.3	69.6	−0.67968	616	0	0	100	0
77327	53779.35888	−164.2439	95.7494	20.4	437.0	170.37	430.9	75.8	−0.96220	85.1	585.1	577.0	128.9	−0.74313	599	0	0	100	0
77327	53789.23747	−165.3090	96.0722	30.6	827.4	21.45	770.2	303.9	0.99413	121.4	1084.7	1010.5	412.4	0.94875	219	0	0	100	0
77327	53790.24516	−165.4556	95.9622	7.6	157.5	23.84	144.1	64.0	0.99165	45.4	248.0	227.6	108.5	0.89012	1399	0	0	100	0
77327	53818.32093	−167.2428	96.1559	14.4	296.3	7.09	294.1	39.3	0.92959	65.0	409.8	406.8	81.9	0.60174	302	0	0	100	0
77327	53865.18143	−170.1031	96.5281	9.6	294.3	5.53	292.9	30.0	0.94621	50.6	407.4	405.5	63.8	0.60562	457	0	1	100	0
77327	53866.15364	−170.3111	96.5471	12.5	373.2	179.72	373.2	12.6	−0.14192	59.0	505.0	504.9	59.1	−0.04122	361	0	1	100	0
77327	54070.54943	−181.8796	97.9328	8.4	124.1	167.85	121.4	27.4	−0.94951	36.0	213.6	209.0	57.1	−0.76462	895	1	1	100	0
77327	54075.56122	−182.0574	97.9003	11.6	190.4	173.89	189.3	23.3	−0.86658	36.9	284.4	282.8	47.5	−0.62588	916	1	1	50	0
77327	54083.56093	−182.6256	97.9823	15.1	249.6	178.94	249.6	15.8	−0.29046	38.1	353.4	353.3	38.7	−0.16710	877	1	1	50	0
77327	54084.53031	−183.5955	98.1133	23.7	930.5	171.99	921.5	131.8	−0.98339	42.3	1217.7	1205.9	174.8	−0.96972	247	1	1	100	0
77327	54090.54319	−183.0315	98.0199	13.3	160.1	179.08	160.1	13.5	−0.18942	37.4	250.8	250.8	37.7	−0.10458	394	1	1	100	0
77327	54138.39563	−185.2061	98.2216	18.1	405.1	174.88	403.5	40.3	−0.89333	39.4	544.9	542.8	62.5	−0.77411	600	1	1	50	0
77327	54174.33117	−187.4601	98.3954	5.8	118.7	3.34	118.5	9.0	0.76319	35.5	208.4	208.0	37.4	0.31481	2341	1	1	50	0
77327	54175.31402	−187.4958	98.4070	5.5	104.1	0.04	104.1	5.5	0.01440	35.4	194.7	194.7	35.4	0.00371	2382	1	1	50	0
77327	54196.22624	−188.4392	98.4568	7.6	167.2	173.34	166.0	20.8	−0.93001	35.8	258.5	256.8	46.5	−0.63204	2942	1	1	50	0
77327	54215.17245	−189.6068	98.5838	3.8	55.4	172.53	54.9	8.1	−0.88042	35.2	157.4	156.2	40.5	−0.48032	4950	1	1	50	0
77327	54216.18008	−189.4611	98.5665	17.4	138.1	175.19	137.6	20.8	−0.54686	39.1	227.7	226.9	43.4	−0.42709	789	1	1	50	0
77327	54229.17768	−190.3568	98.6330	14.4	298.9	4.01	298.2	25.4	0.82180	37.8	413.0	412.0	47.5	0.60250	898	1	1	50	0
77327	54231.17091	−190.2099	98.6405	8.5	170.5	3.56	170.1	13.5	0.77952	36.0	262.2	261.7	39.5	0.40471	1715	1	1	50	0

Table 4
(Continued)

HD Number	HJD 2400000.5	δR.A. (mas)	δDecl. (mas)	σ_{min} (μas)	σ_{maj} (μas)	ϕ_e (deg)	$\sigma_{R.A.}$ (μas)	$\sigma_{Decl.}$ (μas)	$\frac{\sigma^2_{R.A.,decl.}}{\sigma_{R.A.}\sigma_{decl.}}$	$\sigma_{min,c}$ (μas)	$\sigma_{maj,c}$ (μas)	$\sigma_{R.A.,c}$ (μas)	$\sigma_{Decl.,c}$ (μas)	$\frac{\sigma^2_{R.A.,decl.,c}}{\sigma_{R.A.,c}\sigma_{decl.,c}}$	N	LDC	Align	Rate (Hz)	Outlier
77327	54237.17798	−190.3349	98.7236	19.8	921.7	9.21	909.8	148.8	0.99091	40.2	1206.4	1190.8	197.1	0.97841	345	1	1	50	0
77327	54454.51102	−200.4767	99.2497	33.8	2453.1	171.18	2424.1	377.6	−0.99588	48.7	3192.1	3154.4	491.8	−0.99498	318	1	1	50	0
77327	54502.41055	−204.0323	99.4837	30.9	831.4	177.59	830.7	46.6	−0.74872	46.7	1089.8	1088.9	65.4	−0.69953	351	1	1	50	0
77327	54538.28712	−205.6761	99.5105	4.9	50.3	171.51	49.8	8.9	−0.82745	35.3	154.5	152.9	41.7	−0.51765	2140	1	1	100	0
77327	54544.28725	−205.8363	99.4961	8.2	95.6	175.75	95.4	10.8	−0.64870	35.9	187.2	186.7	38.4	−0.34757	1602	1	1	50	0
79096	54056.53627	0.2350	49.9778	27.6	312.7	157.07	288.2	124.5	−0.97070	44.6	429.9	396.3	172.5	−0.95990	345	1	1	50	0
79096	54075.43903	−15.0197	53.2484	22.3	350.3	147.35	295.2	189.9	−0.99025	41.5	476.4	401.8	259.4	−0.98184	272	1	1	50	0
81858	53467.16912	657.2324	−60.1448	25.7	433.9	155.97	396.4	178.3	−0.98749	103.7	581.2	532.5	254.9	−0.89595	421	0	0	100	0
81858	53705.49000	667.1219	−75.1289	25.6	186.3	157.18	172.0	76.0	−0.93123	103.4	279.7	260.9	144.4	−0.64102	498	0	0	100	0
81858	53746.41422	668.7535	−77.5370	20.0	194.3	157.92	180.2	75.4	−0.95801	83.7	288.8	269.5	133.4	−0.74035	542	0	0	100	0
81858	54061.55491	680.2136	−95.9792	10.1	193.6	159.13	181.0	69.6	−0.98791	36.4	288.0	269.4	108.1	−0.93286	1306	1	1	100	0
81858	54063.55814	681.5987	−96.5756	29.5	574.6	160.99	543.3	189.3	−0.98630	45.8	760.0	718.7	251.3	−0.98128	713	1	1	50	0
81858	54083.48145	681.1639	−97.3074	17.1	130.8	154.57	118.4	58.2	−0.94606	39.0	220.3	199.6	100.9	−0.90476	1257	1	1	50	0
81858	54090.48497	681.5160	−97.7666	24.3	659.0	160.67	621.9	219.3	−0.99309	42.6	868.1	819.3	290.1	−0.98782	324	1	1	100	0
81858	54138.34899	683.4584	−100.9094	31.2	537.2	158.58	500.2	198.3	−0.98562	46.9	712.3	663.3	263.8	−0.98161	426	1	1	50	0
81858	54425.54595	694.1319	−118.0261	31.2	325.1	156.94	299.3	130.5	−0.96579	123.6	445.2	412.5	208.2	−0.76767	856	0	1	50	0
81858	54426.56538	693.3936	−117.6748	27.6	635.2	161.30	601.7	205.3	−0.98989	110.6	837.5	794.1	288.2	−0.91450	672	0	1	50	0
81858	54526.25977	696.7234	−123.7262	13.7	252.0	153.11	224.8	114.6	−0.99099	37.6	356.3	318.2	164.6	−0.96676	1439	1	1	50	0
81858	54529.24852	696.8410	−123.9198	20.2	311.0	151.96	274.6	147.3	−0.98781	40.4	427.9	378.1	204.3	−0.97462	1388	1	1	50	0
90537	53474.19167	−248.2523	−281.1256	15.5	96.8	35.60	79.2	57.7	0.94492	68.5	188.2	158.2	122.9	0.74834	3391	0	0	100	1
90537	53494.18377	−243.6561	−292.1790	8.3	83.3	167.45	81.4	19.8	−0.90263	47.1	177.0	173.1	60.0	−0.59501	2396	0	0	100	0
90537	53732.54966	−280.0714	−306.5021	25.5	170.0	169.62	167.3	39.6	−0.75545	103.0	261.6	258.0	111.8	−0.35541	3390	0	0	100	2
90537	53746.45718	−278.8953	−305.0878	17.7	117.9	160.65	111.4	42.5	−0.89713	75.8	207.6	197.5	99.2	−0.59573	2069	0	0	100	2
90537	53780.35698	−269.8591	−314.5219	14.2	161.9	157.59	149.8	63.1	−0.96977	64.3	252.8	235.0	113.2	−0.79160	2692	0	0	100	0
90537	53789.33201	−271.4384	−315.2977	18.5	346.2	27.99	305.9	163.3	0.99177	78.5	471.3	417.8	231.8	0.92411	3785	0	0	100	0
90537	53790.34191	−271.6737	−315.4991	10.6	233.9	31.61	199.3	122.9	0.99484	53.4	334.8	286.5	181.2	0.93895	4970	0	0	100	0
90537	54201.28297	−302.9398	−340.5600	26.4	515.6	175.95	514.3	44.9	−0.80805	43.8	684.7	683.0	65.2	−0.73868	871	1	1	100	0
90537	54217.26207	−304.0353	−341.4965	14.8	319.5	1.04	319.4	15.9	0.36270	38.0	438.3	438.2	38.8	0.20340	1688	1	1	100	0
114378	53034.46586	75.1692	344.7686	12.7	304.2	149.79	263.0	153.5	−0.99543	59.6	419.5	363.8	217.3	−0.94862	1098	0	0	100	0
114378	53109.37898	78.8911	361.2198	13.9	291.6	173.75	289.8	34.6	−0.91458	63.4	404.1	401.8	76.8	−0.55845	360	0	0	100	0
114378	53123.26130	79.5777	364.3108	16.6	424.6	156.62	389.8	169.2	−0.99428	72.1	569.5	523.5	235.5	−0.94284	340	0	0	100	0
114378	53131.27830	81.3717	366.6307	28.3	1269.6	35.71	1031.0	741.3	0.99890	113.1	1656.4	1346.6	971.2	0.98969	456	0	0	100	0
114378	53145.18418	80.9790	368.8005	13.1	378.8	153.39	338.8	170.1	−0.99627	60.9	512.0	458.5	235.7	−0.95755	401	0	0	100	0
114378	53466.31699	94.9611	435.0800	7.1	208.4	155.35	189.4	87.1	−0.99598	44.2	305.0	277.8	133.4	−0.93150	927	0	0	100	0
114378	53467.28332	94.6993	435.3575	25.9	370.5	150.67	323.3	182.9	−0.98673	104.5	501.6	440.3	262.0	−0.89092	108	0	0	100	0
114378	53473.31290	95.8321	436.1674	17.2	609.2	158.06	565.1	228.1	−0.99669	74.1	804.2	746.5	308.3	−0.96585	289	0	0	100	0
114378	53494.26544	96.5771	440.3152	8.4	154.3	160.79	145.7	51.4	−0.98487	47.4	244.6	231.5	92.1	−0.83939	688	0	0	100	0
114378	53753.46614	107.0280	488.4115	23.3	2917.1	145.75	2411.3	1641.9	−0.99985	95.2	3794.8	3137.2	2137.2	−0.99855	390	0	0	100	0
114378	53777.43726	107.3061	492.9796	6.8	199.4	150.50	173.6	98.3	−0.99682	43.5	294.6	257.3	149.9	−0.94320	946	0	0	100	0
114378	53779.45201	107.7889	493.0071	20.0	214.4	154.51	193.7	94.0	−0.97185	83.7	311.9	283.8	154.0	−0.80226	160	0	0	100	0
114378	53790.38787	107.7252	495.0434	27.9	535.5	18.70	507.3	173.7	0.98557	111.6	710.1	673.6	251.0	0.88326	276	0	0	100	0
114378	53832.30416	109.5871	502.1805	29.6	643.7	153.23	574.8	291.2	−0.99349	117.8	848.4	759.4	396.4	−0.94325	129	0	0	100	0
114378	53874.20324	111.2474	509.1821	10.3	144.1	155.99	131.7	59.4	−0.98187	52.5	233.9	214.7	106.6	−0.84376	884	0	1	100	0
114378	53895.19690	111.8346	512.6873	20.5	333.0	167.66	325.3	74.0	−0.95880	85.4	455.0	444.8	128.1	−0.73157	317	0	1	100	0
114378	54196.35212	121.5222	558.2313	18.8	87.9	165.19	85.1	28.9	−0.74147	39.7	180.7	175.0	60.1	−0.73052	478	1	1	50	0

Table 4
(Continued)

HD Number	HJD 2400000.5	δR.A. (mas)	δDecl. (mas)	σ_{min} (μas)	σ_{maj} (μas)	ϕ_e (deg)	$\sigma_{R.A.}$ (μas)	$\sigma_{Decl.}$ (μas)	$\frac{\sigma^2_{R.A.,decl.}}{\sigma_{R.A.}\sigma_{decl.}}$	$\sigma_{min,c}$ (μas)	$\sigma_{maj,c}$ (μas)	$\sigma_{R.A.,c}$ (μas)	$\sigma_{Decl.,c}$ (μas)	$\frac{\sigma^2_{R.A.,decl.,c}}{\sigma_{R.A.,c}\sigma_{decl.,c}}$	N	LDC	Align	Rate (Hz)	Outlier
114378	54230.18384	121.4432	563.5820	15.0	934.8	148.46	796.7	489.1	−0.99935	38.1	1223.3	1042.8	640.7	−0.99757	877	1	1	50	0
114378	54236.23439	123.8259	563.4369	4.5	26.9	159.38	25.2	10.4	−0.88735	35.3	144.3	135.6	60.6	−0.78502	2979	1	1	50	2
114378	54245.19316	122.9457	564.8337	16.1	146.5	156.84	134.9	59.5	−0.95582	38.5	236.4	217.8	99.5	−0.90744	621	1	1	50	0
114378	54273.21611	124.4797	568.6072	25.0	1968.5	0.64	1968.4	33.3	0.65775	43.0	2562.9	2562.7	51.7	0.55393	226	1	1	50	0
114378	54503.48823	128.3515	595.4148	25.8	477.3	157.82	442.1	181.7	−0.98815	43.5	636.1	589.2	243.5	−0.98124	592	1	1	50	0
114378	54524.42212	130.3603	596.9057	11.6	391.2	155.95	357.3	159.8	−0.99685	36.9	527.5	481.9	217.6	−0.98265	947	1	1	50	0
114378	54525.39148	129.7856	597.3709	12.2	150.4	151.14	131.9	73.4	−0.98190	37.1	240.5	211.4	120.5	−0.93679	966	1	1	50	0
129132	54175.38093	47.8813	26.7291	30.6	1082.3	146.96	907.4	590.7	−0.99808	46.5	1413.9	1185.6	771.9	−0.99742	994	1	1	50	0
129246	53467.34466	−608.9232	322.0589	23.3	273.1	149.40	235.4	140.5	−0.98135	95.2	381.6	332.0	210.8	−0.85478	377	0	0	100	2
129246	53495.31448	−594.5117	312.5408	29.4	2687.1	157.23	2477.7	1040.3	−0.99953	117.1	3496.0	3223.9	1357.4	−0.99562	216	0	0	100	0
129246	53746.57095	−583.5150	302.9204	18.1	654.1	148.56	558.2	341.5	−0.99807	77.2	861.8	736.4	454.3	−0.98004	427	0	0	100	0
129246	53775.51962	−581.6762	301.1655	18.1	130.6	154.18	117.9	59.2	−0.94088	77.2	220.1	200.9	118.4	−0.70010	270	0	0	100	0
129246	53779.46998	−582.0267	301.4209	11.5	273.7	147.06	229.8	149.1	−0.99574	56.0	382.4	322.3	213.2	−0.95022	387	0	0	100	0
129246	53790.42751	−579.2605	301.0463	26.9	543.9	13.05	529.9	125.6	0.97549	108.0	720.8	702.6	193.8	0.82034	203	0	0	100	0
129246	53865.22737	−576.7113	296.8973	22.2	1648.0	145.48	1357.9	934.0	−0.99958	91.3	2147.0	1769.7	1219.0	−0.99586	166	0	1	100	0
129246	53874.23660	−577.5548	297.2315	23.2	266.4	150.60	232.4	132.3	−0.97967	94.9	373.5	328.8	201.1	−0.84432	91	0	1	100	0
129246	53915.20514	−575.6900	295.4207	6.5	265.9	166.73	258.8	61.3	−0.99410	42.8	372.9	363.1	95.2	−0.88685	1471	0	1	100	0
129246	53929.19040	−575.5811	295.0325	25.7	860.8	172.99	854.4	108.2	−0.97083	43.4	1127.8	1119.3	144.2	−0.95288	233	1	1	50	0
129246	53930.19601	−573.8361	294.7560	20.3	1199.8	174.81	1194.9	110.3	−0.98285	84.7	1566.0	1559.6	164.9	−0.85666	466	0	1	50	0
129246	54196.38310	−562.3833	283.7157	8.8	56.8	157.83	52.7	22.9	−0.91043	36.1	158.3	147.2	68.4	−0.82375	1843	1	1	50	0
129246	54229.25332	−560.6448	282.2014	10.9	84.8	147.87	72.1	46.1	−0.96040	36.7	178.2	152.2	99.7	−0.90259	1458	1	1	50	0
129246	54231.24985	−560.5548	282.1606	9.7	64.4	149.61	55.8	33.6	−0.94290	36.3	163.1	141.9	88.3	−0.88107	2125	1	1	50	0
129246	54236.30029	−559.8066	281.7239	4.8	78.4	160.75	74.0	26.2	−0.98100	35.3	173.2	163.9	66.1	−0.82543	3432	1	1	50	0
129246	54252.31015	−559.7136	281.2778	16.7	311.7	172.97	309.3	41.6	−0.91488	38.8	428.7	425.5	65.1	−0.79968	831	1	1	50	0
129246	54544.40795	−545.2344	268.7590	6.7	49.4	151.70	43.6	24.1	−0.94938	35.6	154.0	136.7	79.5	−0.86293	3033	1	1	50	0
137107	53109.32634	531.1642	−89.1492	15.3	876.0	145.87	725.2	491.6	−0.99929	67.9	1147.4	950.5	646.2	−0.99193	624	0	0	100	0
137107	53110.37376	531.1031	−89.5071	10.2	280.7	154.52	253.4	121.1	−0.99565	52.2	390.8	353.5	174.6	−0.94376	1113	0	0	100	0
137107	53123.30637	529.9131	−93.3526	7.3	214.7	148.93	183.9	111.0	−0.99701	44.7	312.3	268.4	165.6	−0.94954	2085	0	0	100	0
137107	53145.28003	526.5734	−99.0990	16.4	319.8	155.46	291.0	133.6	−0.99090	71.5	438.7	400.2	193.5	−0.91430	615	0	0	100	0
137107	53168.30554	523.4366	−105.1787	10.1	403.7	173.33	400.9	48.0	−0.97727	51.9	543.2	539.5	81.5	−0.76699	866	0	0	100	0
137107	53172.29417	522.8037	−106.1552	5.2	90.8	174.05	90.3	10.7	−0.87251	40.2	183.1	182.2	44.3	−0.40817	1305	0	0	100	0
137107	53181.19635	521.2515	−108.5494	5.8	179.4	158.19	166.6	66.9	−0.99567	41.4	272.0	253.0	108.1	−0.91149	1570	0	0	100	0
137107	53182.18871	521.3702	−108.9539	8.1	208.5	156.63	191.4	83.0	−0.99432	46.6	305.1	280.7	128.4	−0.91880	1302	0	0	100	0
137107	53199.23352	519.9659	−113.5036	12.4	507.7	176.77	506.9	31.2	−0.91759	58.7	674.7	673.6	69.9	−0.54009	724	0	0	100	0
137107	53466.40129	480.0686	−185.3656	4.9	26.6	155.85	24.4	11.8	−0.89233	39.6	144.2	132.6	69.2	−0.78216	2764	0	0	100	0
137107	53473.42045	478.5369	−187.0777	13.8	131.0	163.22	125.5	40.1	−0.93290	63.0	220.5	211.9	87.7	−0.66377	542	0	0	100	0
137107	53481.36211	476.7500	−189.9505	20.4	766.1	25.41	692.0	329.3	0.99765	85.1	1005.7	909.2	438.3	0.97669	277	0	0	100	2
137107	53508.34722	473.2721	−196.3472	17.7	549.5	167.15	535.8	123.4	−0.98908	75.8	727.9	709.9	178.0	−0.89953	310	0	0	100	0
137107	53552.22505	466.1191	−207.9214	4.6	80.4	166.75	78.2	19.0	−0.96812	39.1	174.7	170.3	55.3	−0.68736	2573	0	0	100	0
137107	53586.18646	459.4907	−216.7858	22.6	607.1	0.14	607.1	22.7	0.06354	92.7	801.6	801.5	92.8	0.02083	224	0	0	100	0
137107	53777.55293	428.7597	−266.5016	11.1	227.5	155.96	207.8	93.2	−0.99144	54.8	327.2	299.7	142.4	−0.90737	603	0	0	100	0
137107	53789.50370	426.9384	−269.7364	12.3	85.2	26.36	76.6	39.4	0.93727	58.4	178.5	162.0	95.0	0.73568	505	0	0	100	0
137107	53838.38366	418.4371	−282.1850	9.7	121.5	154.68	109.9	52.7	−0.97913	50.8	211.1	192.0	101.3	−0.83411	960	0	0	100	0
137107	53858.35734	414.3501	−287.0404	26.1	366.1	160.61	345.4	124.0	−0.97483	105.2	496.1	469.3	192.3	−0.81583	116	0	1	100	0
137107	53873.30193	412.1842	−290.9649	24.6	310.9	158.28	288.9	117.3	−0.97418	99.8	427.7	399.1	183.5	−0.81235	178	0	1	100	0

Table 4
(Continued)

HD Number	HJD 2400000.5	δR.A. (mas)	δDecl. (mas)	$\sigma_{\rm min}$ (μas)	$\sigma_{\rm maj}$ (μas)	$\phi_{\rm e}$ (deg)	$\sigma_{\rm R.A.}$ (μas)	$\sigma_{\rm Decl.}$ (μas)	$\frac{\sigma^2_{\rm R.A.,decl.}}{\sigma_{\rm R.A.}\sigma_{\rm decl.}}$	$\sigma_{\rm min,c}$ (μas)	$\sigma_{\rm maj,c}$ (μas)	$\sigma_{\rm R.A.,c}$ (μas)	$\sigma_{\rm Decl.,c}$ (μas)	$\frac{\sigma^2_{\rm R.A.,decl.,c}}{\sigma_{\rm R.A.,c}\sigma_{\rm decl.,c}}$	N	LDC	Align	Rate (Hz)	Outlier
137107	53894.25519	408.3143	−296.1528	7.2	74.8	160.73	70.6	25.6	−0.95457	44.4	170.5	161.6	70.2	−0.74420	1134	0	1	100	0
137107	53895.28364	409.1704	−296.7199	23.4	419.8	166.29	407.9	102.1	−0.97171	95.6	563.4	547.8	162.6	−0.79676	169	0	1	100	0
137107	53915.24189	404.9289	−301.6093	7.9	93.3	168.46	91.4	20.2	−0.91757	46.1	185.2	181.7	58.4	−0.59411	807	0	1	100	0
137107	53921.21028	402.7064	−302.8913	9.6	623.6	166.23	605.7	148.8	−0.99777	50.6	822.7	799.1	201.9	−0.96620	1083	0	1	50	0
137107	53922.19931	403.0928	−303.1740	9.1	258.3	164.14	248.5	71.1	−0.99106	49.2	363.8	350.2	110.1	−0.88575	1350	0	1	50	0
137107	53929.21811	403.7722	−305.4077	14.4	619.4	173.02	614.8	76.6	−0.98190	37.8	817.3	811.3	106.2	−0.93331	335	1	1	50	0
137107	53930.21680	402.1173	−305.3839	11.9	400.4	173.32	397.6	48.1	−0.96867	57.2	539.0	535.4	84.6	−0.73276	839	0	1	50	0
137107	54173.43915	356.7275	−365.0582	12.5	101.1	151.00	88.6	50.2	−0.95881	37.2	192.0	168.9	98.6	−0.90356	1180	1	1	50	0
137107	54175.43150	356.4653	−365.5890	5.3	147.4	149.89	127.5	74.1	−0.99663	35.4	237.3	206.1	122.9	−0.94340	2730	1	1	50	0
137107	54194.37929	352.9816	−370.1861	21.2	141.3	153.57	126.9	65.7	−0.93305	40.9	231.0	207.6	109.1	−0.90886	583	1	1	50	0
137107	54216.31478	348.8051	−375.4462	35.3	349.1	150.26	303.6	175.9	−0.97306	49.7	474.9	413.1	239.5	−0.97112	413	1	1	50	0
137107	54222.37677	347.3641	−376.7105	23.4	208.4	164.45	200.9	60.2	−0.91539	42.1	305.0	294.0	91.3	−0.87808	139	1	1	100	0
137107	54229.26040	346.2828	−378.5544	9.6	240.5	145.70	198.7	135.7	−0.99632	36.3	342.6	283.7	195.4	−0.97452	1489	1	1	50	0
137107	54230.28549	346.1827	−378.8516	9.8	101.8	152.18	90.2	48.3	−0.97366	36.3	192.6	171.2	95.5	−0.90364	1720	1	1	50	0
137107	54231.27738	345.7634	−378.9567	8.7	121.5	151.31	106.7	58.8	−0.98565	36.1	211.1	186.0	106.2	−0.92266	1801	1	1	50	0
137107	54236.27062	344.7011	−380.0427	4.9	37.2	151.41	32.7	18.3	−0.95174	35.3	148.1	131.2	77.4	−0.85669	2692	1	1	50	0
137107	54238.28216	343.8738	−380.3467	19.8	177.1	153.66	158.9	80.5	−0.96178	40.2	269.5	242.1	124.9	−0.93358	293	1	1	50	0
137107	54245.21340	342.7419	−381.9826	17.5	127.8	146.82	107.4	71.5	−0.95684	39.1	217.3	183.1	123.3	−0.92642	600	1	1	50	0
137107	54250.23538	341.8321	−383.2984	19.6	114.8	157.74	106.5	47.1	−0.89401	40.1	204.6	190.0	85.9	−0.86446	524	1	1	50	0
137107	54266.21481	338.7509	−387.0380	23.8	111.2	158.79	104.0	45.9	−0.83318	42.3	201.2	188.2	82.8	−0.83751	402	1	1	50	0
137107	54272.23057	337.7686	−388.5211	12.2	153.8	162.01	146.4	48.9	−0.96490	37.1	244.1	232.4	83.2	−0.88388	849	1	1	50	0
137107	54273.26744	337.4026	−388.7903	12.7	344.5	170.30	339.6	59.4	−0.97616	37.2	469.2	462.6	87.2	−0.90124	599	1	1	50	0
137107	54279.21881	336.2489	−390.1061	15.1	137.7	162.78	131.6	43.2	−0.93069	38.1	227.3	217.4	76.5	−0.85357	561	1	1	50	0
137107	54280.20686	335.9651	−390.3342	14.8	158.9	161.97	151.2	51.2	−0.95270	38.0	249.5	237.6	85.3	−0.88369	611	1	1	50	0
137107	54524.47585	286.5216	−445.8906	20.4	216.4	151.08	189.7	106.1	−0.97560	40.5	314.2	275.7	156.0	−0.95523	269	1	1	50	0
137107	54529.45024	285.2266	−446.7797	23.7	221.8	149.55	191.6	114.2	−0.97065	42.3	320.5	277.1	166.5	−0.95591	304	1	1	50	0
137107	54544.45168	282.3985	−450.1820	23.9	241.4	155.39	219.7	102.9	−0.96690	42.4	343.6	312.9	148.2	−0.94941	236	1	1	50	0
137107	54627.23049	264.4019	−467.7278	7.4	83.8	155.20	76.2	35.8	−0.97369	35.8	177.4	161.7	81.2	−0.87545	1696	1	1	50	0
137107	54629.29341	264.1297	−468.1424	18.5	127.7	172.48	126.6	24.8	−0.66005	39.6	217.2	215.4	48.5	−0.56685	228	1	1	50	0
137107	54643.20045	262.0685	−471.4366	34.5	766.1	159.00	715.3	276.5	−0.99102	49.1	1005.7	939.1	363.3	−0.98945	62	1	1	50	0
137107	54653.20544	258.8288	−473.2275	16.8	153.1	166.25	148.8	39.9	−0.90105	38.8	243.3	236.5	69.0	−0.81573	207	1	1	50	0
137391	53131.33397	−111.6255	23.7186	26.4	1609.9	28.08	1420.5	758.1	0.99922	106.3	2097.5	1851.3	991.8	0.99261	322	0	0	100	2
137391	53173.23068	−105.2831	14.4002	5.1	111.4	31.21	95.3	57.9	0.99463	40.0	201.4	173.5	109.8	0.90622	2278	0	0	100	0
137391	53207.19820	−101.9431	4.8693	13.9	967.8	42.15	717.6	649.5	0.99958	63.4	1265.9	939.5	850.8	0.99495	993	0	0	100	0
137391	53467.39933	−38.8819	−60.0783	9.8	58.2	155.86	53.3	25.4	−0.90755	51.1	159.1	146.7	80.1	−0.72158	1002	0	0	100	0
137391	53473.42909	−36.6327	−61.1809	9.1	72.0	165.12	69.6	20.5	−0.88881	49.2	168.4	163.2	64.3	−0.61355	862	0	0	100	0
137391	53481.31896	−33.8170	−62.4318	4.4	50.4	15.51	48.6	14.1	0.94585	38.8	154.6	149.3	55.7	0.69334	3500	0	0	100	0
137391	53494.36541	−29.3083	−64.5999	3.9	34.7	161.25	32.9	11.7	−0.93582	38.0	147.1	139.8	59.4	−0.73972	3325	0	0	100	0
137391	53495.29445	−28.4886	−65.0610	18.6	923.3	149.21	793.3	472.8	−0.99895	78.9	1208.4	1038.9	622.3	−0.98907	367	0	0	100	0
137391	53508.36719	−24.0911	−66.7096	15.0	91.1	171.27	90.1	20.2	−0.66460	66.9	183.4	181.5	71.7	−0.33585	402	0	0	100	0
137391	53790.50296	62.2247	−37.8414	15.8	75.5	22.03	70.3	31.9	0.84562	69.5	171.0	160.6	90.9	0.58114	420	0	0	100	0
137391	54173.51167	−57.7890	80.3098	7.6	43.5	162.74	41.6	14.8	−0.84403	35.8	151.0	144.6	56.4	−0.74808	2324	1	1	50	0
137391	54215.42046	−71.1760	78.9631	6.5	58.8	168.93	57.7	13.0	−0.85973	35.6	159.5	156.7	46.5	−0.62578	2493	1	1	50	0
137391	54217.39168	−71.4893	78.7647	5.4	94.4	163.41	90.5	27.4	−0.97880	35.4	186.2	178.7	63.1	−0.81105	1534	1	1	100	0
137391	54222.44236	−72.5317	78.4764	14.6	476.8	178.47	476.6	19.4	−0.65658	37.9	635.5	635.2	41.5	−0.40706	426	1	1	100	0

Table 4
(Continued)

HD Number	HJD 2400000.5	δR.A. (mas)	δDecl. (mas)	σ_{min} (μas)	σ_{maj} (μas)	ϕ_e (deg)	$\sigma_{R.A.}$ (μas)	$\sigma_{Decl.}$ (μas)	$\frac{\sigma^2_{R.A.,decl.}}{\sigma_{R.A.}\sigma_{decl.}}$	$\sigma_{min,c}$ (μas)	$\sigma_{maj,c}$ (μas)	$\sigma_{R.A.,c}$ (μas)	$\sigma_{Decl.,c}$ (μas)	$\frac{\sigma^2_{R.A.,decl.,c}}{\sigma_{R.A.,c}\sigma_{decl.,c}}$	N	LDC	Align	Rate (Hz)	Outlier
137391	54237.34357	−77.2901	77.3107	11.9	144.1	164.32	138.8	40.6	−0.95244	37.0	233.9	225.4	72.5	−0.84874	859	1	1	50	0
137391	54250.33246	−80.8381	76.1257	5.1	22.2	169.86	21.8	6.3	−0.58246	35.4	142.9	140.8	43.0	−0.54939	2892	1	1	50	0
137391	54265.29221	−84.3822	74.4217	10.0	166.7	170.40	164.3	29.5	−0.93922	36.4	258.0	254.5	56.0	−0.75241	2104	1	1	50	0
137391	54273.26986	−86.4135	73.5150	2.6	21.0	168.88	20.6	4.8	−0.82956	35.1	142.6	140.1	44.1	−0.58566	7969	1	1	50	0
137391	54280.24357	−87.9096	72.5765	4.6	41.1	169.30	40.4	8.9	−0.85006	35.3	149.8	147.4	44.5	−0.59038	4123	1	1	50	0
137391	54285.27988	−89.3442	71.9258	4.6	131.5	0.79	131.5	5.0	0.36354	35.3	221.0	220.9	35.4	0.08380	2676	1	1	50	0
137391	54300.23692	−92.1669	69.7310	4.5	111.7	0.54	111.7	4.6	0.22779	35.3	201.7	201.7	35.3	0.05215	2910	1	1	50	0
137391	54628.22039	−93.8692	−9.7530	9.2	230.9	155.39	210.0	96.5	−0.99448	36.2	331.2	301.5	141.8	−0.95990	3013	1	1	50	0
137391	54630.20547	−93.1860	−10.5046	4.7	111.4	153.12	99.4	50.5	−0.99446	35.3	201.4	180.4	96.4	−0.91242	4586	1	1	50	0
137909	53034.51366	53.5645	−194.5843	23.8	1438.6	143.37	1154.5	858.6	−0.99940	97.0	1875.4	1506.1	1121.7	−0.99419	1396	0	0	100	0
137909	53109.41620	66.9564	−209.5610	7.1	163.8	161.51	155.4	52.4	−0.98960	44.2	254.8	242.1	91.0	−0.85960	1980	0	0	100	0
137909	53110.33506	68.4221	−210.5182	27.4	1240.9	146.99	1040.7	676.4	−0.99883	109.8	1619.2	1359.2	886.9	−0.98906	923	0	0	100	0
137909	53116.44145	68.9445	−210.9433	15.9	360.4	171.28	356.2	56.9	−0.95913	69.8	489.0	483.5	101.3	−0.71681	725	0	0	100	0
137909	53123.35186	69.0323	−211.8662	10.4	277.1	156.18	253.5	112.3	−0.99486	52.8	386.5	354.2	163.4	−0.93579	1929	0	0	100	0
137909	53131.35817	72.1608	−212.0850	25.4	1113.7	32.39	940.5	596.9	0.99873	102.7	1454.6	1229.5	784.0	0.98793	831	0	0	100	0
137909	53137.25597	71.0095	−214.0018	20.8	164.9	148.57	141.1	87.8	−0.96110	86.4	256.0	223.1	152.5	−0.75953	1456	0	0	100	0
137909	53144.25226	72.3729	−215.2859	18.8	591.4	149.75	511.0	298.4	−0.99733	79.6	781.5	676.2	399.6	−0.97318	1366	0	0	100	0
137909	53145.25716	72.6629	−215.5332	14.1	62.5	154.89	56.9	29.4	−0.85085	64.0	161.9	149.1	89.9	−0.63406	1572	0	0	100	0
137909	53168.22207	76.1372	−219.1702	11.7	101.5	154.17	91.5	45.5	−0.95813	56.6	192.4	174.9	98.1	−0.77289	1327	0	0	100	0
137909	53172.32119	76.7569	−219.7537	10.8	439.1	178.90	439.0	13.7	−0.61406	53.9	587.7	587.6	55.1	−0.20307	865	0	0	100	0
137909	53173.27098	76.2659	−220.1791	12.8	473.9	37.09	378.1	285.9	0.99842	59.9	631.8	505.3	384.0	0.98078	1082	0	0	100	0
137909	53181.26233	78.2354	−221.1312	7.6	53.8	170.61	53.0	11.5	−0.74656	45.4	156.5	154.6	51.5	−0.45325	1751	0	0	100	0
137909	53182.26133	78.4083	−221.2440	8.5	62.3	169.83	61.3	13.8	−0.78226	47.6	161.7	159.4	54.9	−0.47449	1688	0	0	100	0
137909	53187.23910	79.1434	−222.0794	18.9	161.2	170.72	159.1	32.0	−0.80182	79.9	252.0	249.1	88.7	−0.41156	665	0	0	100	0
137909	53198.21815	80.7524	−223.6743	4.2	36.5	172.04	36.1	6.6	−0.75801	38.5	147.8	146.5	43.2	−0.44099	4250	0	0	100	0
137909	53199.21988	80.8510	−223.8461	7.4	43.5	169.45	42.7	10.7	−0.71852	44.9	151.0	148.7	52.1	−0.48314	1380	0	0	100	0
137909	53208.19574	81.3807	−225.4354	4.4	98.4	40.49	74.9	64.0	0.99582	38.8	189.6	146.4	126.6	0.91791	7065	0	0	100	0
137909	53214.19010	82.8394	−225.9509	7.7	107.2	176.79	107.0	9.7	−0.61289	45.6	197.5	197.2	46.9	−0.22338	2591	0	0	100	0
137909	53228.16998	84.8381	−227.8406	8.4	243.2	0.01	243.2	8.4	0.00464	47.4	345.8	345.8	47.4	0.00125	1683	0	0	100	0
137909	53467.43736	116.5069	−254.1639	15.0	92.7	162.71	88.6	31.1	−0.86317	66.9	184.7	177.5	84.2	−0.56285	924	0	0	100	0
137909	53473.39997	117.0549	−254.6189	9.1	42.9	160.51	40.6	16.7	−0.81754	49.2	150.7	143.0	68.4	−0.65233	2205	0	0	100	0
137909	53474.37831	116.7379	−254.8786	24.4	262.9	24.46	239.5	111.1	0.97044	99.1	369.3	338.7	177.6	0.79340	567	0	0	100	0
137909	53487.43377	118.9563	−255.3060	35.3	3552.5	40.93	2684.1	2327.5	0.99980	138.6	4620.4	3491.9	3028.8	0.99816	524	0	0	100	0
137909	53494.32489	119.5240	−256.2291	4.5	37.1	153.62	33.3	17.0	−0.95559	39.0	148.1	133.8	74.5	−0.81537	3702	0	0	100	0
137909	53495.27147	117.5046	−254.8422	26.4	2313.6	145.58	1908.6	1307.9	−0.99970	106.3	3010.9	2484.5	1704.2	−0.99714	619	0	0	100	0
137909	53508.37081	120.8718	−257.3319	16.6	491.2	171.53	485.9	74.2	−0.97412	72.1	653.7	646.7	119.8	−0.79356	588	0	0	100	0
137909	53509.37190	120.5678	−257.3634	24.4	1039.8	172.70	1031.4	134.3	−0.98314	99.1	1359.0	1348.0	198.7	−0.86438	396	0	0	100	0
137909	53550.22220	126.2598	−260.2868	20.0	294.2	162.93	281.3	88.5	−0.97152	83.7	407.3	390.1	143.8	−0.79448	851	0	0	100	0
137909	53552.22051	126.0813	−260.2757	6.1	67.4	163.60	64.7	19.9	−0.94827	42.0	165.2	158.9	61.6	−0.70596	2608	0	0	100	0
137909	53571.22733	128.1939	−261.4554	5.1	92.0	178.85	92.0	5.4	−0.34165	40.0	184.1	184.1	40.2	−0.08765	3061	0	0	100	0
137909	53585.20008	129.7290	−262.1885	8.4	168.2	1.29	168.1	9.3	0.40776	47.4	259.6	259.6	47.7	0.11842	1479	0	0	100	0
137909	53747.57361	145.7598	−268.5562	24.5	642.3	145.69	530.7	362.6	−0.99664	99.5	846.6	701.6	484.2	−0.96879	2165	0	0	100	0
137909	53748.56579	145.8894	−268.3788	21.1	334.9	11.49	328.2	69.8	0.95125	87.5	457.3	448.5	125.1	0.70105	1179	0	0	100	0
137909	53755.57238	146.9995	−269.0019	19.9	443.1	148.55	378.2	231.8	−0.99492	83.3	592.8	507.6	317.4	−0.95182	876	0	0	100	0
137909	53769.54876	147.4389	−268.6635	22.2	338.7	150.13	293.9	169.7	−0.98856	91.3	462.0	403.2	243.4	−0.90281	900	0	0	100	0

Table 4
(Continued)

HD Number	HJD 2400000.5	δR.A. (mas)	δDecl. (mas)	$\sigma_{\rm min}$ (μas)	$\sigma_{\rm maj}$ (μas)	$\phi_{\rm e}$ (deg)	$\sigma_{\rm R.A.}$ (μas)	$\sigma_{\rm Decl.}$ (μas)	$\frac{\sigma^2_{\rm R.A.,decl.}}{\sigma_{\rm R.A.}\sigma_{\rm decl.}}$	$\sigma_{\rm min,c}$ (μas)	$\sigma_{\rm maj,c}$ (μas)	$\sigma_{\rm R.A.,c}$ (μas)	$\sigma_{\rm Decl.,c}$ (μas)	$\frac{\sigma^2_{\rm R.A.,decl.,c}}{\sigma_{\rm R.A.,c}\sigma_{\rm decl.,c}}$	N	LDC	Align	Rate (Hz)	Outlier
137909	53774.52483	147.7766	−268.7643	23.4	443.3	148.64	378.7	231.6	−0.99301	95.6	593.1	508.9	319.2	−0.93717	922	0	0	100	0
137909	53775.53474	148.0964	−268.9414	14.4	266.7	150.97	233.3	130.0	−0.99193	65.0	373.9	328.4	190.1	−0.92127	1067	0	0	100	0
137909	53778.54697	149.1976	−269.3447	19.2	254.8	155.16	231.3	108.4	−0.98079	80.9	359.6	328.1	168.0	−0.84924	1371	0	0	100	0
137909	53789.51750	149.3117	−269.1943	6.9	39.2	27.70	34.9	19.2	0.91372	43.7	149.0	133.5	79.3	0.78833	2654	0	0	100	0
137909	53817.37249	152.2839	−269.7881	38.2	2074.0	143.36	1664.4	1238.1	−0.99926	149.3	2699.8	2168.2	1615.7	−0.99336	437	0	0	100	0
137909	53818.39216	151.7108	−269.4217	9.7	96.7	146.36	80.7	54.2	−0.97671	50.8	188.2	159.2	112.5	−0.84538	1430	0	0	100	0
137909	53838.39716	153.2793	−269.4958	12.9	146.1	157.47	135.1	57.2	−0.96978	60.2	236.0	219.2	106.2	−0.79174	1300	0	0	100	0
137909	53865.31336	155.4860	−269.5653	14.1	62.6	158.88	58.6	26.1	−0.81719	64.0	161.9	152.8	83.5	−0.58304	664	0	1	100	0
137909	53874.31771	156.2805	−269.5344	9.1	60.6	163.98	58.3	18.9	−0.86421	49.2	160.6	155.0	64.8	−0.61739	1390	0	1	100	0
137909	53894.27169	157.4676	−269.2663	7.0	77.5	162.01	73.8	24.8	−0.95536	44.0	172.5	164.6	67.7	−0.73303	2175	0	1	100	0
137909	53895.33336	158.1374	−269.3299	14.7	199.9	176.75	199.5	18.5	−0.60708	65.9	295.2	294.7	67.9	−0.23413	670	0	1	100	0
137909	54174.51072	173.2814	−259.3431	4.7	37.1	163.07	35.5	11.7	−0.90640	35.3	148.1	142.0	54.8	−0.74045	4830	1	1	50	0
137909	54196.35398	173.8172	−257.7037	18.5	140.2	147.30	118.4	77.3	−0.95920	39.6	229.8	194.6	128.6	−0.93150	1398	1	1	50	0
137909	54201.42990	174.0685	−257.5548	13.6	81.2	161.50	77.1	28.8	−0.86791	37.5	175.3	166.7	66.1	−0.80157	1036	1	1	100	0
137909	54215.33362	174.7108	−256.5834	8.0	93.3	151.65	82.2	44.9	−0.97930	35.9	185.2	163.9	93.5	−0.90085	3722	1	1	50	0
137909	54217.33404	174.8460	−256.4839	4.7	56.6	152.93	50.5	26.1	−0.97947	35.3	158.2	141.7	78.5	−0.86506	4176	1	1	100	0
137909	54222.39790	175.0331	−256.1332	9.0	60.6	167.56	59.2	15.7	−0.81238	36.1	160.6	157.1	49.4	−0.66390	1588	1	1	100	0
137909	54229.33268	175.1202	−255.5651	6.3	52.9	156.30	48.5	22.0	−0.95045	35.6	156.0	143.5	70.6	−0.83713	2913	1	1	50	0
137909	54237.25545	175.3859	−254.9517	5.6	55.8	146.46	46.6	31.2	−0.97622	35.4	157.7	132.9	92.0	−0.88935	4092	1	1	50	0
137909	54245.26139	175.3279	−254.2065	9.5	285.4	151.94	251.9	134.5	−0.99682	36.3	396.6	350.4	189.3	−0.97620	2755	1	1	50	0
137909	54250.30278	175.8783	−254.0458	5.7	27.6	169.63	27.2	7.5	−0.63349	35.5	144.5	142.3	43.5	−0.56129	3535	1	1	50	0
137909	54265.27036	176.3798	−252.8642	7.1	64.6	164.58	62.3	18.5	−0.91772	35.7	163.3	157.7	55.4	−0.74465	3762	1	1	50	0
137909	54266.28963	176.3737	−252.6923	27.1	182.1	171.62	180.2	37.7	−0.68732	44.3	275.0	272.2	59.4	−0.65749	741	1	1	50	0
137909	54272.26863	176.4879	−252.2592	6.1	44.7	169.89	44.0	9.9	−0.78055	35.5	151.6	149.4	43.9	−0.57171	3020	1	1	50	0
137909	54287.20214	177.0428	−251.1696	7.6	91.2	162.84	87.1	27.9	−0.95818	35.8	183.5	175.6	64.0	−0.81155	3375	1	1	50	0
137909	54293.24597	176.8140	−250.5425	25.3	198.6	174.40	197.6	31.8	−0.59930	43.2	293.7	292.3	51.7	−0.54273	404	1	1	50	0
137909	54299.24298	176.9458	−250.0570	11.2	266.4	1.32	266.3	12.8	0.47686	36.7	373.5	373.4	37.7	0.22585	1083	1	1	50	0
137909	54301.23328	177.0013	−249.8160	10.2	234.1	0.11	234.1	10.2	0.04578	36.5	335.0	335.0	36.5	0.01743	1473	1	1	50	0
137909	54481.59273	179.0538	−231.1182	9.4	316.0	150.26	274.4	157.0	−0.99763	36.2	434.0	377.3	217.6	−0.98147	2048	1	1	100	0
137909	54515.53384	178.4511	−226.7391	14.3	138.6	156.86	127.6	56.0	−0.96057	37.8	228.2	210.3	96.2	−0.90451	3350	1	1	50	0
137909	54546.42115	178.6146	−223.0048	27.3	179.7	148.17	153.4	97.6	−0.94471	44.4	272.3	232.6	148.5	−0.93674	1638	1	1	50	0
137909	54627.28557	176.7394	−211.3458	4.3	26.0	164.92	25.1	7.9	−0.82781	35.3	144.0	139.4	50.6	−0.69421	5439	1	1	50	0
137909	54628.32452	176.8688	−211.1799	11.3	105.1	178.34	105.1	11.7	−0.25711	36.8	195.6	195.5	37.2	−0.14696	1529	1	1	50	0
137909	54630.29708	176.4618	−210.7976	9.3	88.1	169.86	86.7	18.0	−0.85225	36.2	180.9	178.2	47.8	−0.63908	2230	1	1	50	0
137909	54643.21607	177.3337	−209.2726	11.4	485.1	161.47	460.0	154.5	−0.99698	36.8	646.0	612.6	208.2	−0.98247	1053	1	1	50	0
137909	54652.20867	175.6355	−207.4353	9.7	236.6	165.11	228.7	61.5	−0.98660	36.3	337.9	326.7	93.7	−0.91605	2546	1	1	50	0
137909	54653.20993	175.6903	−207.3676	4.9	126.5	166.21	122.9	30.5	−0.98642	35.3	216.0	209.9	61.9	−0.80910	3666	1	1	50	0
138629	53909.23586	23.5841	47.8180	10.4	412.7	163.33	395.3	118.8	−0.99580	52.8	554.5	531.4	166.9	−0.94397	2659	0	0	50	0
140159	53110.41886	173.2006	54.5009	14.9	420.9	159.96	395.4	144.9	−0.99396	66.6	564.8	531.1	203.4	−0.93748	342	0	0	100	0
140159	53123.41078	171.7168	54.1016	14.8	297.5	165.86	288.5	74.1	−0.97862	66.2	411.3	399.2	119.3	−0.82002	401	0	0	100	0
140159	53181.26600	167.5849	51.3957	11.9	248.8	169.02	244.2	48.8	−0.96886	57.2	352.4	346.2	87.5	−0.74656	581	0	0	100	0
140159	53182.26697	167.5830	51.2650	21.9	584.5	169.77	575.2	106.1	−0.97771	90.3	772.6	760.5	163.5	−0.82777	274	0	0	100	0
140159	53199.21014	167.6260	50.2550	14.9	602.4	167.75	588.6	128.7	−0.99296	66.6	795.5	777.6	180.9	−0.92642	585	0	0	100	0
140159	53215.18210	164.4576	49.8117	11.6	242.2	171.71	239.6	36.8	−0.94788	56.3	344.6	341.1	74.6	−0.64772	784	0	0	100	0
140159	53221.18430	164.1972	48.9769	39.7	2476.7	41.94	1842.4	1655.6	0.99948	154.9	3222.8	2399.5	2157.0	0.99534	274	0	0	100	0

Table 4
(Continued)

HD Number	HJD 2400000.5	δR.A. (mas)	δDecl. (mas)	σ_{min} (μas)	σ_{maj} (μas)	ϕ_e (deg)	$\sigma_{R.A.}$ (μas)	$\sigma_{Decl.}$ (μas)	$\frac{\sigma^2_{R.A.,decl.}}{\sigma_{R.A.}\sigma_{decl.}}$	$\sigma_{min,c}$ (μas)	$\sigma_{maj,c}$ (μas)	$\sigma_{R.A.,c}$ (μas)	$\sigma_{Decl.,c}$ (μas)	$\frac{\sigma^2_{R.A.,decl.,c}}{\sigma_{R.A.,c}\sigma_{decl.,c}}$	N	LDC	Align	Rate (Hz)	Outlier
140159	53551.26199	130.1927	31.4453	7.0	171.2	171.33	169.2	26.7	−0.96431	44.0	262.9	260.0	58.8	−0.65481	1292	0	0	100	0
140159	54524.53447	−21.0858	−30.5862	12.0	111.8	157.94	103.7	43.5	−0.95456	37.0	201.8	187.5	83.2	−0.87804	1490	1	1	50	0
140159	54529.52522	−22.1019	−30.8333	12.6	119.7	159.60	112.3	43.3	−0.95109	37.2	209.3	196.6	80.9	−0.87188	1287	1	1	50	0
140159	54630.26695	−39.3695	−36.5049	9.7	97.6	160.71	92.1	33.5	−0.95231	36.3	188.9	178.7	71.2	−0.84221	1493	1	1	50	0
140159	54635.30502	−40.7530	−36.7617	11.7	299.2	173.35	297.2	36.5	−0.94679	36.9	413.4	410.6	60.3	−0.78761	1325	1	1	50	0
140159	54636.28083	−40.7402	−36.8224	25.1	218.0	167.94	213.3	51.8	−0.86812	43.1	316.1	309.2	78.3	−0.82713	411	1	1	50	0
140159	54657.19365	−40.9334	−38.9513	23.0	997.2	162.29	950.0	304.1	−0.99684	41.9	1303.9	1242.2	398.6	−0.99390	697	1	1	50	0
140159	54671.21541	−45.3294	−38.8512	21.4	708.5	176.24	707.0	51.1	−0.90812	41.0	931.6	929.6	73.5	−0.82914	316	1	1	50	0
140436	53109.45226	664.3435	−294.4134	7.7	256.9	166.88	250.2	58.8	−0.99098	45.6	362.1	352.8	93.4	−0.86539	1682	0	0	100	0
140436	53110.45365	664.9826	−294.5821	6.9	206.7	167.54	201.8	45.1	−0.98758	43.7	303.0	296.0	78.1	−0.81936	2174	0	0	100	0
140436	53145.33169	664.2835	−293.9576	12.5	267.8	161.81	254.4	84.4	−0.98778	59.0	375.2	357.0	129.9	−0.87857	1661	0	0	100	0
140436	53168.25220	663.9125	−293.5786	10.4	94.5	160.74	89.3	32.7	−0.94109	52.8	186.3	176.7	79.1	−0.71076	1847	0	0	100	0
140436	53187.22658	663.4442	−293.3415	14.3	324.4	164.08	312.0	90.0	−0.98624	64.6	444.4	427.7	136.8	−0.87125	1244	0	0	100	0
140436	53199.18576	664.6341	−293.4290	7.8	369.0	162.49	351.9	111.3	−0.99728	45.9	499.7	476.8	156.6	−0.95171	2995	0	0	100	0
140436	53229.18064	664.7532	−292.6397	20.3	658.6	0.57	658.6	21.3	0.30773	84.7	867.6	867.5	85.1	0.10040	396	0	0	100	0
140436	53466.42563	661.2097	−289.5648	7.2	37.5	160.03	35.3	14.5	−0.84895	44.4	148.2	140.2	65.6	−0.69808	3806	0	0	100	0
140436	53494.34069	660.4979	−288.9465	6.6	58.1	154.64	52.6	25.6	−0.95883	43.1	159.1	144.9	78.5	−0.79821	3819	0	0	100	0
140436	53777.49192	654.9326	−283.3120	27.2	653.9	143.52	526.0	389.4	−0.99622	109.1	861.5	695.8	519.7	−0.96560	553	0	0	100	0
140436	53818.41258	655.4666	−283.6246	13.3	378.4	148.20	321.7	199.7	−0.99692	61.5	511.5	435.9	274.5	−0.96486	1530	0	0	100	0
140436	53858.42205	654.2191	−282.6916	21.7	608.1	171.06	600.7	96.9	−0.97404	89.6	802.8	793.2	153.0	−0.80537	206	0	1	100	0
140436	53872.26085	654.0747	−282.4653	24.7	283.9	147.12	238.8	155.5	−0.98206	100.2	394.7	335.9	230.2	−0.85940	257	0	1	100	0
140436	53916.19326	653.2698	−281.6721	5.2	85.2	155.93	77.9	35.1	−0.98660	40.2	178.5	163.8	81.5	−0.84346	5781	0	1	50	0
140436	53921.23061	652.4034	−281.4666	9.0	521.8	167.32	509.1	114.9	−0.99674	48.9	692.6	675.8	159.4	−0.94919	1933	0	1	50	0
140436	53922.23305	652.5061	−281.3333	16.5	977.7	168.64	958.6	193.2	−0.99620	71.8	1278.7	1253.7	261.5	−0.95999	899	0	1	50	0
140436	53957.17243	652.0252	−280.8090	8.7	148.9	176.88	148.7	11.9	−0.67980	36.1	238.9	238.5	38.3	−0.33185	1641	1	1	50	0
140436	53965.16468	652.0843	−280.5933	12.7	395.2	0.51	395.1	13.2	0.26534	37.2	532.5	532.5	37.5	0.12567	581	1	1	100	0
140436	54173.49376	672.3551	−288.1985	31.0	200.7	153.93	180.8	92.5	−0.92809	46.8	296.1	266.8	136.7	−0.92518	2559	1	1	50	2
140436	54194.39957	658.7929	−283.7464	19.6	201.9	150.29	175.7	101.5	−0.97497	40.1	297.5	259.1	151.5	−0.95268	2011	1	1	50	2
140436	54201.38883	645.6054	−275.5323	23.7	188.2	151.87	166.4	91.2	−0.95563	42.3	281.9	249.4	138.0	−0.93818	688	1	1	100	0
140436	54215.37171	671.2683	−285.4691	23.6	148.8	159.02	139.2	57.6	−0.89913	42.2	238.8	223.5	94.1	−0.87774	3407	1	1	50	2
140436	54217.34740	658.2211	−282.5661	9.3	102.8	151.69	90.6	49.5	−0.97710	36.2	193.5	171.3	97.2	−0.90697	2724	1	1	100	2
140436	54229.30007	644.8058	−274.7562	11.1	120.0	150.01	104.0	60.7	−0.97752	36.7	209.6	182.5	109.5	−0.92282	2002	1	1	50	0
140436	54230.32399	670.5271	−285.4471	25.6	262.1	150.95	229.4	129.2	−0.97398	43.4	368.4	322.7	182.8	−0.96266	3035	1	1	50	1
140436	54231.28180	644.9348	−274.9056	10.1	188.8	147.58	159.5	101.6	−0.99307	36.4	282.6	239.3	154.6	−0.96051	2478	1	1	50	0
140436	54237.28511	645.0730	−274.8959	14.0	113.1	150.72	98.9	56.6	−0.95909	37.7	203.0	178.0	104.6	−0.91165	1358	1	1	50	0
140436	54238.36791	644.6951	−274.7607	16.6	435.9	168.12	426.6	91.2	−0.98250	38.7	583.7	571.3	126.0	−0.94938	975	1	1	50	0
140436	54245.24557	644.9259	−274.7434	21.9	256.2	147.36	216.1	139.4	−0.98256	41.3	361.3	305.0	197.9	−0.96901	1135	1	1	50	0
140436	54250.30133	644.4289	−274.4704	7.6	58.6	166.08	56.9	15.9	−0.86938	35.8	159.4	154.9	51.8	−0.70234	2683	1	1	50	0
140436	54251.30630	644.4088	−274.4683	18.6	348.3	162.59	332.4	105.7	−0.98288	39.6	473.9	452.4	146.8	−0.95914	1673	1	1	50	0
140436	54272.29098	644.0494	−273.9947	15.4	389.7	171.33	385.3	60.7	−0.96654	38.2	525.6	519.6	87.8	−0.89771	755	1	1	50	0
140436	54279.25251	643.5091	−273.8182	8.2	181.0	167.37	176.6	40.4	−0.97820	35.9	273.8	267.3	69.4	−0.84756	2773	1	1	50	0
140436	54285.24771	643.6299	−273.8924	11.0	388.3	170.31	382.7	66.2	−0.98566	36.7	523.8	516.4	95.3	−0.92060	1373	1	1	50	0
140436	54294.23032	641.4189	−273.2504	20.6	464.1	172.31	459.9	65.4	−0.94831	40.6	619.4	613.8	92.1	−0.89564	783	1	1	50	0
140436	54300.18894	671.0123	−281.5017	23.5	314.5	165.38	304.3	82.6	−0.95566	42.2	432.2	418.3	116.5	−0.92743	3934	1	1	50	2
140436	54320.17781	641.9314	−272.6939	24.3	611.5	176.50	610.4	44.5	−0.83778	98.8	807.2	805.7	110.2	−0.44047	479	0	1	50	0

Table 4
(Continued)

HD Number	HJD 2400000.5	δR.A. (mas)	δDecl. (mas)	$\sigma_{\rm min}$ (μas)	$\sigma_{\rm maj}$ (μas)	$\phi_{\rm e}$ (deg)	$\sigma_{\rm R.A.}$ (μas)	$\sigma_{\rm Decl.}$ (μas)	$\frac{\sigma^2_{\rm R.A.,decl.}}{\sigma_{\rm R.A.}\sigma_{\rm decl.}}$	$\sigma_{\rm min,c}$ (μas)	$\sigma_{\rm maj,c}$ (μas)	$\sigma_{\rm R.A.,c}$ (μas)	$\sigma_{\rm Decl.,c}$ (μas)	$\frac{\sigma^2_{\rm R.A.,decl.,c}}{\sigma_{\rm R.A.,c}\sigma_{\rm decl.,c}}$	N	LDC	Align	Rate (Hz)	Outlier
140436	54525.53453	635.6122	−267.9561	12.2	75.4	159.51	70.7	28.8	−0.89179	37.1	170.9	160.6	69.2	−0.82151	2925	1	1	50	0
140436	54544.48538	635.0145	−267.4932	8.0	40.1	161.82	38.1	14.6	−0.81809	35.9	149.4	142.4	57.8	−0.75802	2986	1	1	50	0
140436	54627.22639	632.2443	−265.5922	6.1	47.6	151.41	41.9	23.4	−0.95574	35.5	153.1	135.5	79.6	−0.86359	4896	1	1	50	0
140436	54629.25668	631.7883	−265.3466	13.2	52.6	164.94	50.9	18.7	−0.68433	37.4	155.8	150.8	54.3	−0.70169	1253	1	1	50	0
140436	54670.20834	630.7171	−264.2290	9.1	207.4	173.78	206.2	24.2	−0.92566	36.2	303.8	302.0	48.7	−0.66566	1473	1	1	50	0
140436	54671.19106	629.5806	−264.2138	11.4	171.2	170.65	168.9	30.0	−0.92305	36.8	262.9	259.5	56.1	−0.74671	1154	1	1	50	0
149630	54279.23100	33.9523	93.2975	19.0	256.5	154.72	232.1	110.9	−0.98189	39.8	361.6	327.5	158.6	−0.96077	3101	1	1	50	0
149630	54286.26316	34.9403	93.5250	13.2	206.7	166.46	201.0	50.1	−0.96225	37.4	303.0	294.7	79.7	−0.87593	4977	1	1	50	0
149630	54292.30173	34.5264	94.1038	21.1	523.5	178.78	523.4	23.8	−0.46562	40.9	694.8	694.6	43.5	−0.33925	1835	1	1	50	0
150680	53474.47129	−660.9775	−688.2772	17.5	191.7	35.49	156.4	112.2	0.98163	75.1	285.8	236.8	176.9	0.85845	3147	0	0	100	0
150680	53481.43115	−667.7688	−688.7846	27.4	246.5	26.34	221.2	112.1	0.96222	109.8	349.7	317.2	183.8	0.75204	3126	0	0	100	0
150680	53558.24741	−625.5231	−722.2271	38.2	622.1	33.23	520.8	342.4	0.99106	149.3	820.8	691.4	466.8	0.92510	2900	0	0	100	0
150680	53572.24044	−622.1670	−729.4186	20.1	282.1	38.41	221.4	176.0	0.98930	84.0	392.5	312.0	252.6	0.90823	1767	0	0	100	0
155103	53916.26197	10.0037	64.9505	8.6	51.9	157.30	48.0	21.6	−0.90207	47.9	155.4	144.6	74.5	−0.72273	2254	0	1	50	0
155103	53958.17528	3.0330	65.7742	9.0	169.5	164.61	163.5	45.8	−0.97895	36.1	261.1	251.9	77.6	−0.87563	2065	1	1	50	0
155103	53978.18708	0.0185	65.9289	25.2	550.8	179.45	550.8	25.8	−0.20511	43.1	729.6	729.6	43.7	−0.15974	318	1	1	50	0
155103	54174.52214	−30.8860	59.4502	14.0	431.2	152.71	383.2	198.1	−0.99682	37.7	577.8	513.8	267.0	−0.98732	749	1	1	50	0
155103	54215.49147	−36.5327	55.5474	29.2	427.7	167.55	417.6	96.5	−0.95076	45.6	573.4	560.0	131.4	−0.93477	366	1	1	50	0
155103	54252.37253	−41.0015	50.9033	29.8	850.3	164.26	818.4	232.5	−0.99107	46.0	1114.2	1072.5	305.5	−0.98770	544	1	1	50	0
155103	54300.28308	−44.3879	42.8265	21.4	458.5	174.08	456.0	51.8	−0.90995	41.0	612.3	609.0	75.2	−0.83612	432	1	1	50	0
155103	54315.23535	−45.0469	39.8706	11.3	228.7	172.65	226.8	31.3	−0.93204	55.4	328.6	326.0	69.2	−0.59028	1242	0	1	50	0
155103	54349.15893	−46.2630	32.3331	12.2	264.3	176.56	263.9	20.0	−0.79098	58.1	371.0	370.4	62.1	−0.34963	1076	0	1	50	0
155103	54670.26295	20.6203	−51.4981	16.5	455.7	172.80	452.1	59.4	−0.96020	38.7	608.7	603.9	85.4	−0.88965	463	1	1	50	0
157482	53109.48025	49.6406	−84.4966	7.3	282.5	158.77	263.4	102.5	−0.99707	44.7	393.0	366.7	148.3	−0.94647	2011	0	0	100	0
157482	53110.48257	48.0945	−84.1334	11.9	600.3	159.53	562.4	210.3	−0.99818	57.2	792.8	743.1	282.4	−0.97638	1334	0	0	100	0
157482	53123.45846	49.1860	−85.9318	18.1	507.8	162.47	484.3	153.9	−0.99240	77.2	674.8	643.9	216.2	−0.92737	1378	0	0	100	0
157482	53130.44282	48.4777	−86.4134	6.6	205.8	162.94	196.7	60.7	−0.99360	43.1	302.0	288.9	97.7	−0.88758	2537	0	0	100	0
157482	53137.43118	48.3928	−87.1396	14.0	280.2	164.34	269.9	76.8	−0.98202	63.7	390.2	376.1	121.9	−0.84035	1226	0	0	100	0
157482	53144.42500	47.7018	−87.6613	25.1	1039.7	167.13	1013.5	232.9	−0.99386	101.6	1358.8	1324.9	318.5	−0.94495	897	0	0	100	0
157482	53145.39616	48.3082	−87.8014	13.7	316.5	161.59	300.4	100.8	−0.98963	62.7	434.6	412.8	149.6	−0.89730	1673	0	0	100	0
157482	53168.34023	47.0275	−89.7513	15.0	340.0	162.93	325.0	100.8	−0.98777	66.9	463.6	443.7	150.4	−0.88538	1409	0	0	100	0
157482	53172.35295	47.3440	−90.1337	6.3	170.0	168.29	166.5	35.1	−0.98309	42.4	261.6	256.3	67.4	−0.76661	2560	0	0	100	0
157482	53173.33276	47.1603	−90.3599	8.0	77.4	33.97	64.4	43.8	0.97548	46.4	172.4	145.3	103.7	0.84781	2904	0	0	100	0
157482	53181.33465	46.4333	−90.7858	7.5	174.6	169.71	171.8	32.1	−0.97114	45.1	266.7	262.5	65.1	−0.71017	2795	0	0	100	0
157482	53182.33238	46.5646	−91.0137	13.9	333.2	169.62	327.7	61.6	−0.97328	63.4	455.2	447.9	103.0	−0.78052	2014	0	0	100	0
157482	53186.30522	45.6585	−91.1213	18.2	426.5	166.80	415.2	99.0	−0.98196	77.5	571.9	557.0	150.8	−0.84948	706	0	0	100	0
157482	53187.30536	46.1426	−91.2225	13.0	441.4	166.94	430.0	100.6	−0.99110	60.5	590.7	575.5	145.9	−0.90482	1578	0	0	100	0
157482	53197.26925	46.1852	−92.1523	4.8	117.1	164.87	113.0	30.9	−0.98714	39.5	206.8	199.9	66.1	−0.78621	5218	0	0	100	0
157482	53198.24332	46.2937	−92.2555	5.7	54.6	160.36	51.5	19.1	−0.94837	41.2	157.0	148.5	65.5	−0.74717	5404	0	0	100	0
157482	53199.29260	44.0251	−91.9446	24.7	1645.4	171.42	1627.0	246.7	−0.99488	100.2	2143.6	2119.7	334.8	−0.95312	946	0	0	100	0
157482	53208.25310	46.4304	−92.4901	6.6	181.7	37.67	143.9	111.1	0.99718	43.1	274.6	218.9	171.2	0.94896	6558	0	0	100	0
157482	53214.24152	45.6336	−93.3429	5.5	125.9	169.45	123.8	23.7	−0.97194	40.8	215.4	211.9	56.2	−0.67583	5251	0	0	100	0
157482	53215.23168	45.6364	−93.5172	4.8	110.7	167.53	108.1	24.3	−0.97962	39.5	200.8	196.2	58.0	−0.71784	5723	0	0	100	0
157482	53221.22283	46.2560	−92.9726	8.8	342.3	38.91	266.4	215.1	0.99860	48.4	466.5	364.3	295.4	0.97773	3998	0	0	100	0
157482	53228.21020	45.0884	−94.3310	7.2	100.6	169.45	98.9	19.7	−0.92813	44.4	191.6	188.5	56.0	−0.59198	3180	0	0	100	0

Table 4
(Continued)

HD Number	HJD 2400000.5	δR.A. (mas)	δDecl. (mas)	$\sigma_{\rm min}$ (μas)	$\sigma_{\rm maj}$ (μas)	$\phi_{\rm e}$ (deg)	$\sigma_{\rm R.A.}$ (μas)	$\sigma_{\rm Decl.}$ (μas)	$\frac{\sigma^2_{\rm R.A.,decl.}}{\sigma_{\rm R.A.}\sigma_{\rm decl.}}$	$\sigma_{\rm min,c}$ (μas)	$\sigma_{\rm maj,c}$ (μas)	$\sigma_{\rm R.A.,c}$ (μas)	$\sigma_{\rm Decl.,c}$ (μas)	$\frac{\sigma^2_{\rm R.A.,decl.,c}}{\sigma_{\rm R.A.,c}\sigma_{\rm decl.,c}}$	N	LDC	Align	Rate (Hz)	Outlier
157482	53229.22147	45.2196	−94.5160	6.4	80.0	172.84	79.4	11.8	−0.83913	42.6	174.4	173.1	47.5	−0.42967	3905	0	0	100	0
157482	53233.18369	45.0993	−94.8458	6.0	64.7	167.67	63.2	15.0	−0.91188	41.8	163.3	159.8	53.7	−0.60625	3303	0	0	100	0
157482	53234.20226	44.8269	−94.7637	7.6	37.8	172.74	37.5	8.9	−0.51350	45.4	148.4	147.3	48.8	−0.34830	3701	0	0	100	0
157482	53235.21839	45.2153	−94.9183	8.5	107.1	176.57	106.9	10.6	−0.60012	47.6	197.4	197.1	49.0	−0.22709	2094	0	0	100	0
157482	53236.16808	44.4598	−94.8862	4.7	78.1	166.59	76.0	18.7	−0.96551	39.3	172.9	168.5	55.4	−0.68554	6684	0	0	100	0
157482	53249.16080	44.2467	−95.8032	4.3	87.9	172.71	87.2	12.0	−0.93122	38.6	180.7	179.3	44.7	−0.48991	5428	0	0	100	0
157482	53466.52339	31.4133	−102.8882	9.9	204.2	163.01	195.3	60.4	−0.98523	51.4	300.1	287.4	100.5	−0.84564	3031	0	0	100	0
157482	53481.50702	30.4434	−103.3347	11.1	311.1	38.18	244.7	192.5	0.99731	54.8	428.0	338.1	268.0	0.96592	3301	0	0	100	0
157482	53494.45379	29.5257	−103.1672	18.6	251.9	163.98	242.2	71.8	−0.96315	78.9	356.1	343.0	124.1	−0.75148	1355	0	0	100	0
157482	53585.25004	23.9817	−102.6116	10.1	114.7	174.02	114.0	15.6	−0.76046	51.9	204.5	203.5	55.9	−0.35659	1479	0	0	100	0
157482	53874.42903	1.2460	−88.7776	6.8	99.5	168.07	97.4	21.6	−0.94661	43.5	190.6	186.7	58.0	−0.64317	2358	0	1	100	0
157482	53956.21473	−5.0781	−81.9131	9.2	341.7	170.23	336.8	58.7	−0.98729	36.2	465.7	459.0	86.7	−0.90591	4028	1	1	50	0
157482	54216.50608	−22.1555	−45.7120	8.7	202.1	171.22	199.7	32.0	−0.96157	36.1	297.7	294.3	57.8	−0.77515	2492	1	1	100	1
157482	54217.49399	−23.6355	−49.4281	9.6	162.5	169.30	159.7	31.6	−0.95109	36.3	253.4	249.1	59.0	−0.78034	2731	1	1	100	0
157482	54222.50033	−28.3453	−48.1186	15.6	453.9	172.74	450.3	59.4	−0.96421	38.3	606.5	601.6	85.5	−0.89225	1604	1	1	100	2
163840	54229.48700	32.9814	−47.2685	17.1	267.9	168.21	262.2	57.2	−0.95254	39.0	375.4	367.5	85.7	−0.88558	2368	1	1	50	0
163840	54336.19699	29.6432	−81.4727	17.6	163.5	168.93	160.5	35.8	−0.86590	75.5	254.5	250.2	88.7	−0.50137	2058	0	1	50	0
163840	54350.16298	28.9940	−84.8398	20.4	327.5	170.79	323.3	56.2	−0.92952	85.1	448.2	442.6	110.4	−0.62589	2030	0	1	50	0
171779	52808.35348	222.2909	−118.7665	31.3	424.5	105.79	119.4	408.6	−0.96212	124.0	569.3	195.5	548.9	−0.75329	205	0	0	100	0
171779	52834.36024	225.6783	−119.4033	20.4	1868.3	175.56	1862.7	145.9	−0.99015	85.1	2432.8	2425.5	206.5	−0.91072	366	0	0	100	0
171779	52862.30296	221.9964	−119.4218	5.7	100.4	179.91	100.4	5.7	−0.02887	41.2	191.4	191.4	41.2	−0.00697	1903	0	0	100	0
171779	52863.28434	222.1970	−119.4295	9.8	127.3	175.62	126.9	13.8	−0.69960	51.1	216.8	216.2	53.6	−0.29176	711	0	0	100	0
171779	52864.31303	222.3216	−119.3997	9.5	180.2	4.43	179.6	16.8	0.82539	50.3	272.9	272.1	54.4	0.37442	787	0	0	100	0
171779	52865.30141	221.9020	−119.4603	10.4	117.0	1.66	116.9	11.0	0.30652	52.8	206.7	206.6	53.1	0.10541	829	0	0	100	0
171779	52891.21310	221.9119	−119.7123	13.9	417.5	177.49	417.1	23.0	−0.79584	63.4	560.5	560.0	67.9	−0.35692	459	0	0	100	0
171779	52894.23156	221.9503	−119.7423	7.8	234.7	3.92	234.1	17.8	0.89999	45.9	335.7	334.9	51.2	0.43993	1190	0	0	100	0
171779	52896.20046	221.6371	−119.6784	6.0	62.7	177.22	62.6	6.7	−0.45030	41.8	162.0	161.8	42.5	−0.17275	1701	0	0	100	0
171779	52897.22741	222.9335	−119.6507	11.7	348.7	5.15	347.3	33.4	0.93643	56.6	474.4	472.5	70.6	0.59429	594	0	0	100	0
171779	52917.13191	221.1082	−119.9472	4.9	147.1	175.12	146.6	13.4	−0.93027	39.6	237.0	236.2	44.3	−0.44184	1804	0	0	100	0
171779	52918.16098	221.2135	−119.9961	15.7	937.9	2.98	936.6	51.2	0.95168	69.2	1227.3	1225.6	94.0	0.67636	326	0	0	100	0
171779	52920.14902	221.2713	−120.0294	12.3	408.3	1.61	408.2	16.8	0.68297	58.4	548.9	548.7	60.4	0.25258	590	0	0	100	0
171779	52929.11933	221.3020	−120.0970	4.5	137.1	0.23	137.1	4.6	0.12035	39.0	226.6	226.6	39.0	0.02266	1960	0	0	100	0
171779	52930.10995	221.1524	−120.0815	7.2	185.5	178.74	185.5	8.3	−0.49262	44.4	278.8	278.8	44.8	−0.13329	1551	0	0	100	0
171779	53131.44662	219.4510	−122.5100	19.0	403.5	25.15	365.3	172.4	0.99258	80.2	542.9	492.6	241.9	0.93079	407	0	0	100	0
171779	53168.47198	219.4481	−122.6406	4.1	70.4	1.94	70.3	4.7	0.50092	38.3	167.3	167.2	38.7	0.13861	2344	0	0	100	0
171779	53173.33134	219.3735	−122.8492	4.8	116.6	24.98	105.8	49.5	0.99416	39.5	206.3	187.8	94.2	0.88771	1980	0	0	100	0
171779	53199.36474	219.6117	−123.0555	9.7	328.0	176.46	327.4	22.5	−0.90134	50.8	448.8	447.9	57.8	−0.47321	825	0	0	100	0
171779	53207.24884	219.5253	−123.0926	13.3	462.9	27.06	412.3	210.9	0.99749	61.5	617.8	550.9	286.4	0.97058	1254	0	0	100	0
171779	53214.34597	219.1263	−123.1707	3.1	77.3	1.40	77.2	3.7	0.51293	36.9	172.3	172.3	37.2	0.10811	3675	0	0	100	0
171779	53236.26985	218.8993	−123.4054	2.5	81.0	177.98	80.9	3.8	−0.75752	36.3	175.2	175.1	36.8	−0.16075	4097	0	0	100	0
171779	53251.23408	218.7086	−123.5691	5.0	118.4	179.22	118.4	5.2	−0.30556	39.8	208.1	208.0	39.9	−0.06835	2272	0	0	100	0
171779	53585.32238	216.3509	−126.8928	11.2	333.2	179.80	333.2	11.3	−0.10360	55.1	455.2	455.2	55.1	−0.02840	350	0	0	100	0
171779	53620.20055	213.6541	−127.0893	24.2	1559.2	173.71	1549.8	172.6	−0.98999	98.4	2031.8	2019.6	243.1	−0.91337	322	0	0	100	0
171779	53636.19192	216.2497	−127.4120	11.1	370.6	2.65	370.2	20.4	0.83741	54.8	501.7	501.2	59.5	0.38544	697	0	0	100	0
171779	53894.49167	213.7129	−129.9290	10.9	291.4	3.74	290.8	21.9	0.86728	54.2	403.9	403.0	60.2	0.42981	613	0	1	100	0

Table 4
(Continued)

HD Number	HJD 2400000.5	δR.A. (mas)	δDecl. (mas)	σ_{min} (μas)	σ_{maj} (μas)	ϕ_e (deg)	$\sigma_{R.A.}$ (μas)	$\sigma_{Decl.}$ (μas)	$\frac{\sigma^2_{R.A.,decl.}}{\sigma_{R.A.}\sigma_{decl.}}$	$\sigma_{min,c}$ (μas)	$\sigma_{maj,c}$ (μas)	$\sigma_{R.A.,c}$ (μas)	$\sigma_{Decl.,c}$ (μas)	$\frac{\sigma^2_{R.A.,decl.,c}}{\sigma_{R.A.,c}\sigma_{decl.,c}}$	N	LDC	Align	Rate (Hz)	Outlier
171779	53929.37774	213.3161	−130.3377	5.3	132.4	178.98	132.4	5.8	−0.40983	35.4	221.9	221.8	35.6	−0.10808	2461	1	1	50	0
171779	53930.37774	213.1329	−130.3739	3.2	71.6	0.08	71.6	3.2	0.03067	37.1	168.1	168.1	37.1	0.00603	5332	0	1	50	0
171779	53936.35814	213.1750	−130.4222	4.5	110.2	178.59	110.1	5.2	−0.51567	35.3	200.3	200.2	35.6	−0.13408	3012	1	1	50	0
171779	53937.35615	213.2334	−130.4124	3.6	82.9	178.86	82.9	4.0	−0.41030	37.6	176.7	176.6	37.7	−0.08894	3655	0	1	50	0
171779	53942.33879	212.8086	−130.4947	9.8	455.0	178.07	454.7	18.2	−0.84189	36.3	607.8	607.5	41.7	−0.48920	1213	1	1	50	0
171779	53949.32378	213.4291	−130.5064	17.8	1009.2	179.18	1009.1	23.0	−0.62961	39.3	1319.4	1319.3	43.6	−0.43303	375	1	1	50	0
171779	53951.31374	212.7836	−130.5483	2.8	47.5	178.39	47.5	3.1	−0.42651	35.1	153.0	153.0	35.4	−0.11518	6370	1	1	50	0
171779	53956.31011	212.9765	−130.6239	4.9	123.4	0.78	123.4	5.1	0.32578	35.3	212.9	212.9	35.5	0.07950	3646	1	1	50	0
171779	53957.28590	212.6294	−130.6101	6.4	398.4	175.46	397.2	32.2	−0.97984	35.6	536.5	534.8	55.3	−0.76413	2167	1	1	50	0
171779	53958.29026	212.9650	−130.5947	5.2	59.5	176.45	59.4	6.3	−0.57588	35.4	159.9	159.7	36.7	−0.25678	2953	1	1	50	0
171779	53963.26954	212.7146	−130.6330	24.5	686.3	175.85	684.5	55.4	−0.89612	42.7	903.1	900.7	78.0	−0.83580	496	1	1	50	0
171779	53964.26536	213.2967	−130.7210	17.1	480.8	175.35	479.2	42.6	−0.91533	39.0	640.5	638.4	64.8	−0.79791	874	1	1	50	0
171779	53965.26415	212.6975	−130.6755	3.2	86.8	175.73	86.6	7.2	−0.89600	35.1	179.8	179.3	37.5	−0.34318	4673	1	1	50	0
171779	53970.26381	212.9056	−130.7631	3.3	112.3	178.66	112.3	4.2	−0.62001	35.2	202.3	202.2	35.5	−0.12935	3863	1	1	50	0
171779	53971.25825	212.8738	−130.7368	4.1	110.2	178.54	110.2	5.0	−0.56223	35.2	200.3	200.2	35.6	−0.13894	3413	1	1	50	0
171779	53979.25553	212.8052	−130.7791	6.5	206.8	2.34	206.6	10.6	0.79376	35.6	303.1	302.9	37.7	0.32408	2141	1	1	50	0
171779	53992.19426	212.8410	−130.9400	7.1	89.4	175.99	89.2	9.5	−0.65598	35.7	182.0	181.5	37.8	−0.32337	2370	1	1	50	0
171779	53993.17934	211.6802	−130.8416	19.3	1407.9	173.68	1399.3	156.3	−0.99225	40.0	1835.6	1824.5	205.9	−0.98075	221	1	1	100	0
171779	54003.17235	212.6577	−131.0548	16.8	165.0	177.52	164.8	18.2	−0.38794	38.8	256.1	255.9	40.3	−0.26844	970	1	1	50	0
171779	54006.17808	212.6724	−131.1255	3.4	96.4	1.81	96.3	4.6	0.66686	35.2	187.9	187.8	35.6	0.16066	3925	1	1	50	0
171779	54007.18032	212.5338	−131.1279	4.4	141.7	2.92	141.5	8.4	0.85380	35.3	231.4	231.1	37.1	0.30989	3051	1	1	50	0
171779	54251.49209	210.5304	−133.4152	8.0	209.9	178.19	209.8	10.4	−0.63936	35.9	306.7	306.5	37.2	−0.25704	2227	1	1	50	0
171779	54252.48964	209.8767	−133.4837	9.2	259.3	178.18	259.1	12.4	−0.66493	36.2	365.0	364.8	38.0	−0.30220	2229	1	1	50	0
171779	54376.17462	210.2435	−134.6941	9.8	303.1	4.02	302.4	23.4	0.90812	51.1	418.2	417.1	58.8	0.49103	1934	0	1	50	0
171779	54728.18950	206.8926	−138.0488	21.6	862.4	179.21	862.3	24.7	−0.48004	41.1	1129.8	1129.7	44.0	−0.35376	446	1	1	50	0
171779	54741.17373	205.9022	−138.2655	7.3	172.2	3.69	171.9	13.3	0.83253	35.8	264.0	263.5	39.5	0.42209	1746	1	1	50	0
171779	54748.15753	206.6104	−138.2506	9.4	309.9	4.61	308.9	26.6	0.93500	36.2	426.5	425.1	49.8	0.68337	1204	1	1	50	0
176051	52865.18946	−716.3549	217.1509	33.2	3587.6	153.57	3212.7	1597.0	−0.99973	130.9	4666.0	4178.7	2080.2	−0.99753	314	0	0	100	0
176051	52891.15205	−725.7708	214.5872	38.3	2736.4	160.45	2578.8	916.2	−0.99902	149.7	3560.1	3355.2	1199.6	−0.99120	370	0	0	100	0
176051	53109.51640	−764.3662	172.3603	9.2	274.0	153.10	244.4	124.3	−0.99654	49.5	382.7	342.0	178.7	−0.95081	1285	0	0	100	0
176051	53110.52340	−763.8966	171.9603	20.2	787.2	155.34	715.5	329.0	−0.99772	84.4	1032.9	939.4	437.7	−0.97729	664	0	0	100	0
176051	53123.50203	−766.5383	169.5217	13.7	337.0	157.50	311.4	129.6	−0.99348	62.7	459.9	425.6	185.3	−0.93068	1192	0	0	100	0
176051	53145.43757	−770.5581	165.2904	30.1	1532.4	156.75	1408.0	605.5	−0.99853	119.6	1997.0	1835.5	795.9	−0.98654	294	0	0	100	0
176051	53168.38529	−773.5629	160.5122	24.5	609.6	158.86	568.7	221.1	−0.99292	99.5	804.8	751.4	304.7	−0.93691	434	0	0	100	0
176051	53172.39036	−774.8076	159.7908	9.3	294.8	161.87	280.2	92.1	−0.99433	49.7	408.0	388.1	135.5	−0.92249	1386	0	0	100	0
176051	53187.34070	−777.2660	156.8094	8.9	248.8	160.08	233.9	85.2	−0.99387	48.7	352.4	331.8	128.5	−0.91549	1689	0	0	100	0
176051	53197.36964	−779.0516	154.9404	5.0	36.4	171.53	36.0	7.3	−0.72343	39.8	147.8	146.3	45.0	−0.44818	2882	0	0	100	0
176051	53198.38049	−779.4953	154.7126	5.6	224.0	175.37	223.2	18.9	−0.95426	41.0	323.1	322.1	48.4	−0.52966	2844	0	0	100	0
176051	53215.29575	−782.3349	151.3896	3.3	28.7	165.72	27.9	7.8	−0.89815	37.2	144.9	140.7	50.7	−0.65645	5997	0	0	100	0
176051	53222.32431	−783.3567	149.9677	7.8	395.9	177.60	395.5	18.3	−0.90375	45.9	533.4	532.9	51.0	−0.43490	2112	0	0	100	0
176051	53228.28183	−784.3775	148.7425	4.9	31.3	170.87	30.9	6.9	−0.69885	39.6	145.8	144.1	45.5	−0.47073	2825	0	0	100	0
176051	53233.19737	−784.9444	147.7408	13.5	535.9	156.45	491.3	214.5	−0.99764	62.1	710.6	651.9	289.6	−0.97229	801	0	0	100	0
176051	53235.29812	−784.4927	147.5957	14.1	627.5	179.93	627.5	14.2	−0.05756	64.0	827.7	827.7	64.0	−0.01570	1111	0	0	100	0
176051	53242.16492	−786.6680	146.5146	18.0	357.0	25.76	321.6	156.0	0.99173	76.8	484.8	437.9	221.7	0.92350	1383	0	0	100	0
176051	53250.20055	−788.5477	144.6414	5.3	33.4	167.11	32.6	9.1	−0.79918	40.4	146.6	143.2	51.2	−0.58932	3581	0	0	100	0

Table 4
(Continued)

HD Number	HJD 2400000.5	δR.A. (mas)	δDecl. (mas)	σ_{min} (μas)	σ_{maj} (μas)	ϕ_e (deg)	$\sigma_{R.A.}$ (μas)	$\sigma_{Decl.}$ (μas)	$\frac{\sigma^2_{R.A.,decl.}}{\sigma_{R.A.}\sigma_{decl.}}$	$\sigma_{min,c}$ (μas)	$\sigma_{maj,c}$ (μas)	$\sigma_{R.A.,c}$ (μas)	$\sigma_{Decl.,c}$ (μas)	$\frac{\sigma^2_{R.A.,decl.,c}}{\sigma_{R.A.,c}\sigma_{decl.,c}}$	N	LDC	Align	Rate (Hz)	Outlier
176051	53251.16205	−788.1705	144.2936	13.6	748.1	159.65	701.4	260.4	−0.99844	62.4	982.6	921.5	346.7	−0.98140	1397	0	0	100	0
176051	53263.19272	−790.7290	142.0380	7.9	62.7	172.83	62.2	11.1	−0.69416	46.1	162.0	160.8	50.0	−0.37125	3034	0	0	100	0
176051	53271.17385	−791.8338	140.3757	5.8	59.3	173.45	59.0	8.9	−0.75487	41.4	159.8	158.8	45.0	−0.37822	2785	0	0	100	0
176051	53481.42532	−824.7575	100.0525	19.6	172.2	6.55	171.1	27.7	0.70016	82.3	264.0	262.5	87.1	0.31190	660	0	0	100	2
176051	53544.44519	−836.0487	86.2634	13.8	106.8	178.40	106.7	14.1	−0.20740	63.0	197.2	197.1	63.3	−0.07812	967	0	0	100	0
176051	53551.33624	−837.0295	85.0116	6.8	57.0	157.72	52.8	22.5	−0.94589	43.5	158.4	147.5	72.3	−0.76316	3226	0	0	100	0
176051	53565.34142	−839.7999	82.3298	29.3	1014.0	167.65	990.6	218.7	−0.99058	116.7	1325.6	1295.2	305.6	−0.92043	753	0	0	100	0
176051	53585.30412	−841.6259	78.3693	7.0	41.6	168.17	40.7	10.9	−0.75737	44.0	150.1	147.2	52.9	−0.53077	2232	0	0	100	0
176051	53599.23162	−844.0472	75.5130	15.9	822.8	164.08	791.3	226.2	−0.99733	69.8	1078.8	1037.6	303.4	−0.97095	714	0	0	100	0
176051	53600.24883	−844.2410	75.2877	6.2	39.8	167.20	38.9	10.7	−0.80367	42.2	149.3	145.8	52.8	−0.57522	3045	0	0	100	0
176051	53607.17364	−845.4474	73.9736	4.5	77.1	156.57	70.8	30.9	−0.98763	39.0	172.2	158.7	77.2	−0.83708	4516	0	0	100	0
176051	53613.18114	−846.0260	72.6663	12.1	362.8	161.82	344.7	113.8	−0.99374	57.8	492.0	467.8	163.0	−0.92791	1231	0	0	100	0
176051	53614.17295	−846.2973	72.5875	6.7	182.5	160.40	171.9	61.5	−0.99328	43.3	275.5	259.9	101.0	−0.89093	2355	0	0	100	0
176051	53639.15941	−850.7464	67.6243	11.0	129.4	170.33	127.6	24.3	−0.88789	54.5	218.9	215.9	65.1	−0.52907	2078	0	0	100	0
176051	53858.50224	−884.1126	24.0259	12.8	202.7	161.15	191.9	66.6	−0.97934	59.9	298.4	283.1	111.9	−0.82524	532	0	1	100	0
176051	53872.43887	−885.9335	21.1953	13.6	244.8	155.54	222.9	102.1	−0.98925	62.4	347.7	317.5	154.8	−0.89721	313	0	1	100	0
176051	53873.46821	−885.9209	20.8900	23.2	168.6	162.71	161.1	54.8	−0.89612	94.9	260.1	249.9	119.1	−0.55924	534	0	1	100	0
176051	53895.43043	−889.0916	16.3485	10.7	100.8	165.33	97.6	27.5	−0.91632	53.6	191.8	186.0	71.1	−0.62808	925	0	1	100	0
176051	53915.38557	−892.7212	12.5358	13.7	114.1	166.41	110.9	29.9	−0.88184	62.7	204.0	198.8	77.6	−0.55796	2133	0	1	50	0
176051	53922.36301	−893.3954	11.0379	8.3	87.2	168.77	85.6	18.9	−0.89263	47.1	180.1	176.9	58.0	−0.56253	3364	0	1	50	0
176051	53923.36821	−892.8996	10.8388	25.6	286.8	169.75	282.3	56.9	−0.88924	43.4	398.3	392.0	82.7	−0.84637	880	1	1	50	0
176051	53942.29756	−895.8330	7.1329	7.6	179.7	164.73	173.4	47.9	−0.98651	35.8	272.3	262.9	79.6	−0.88477	2492	1	1	50	0
176051	53956.26896	−897.8470	4.2030	11.3	302.7	166.90	294.8	69.5	−0.98584	36.8	417.7	406.9	101.2	−0.92783	2589	1	1	50	0
176051	53970.18199	−900.4581	1.4808	11.6	441.3	157.30	407.2	170.6	−0.99727	36.9	590.5	545.0	230.4	−0.98485	1308	1	1	50	0
176051	53971.17568	−899.9728	1.0645	14.3	435.3	156.27	398.6	175.7	−0.99603	37.8	583.0	533.9	237.1	−0.98473	1157	1	1	50	0
176051	53977.17968	−901.3281	0.0533	7.2	165.7	160.31	156.0	56.2	−0.99060	35.7	256.9	242.2	92.9	−0.91291	2569	1	1	50	0
176051	53995.17191	−903.8195	−3.4528	23.0	219.8	168.21	215.2	50.2	−0.88379	41.9	318.2	311.6	76.9	−0.83090	609	1	1	100	0
176051	53996.14451	−903.1964	−3.7579	6.6	212.6	164.38	204.8	57.6	−0.99281	35.6	309.8	298.5	90.2	−0.91217	1741	1	1	100	0
176051	54007.15384	−905.5950	−5.9761	12.2	328.3	173.17	325.9	40.9	−0.95376	37.1	449.2	446.0	64.9	−0.81783	2094	1	1	50	0
176051	54272.42185	−941.4152	−58.8231	8.2	178.0	171.15	175.9	28.6	−0.95711	35.9	270.5	267.3	54.7	−0.74697	2112	1	1	50	0
176051	54279.41740	−942.6064	−60.2317	21.1	412.9	174.28	410.9	46.2	−0.88822	40.9	554.7	552.0	68.6	−0.80118	1468	1	1	50	0
176051	54285.40351	−943.1286	−61.3424	8.4	177.9	174.84	177.2	18.0	−0.88472	36.0	270.3	269.3	43.3	−0.55133	2534	1	1	50	0
176051	54294.37511	−944.2659	−63.1919	23.9	439.3	172.89	435.9	59.3	−0.91382	42.4	588.0	583.5	84.1	−0.86130	1685	1	1	50	0
176051	54300.34759	−945.6096	−64.3333	12.4	263.2	171.49	260.3	40.8	−0.95148	37.1	369.7	365.7	65.9	−0.82182	1854	1	1	50	0
176051	54315.30463	−946.8404	−67.5020	16.5	314.6	170.89	310.6	52.4	−0.94785	71.8	432.3	427.0	98.5	−0.67512	1165	0	1	50	0
176051	54320.30936	−948.1228	−68.3782	8.5	149.5	175.48	149.0	14.5	−0.80962	47.6	239.5	238.8	51.1	−0.35480	2326	0	1	50	0
176051	54336.27158	−950.2820	−71.6059	6.6	127.1	176.69	126.9	9.9	−0.74162	43.1	216.6	216.2	44.8	−0.26825	4109	0	1	50	0
176051	54343.25058	−950.7254	−73.0148	7.1	157.2	176.16	156.9	12.7	−0.82899	44.2	247.7	247.2	47.1	−0.34091	3771	0	1	50	0
176051	54348.23686	−951.5093	−74.1000	8.2	154.6	175.66	154.2	14.3	−0.81731	46.9	244.9	244.3	50.3	−0.35519	2822	0	1	50	0
176051	54350.22324	−951.8030	−74.3261	9.3	154.1	174.08	153.3	18.4	−0.86105	49.7	244.4	243.2	55.5	−0.43509	2658	0	1	50	0
176051	54357.21302	−952.8741	−75.8207	8.0	187.2	176.55	186.8	13.8	−0.81357	46.4	280.8	280.3	49.3	−0.33359	3494	0	1	50	0
176051	54376.14606	−954.9497	−79.6896	16.2	480.6	173.99	478.0	52.8	−0.95099	70.8	640.3	636.8	97.2	−0.68100	1499	0	1	50	0
176051	54377.14482	−955.1633	−79.7522	7.0	121.7	173.41	120.9	15.6	−0.89110	44.0	211.3	209.9	49.9	−0.46424	3739	0	1	50	0
176051	54383.13838	−955.5471	−80.9643	10.9	289.2	176.14	288.6	22.3	−0.87166	54.2	401.2	400.3	60.5	−0.43844	2283	0	1	50	0
176051	54671.37080	−991.1354	−137.7092	12.9	223.4	0.29	223.4	13.0	0.08820	37.3	322.4	322.4	37.3	0.04312	2378	1	1	50	0

Table 4
(Continued)

HD Number	HJD 2400000.5	δR.A. (mas)	δDecl. (mas)	$\sigma_{\rm min}$ (μas)	$\sigma_{\rm maj}$ (μas)	$\phi_{\rm e}$ (deg)	$\sigma_{\rm R.A.}$ (μas)	$\sigma_{\rm Decl.}$ (μas)	$\frac{\sigma^2_{\rm R.A.,decl.}}{\sigma_{\rm R.A.}\sigma_{\rm decl.}}$	$\sigma_{\rm min,c}$ (μas)	$\sigma_{\rm maj,c}$ (μas)	$\sigma_{\rm R.A.,c}$ (μas)	$\sigma_{\rm Decl.,c}$ (μas)	$\frac{\sigma^2_{\rm R.A.,decl.,c}}{\sigma_{\rm R.A.,c}\sigma_{\rm decl.,c}}$	N	LDC	Align	Rate (Hz)	Outlier
176051	54685.33104	−993.4281	−140.4674	15.4	328.6	179.70	328.6	15.5	−0.11255	38.2	449.5	449.5	38.3	−0.06100	1501	1	1	50	0
176051	54698.29734	−994.6124	−143.2756	21.0	471.1	0.96	471.1	22.4	0.35095	40.8	628.2	628.1	42.1	0.24868	1142	1	1	50	0
176051	54706.27220	−994.4562	−144.6023	16.0	225.3	179.41	225.3	16.2	−0.14317	38.5	324.6	324.6	38.6	−0.08533	2214	1	1	50	0
187362	53909.36616	−20.1136	−131.3605	10.8	107.6	153.40	96.3	49.2	−0.96914	53.9	197.9	178.6	100.9	−0.80563	1622	0	1	50	0
187362	53930.34694	−18.6589	−133.4846	15.3	559.1	159.72	524.5	194.3	−0.99649	67.9	740.2	694.7	264.3	−0.96186	776	0	1	50	0
187362	53958.21750	−21.2649	−134.0831	32.2	995.3	150.17	863.5	495.9	−0.99720	47.6	1301.4	1129.3	648.7	−0.99642	409	1	1	50	0
187362	53964.18964	−18.4896	−136.0483	27.0	662.2	148.42	564.4	347.5	−0.99584	44.2	872.2	743.4	458.3	−0.99358	452	1	1	50	0
187362	53972.17329	−18.5223	−136.5315	13.0	343.0	149.56	295.8	174.2	−0.99623	37.3	467.4	403.4	239.0	−0.98348	1372	1	1	50	0
187362	54006.14033	−17.4188	−139.4907	9.0	194.7	160.75	183.9	64.8	−0.98920	36.1	289.2	273.3	101.3	−0.92598	1925	1	1	50	0
187362	54008.14292	−17.8290	−139.4114	14.5	387.7	162.47	369.8	117.6	−0.99158	37.9	523.1	498.9	161.6	−0.96934	795	1	1	50	0
187362	54336.22798	−7.2546	−163.6643	20.8	121.6	157.15	112.3	51.0	−0.89703	86.4	211.2	197.5	114.3	−0.58837	429	0	1	50	0
187362	54341.24525	−7.3695	−163.9836	30.6	987.2	164.92	953.3	258.5	−0.99246	121.4	1291.0	1246.9	355.7	−0.93547	303	0	1	50	0
187362	54356.19475	−6.7854	−164.9968	20.7	228.9	163.69	219.8	67.3	−0.94715	86.1	328.9	316.5	123.9	−0.69215	438	0	1	50	0
196524	52919.15033	−52.7322	586.2133	15.7	526.6	160.79	497.3	173.9	−0.99544	69.2	698.7	660.2	239.0	−0.95194	779	0	0	100	0
196524	53200.34646	−25.0494	585.6767	33.2	568.9	25.92	511.9	250.5	0.98910	130.9	752.7	679.4	349.5	0.90979	297	0	0	100	0
196524	53207.32515	−25.0499	585.3716	14.0	238.4	27.77	211.1	111.8	0.98988	63.7	340.1	302.4	168.2	0.90477	1258	0	0	100	0
196524	53214.28543	−24.9518	585.1530	10.9	371.2	149.74	320.7	187.3	−0.99772	54.2	502.5	434.9	257.5	−0.96994	1226	0	0	100	0
196524	53221.31357	−23.5277	584.9481	6.4	162.6	31.14	139.2	84.2	0.99606	42.6	253.5	218.1	136.1	0.93139	2780	0	0	100	0
196524	53234.20413	−22.8423	584.6511	6.8	111.1	146.51	92.7	61.5	−0.99113	43.5	201.1	169.5	116.8	−0.89690	1774	0	0	100	0
196524	53242.26045	−21.4859	584.4005	12.7	125.2	34.15	103.9	71.1	0.97667	59.6	214.7	180.8	130.2	0.83934	1529	0	0	100	0
196524	53250.19842	−21.8239	584.4826	13.1	377.7	151.42	331.7	181.0	−0.99659	60.9	510.6	449.3	250.0	−0.96099	1314	0	0	100	0
196524	53263.18972	−20.6518	584.1074	8.8	545.8	156.11	499.1	221.2	−0.99905	48.4	723.2	661.5	296.2	−0.98391	1148	0	0	100	0
196524	53271.15653	−18.4303	583.2751	8.0	286.3	154.14	257.7	125.1	−0.99746	46.4	397.6	358.4	178.4	−0.95753	1394	0	0	100	0
196524	53284.15401	−17.3960	583.3073	9.1	141.1	33.76	117.4	78.8	0.99034	49.2	230.8	193.8	134.6	0.90029	2011	0	0	100	0
196524	53294.15110	−17.0894	582.9895	12.3	286.9	166.14	278.5	69.7	−0.98348	58.4	398.4	387.0	111.0	−0.84072	1184	0	0	100	0
196524	53508.45604	3.3893	574.5971	17.7	814.7	146.57	680.0	449.1	−0.99888	75.8	1068.3	892.6	591.9	−0.98818	726	0	0	100	0
196524	53509.45813	2.4331	575.3321	13.4	488.2	147.44	411.5	263.0	−0.99817	61.8	649.9	548.8	353.6	−0.97836	886	0	0	100	0
196524	53551.39533	7.5489	572.2611	7.3	40.0	153.01	35.8	19.3	−0.90692	44.7	149.3	134.6	78.6	−0.77628	2106	0	0	100	0
196524	53565.33746	9.1612	571.3476	25.4	345.7	148.61	295.4	181.4	−0.98643	102.7	470.7	405.4	260.4	−0.88901	518	0	0	100	0
196524	53572.43002	10.2995	571.4202	25.3	591.3	42.84	434.0	402.5	0.99632	102.3	781.3	577.1	536.5	0.96610	556	0	0	100	0
196524	53584.35475	10.9113	570.1280	12.8	87.1	162.71	83.2	28.6	−0.88391	59.9	180.1	172.8	78.3	−0.60420	923	0	0	100	0
196524	53586.26593	10.3136	570.4053	7.7	61.4	154.46	55.5	27.4	−0.94981	45.6	161.2	146.7	80.8	−0.78427	1675	0	0	100	0
196524	53599.20180	13.2131	568.6734	10.1	542.5	145.53	447.3	307.1	−0.99920	51.9	719.0	593.5	409.2	−0.98810	1407	0	0	100	0
196524	53600.22267	12.5157	569.0969	6.2	64.0	148.22	54.5	34.1	−0.97694	42.2	162.9	140.2	93.0	−0.84979	2119	0	0	100	0
196524	53606.34340	13.3513	569.0109	7.1	122.4	176.93	122.3	9.6	−0.67791	44.2	211.9	211.7	45.6	−0.23827	1336	0	0	100	0
196524	53607.34297	13.1690	568.9778	5.9	140.2	177.63	140.1	8.3	−0.69693	41.6	229.8	229.6	42.6	−0.21577	2015	0	0	100	0
196524	53613.32596	13.4970	568.6135	13.7	281.8	177.57	281.6	18.2	−0.65715	62.7	392.2	391.8	64.8	−0.24987	630	0	0	100	0
196524	53614.32379	13.8057	568.5047	10.7	237.1	177.41	236.9	15.1	−0.70819	53.6	338.5	338.2	55.7	−0.26758	1128	0	0	100	0
196524	53621.20009	14.3445	568.0796	42.6	232.6	30.11	202.3	122.4	0.91643	165.6	333.2	300.0	220.2	0.54934	458	0	0	100	0
196524	53639.21868	16.1788	566.7894	5.3	29.0	169.26	28.5	7.5	−0.69481	40.4	145.0	142.6	48.0	−0.51850	2236	0	0	100	0
196524	53649.19784	17.2474	566.1405	8.7	53.6	171.31	53.0	11.8	−0.66896	48.1	156.4	154.8	53.1	−0.40208	1152	0	0	100	0
196524	53655.15772	18.0352	565.7046	12.2	124.4	163.42	119.3	37.4	−0.93988	58.1	213.9	205.7	82.6	−0.68211	558	0	0	100	0
196524	53676.11652	19.0929	564.5358	11.6	106.5	167.66	104.1	25.4	−0.88469	56.3	196.9	192.7	69.2	−0.55699	1047	0	0	100	0
196524	53957.25341	46.1307	541.1888	6.0	212.2	149.99	183.8	106.3	−0.99787	35.5	309.4	268.5	157.7	−0.96577	2980	1	1	50	0
196524	53972.24316	47.8343	539.5585	5.9	61.4	153.88	55.2	27.5	−0.97100	35.5	161.2	145.5	77.8	−0.86294	3320	1	1	50	0

Table 4
(Continued)

HD Number	HJD 2400000.5	δR.A. (mas)	δDecl. (mas)	σ_{min} (μas)	σ_{maj} (μas)	ϕ_e (deg)	$\sigma_{R.A.}$ (μas)	$\sigma_{Decl.}$ (μas)	$\frac{\sigma^2_{R.A.,decl.}}{\sigma_{R.A.}\sigma_{decl.}}$	$\sigma_{min,c}$ (μas)	$\sigma_{maj,c}$ (μas)	$\sigma_{R.A.,c}$ (μas)	$\sigma_{Decl.,c}$ (μas)	$\frac{\sigma^2_{R.A.,decl.,c}}{\sigma_{R.A.,c}\sigma_{decl.,c}}$	N	LDC	Align	Rate (Hz)	Outlier
196524	53978.26170	47.9166	539.0539	5.3	50.2	161.93	47.7	16.3	−0.94110	35.4	154.5	147.3	58.5	−0.77317	3788	1	1	50	0
196524	53996.19517	49.3756	537.4114	6.1	179.1	158.12	166.2	67.0	−0.99518	35.5	271.7	252.5	106.5	−0.93331	2820	1	1	50	0
196524	54004.19705	50.5316	536.5239	9.0	123.1	163.02	117.8	37.0	−0.96727	36.1	212.6	203.6	71.1	−0.84738	2365	1	1	50	0
196524	54008.20254	50.9299	536.2051	4.7	47.6	166.28	46.2	12.2	−0.91753	35.3	153.1	148.9	49.9	−0.68704	3058	1	1	50	2
196524	54032.12437	53.3578	533.5132	13.8	86.1	164.70	83.1	26.3	−0.83963	37.6	179.2	173.2	59.6	−0.75718	1151	1	1	50	0
196524	54037.14931	54.0282	532.9612	9.3	250.6	174.23	249.3	26.9	−0.93734	36.2	354.6	352.8	50.7	−0.69595	1311	1	1	100	0
196524	54245.44853	72.1388	508.7330	8.9	283.7	147.81	240.2	151.3	−0.99760	36.1	394.5	334.4	212.4	−0.97967	2246	1	1	50	0
196524	54250.43334	72.6182	508.1093	7.8	336.1	147.64	284.0	180.0	−0.99867	35.9	458.8	388.0	247.4	−0.98521	3096	1	1	50	0
196524	54251.43698	73.5329	507.3488	9.4	140.3	149.45	120.9	71.8	−0.98827	36.2	229.9	198.9	121.0	−0.93809	3068	1	1	50	0
196524	54252.42277	73.6944	507.3307	16.0	219.3	147.26	184.7	119.4	−0.98723	38.5	317.6	268.0	174.8	−0.96535	1874	1	1	50	0
196524	54266.41214	74.9599	505.4144	8.5	108.9	152.83	97.0	50.3	−0.98168	36.0	199.1	177.9	96.4	−0.90837	3479	1	1	50	0
196524	54272.37663	74.8844	505.0680	6.4	238.9	148.02	202.7	126.6	−0.99825	35.6	340.7	289.6	182.9	−0.97347	3309	1	1	50	0
196524	54278.34417	75.5951	504.2017	21.2	1711.5	145.35	1408.1	973.1	−0.99965	40.9	2229.4	1834.1	1268.0	−0.99923	1014	1	1	50	0
196524	54279.42309	75.8577	503.7161	7.6	80.9	163.23	77.5	24.4	−0.94577	35.8	175.1	168.0	61.1	−0.79129	2795	1	1	50	0
196524	54280.36975	76.2560	503.6052	6.0	50.8	150.78	44.4	25.3	−0.96314	35.5	154.8	136.2	81.7	−0.86939	3371	1	1	50	0
196524	54292.34064	75.8990	502.8724	14.9	655.3	150.39	569.7	324.0	−0.99860	38.0	863.3	750.8	427.8	−0.99476	1049	1	1	50	0
196524	54294.37850	77.2536	501.7908	6.5	45.7	160.85	43.3	16.2	−0.90443	35.6	152.1	144.1	60.2	−0.78120	3512	1	1	50	0
196524	54299.35356	77.5955	501.1723	9.5	303.8	156.17	277.9	123.1	−0.99644	36.3	419.0	383.6	172.5	−0.97327	2217	1	1	50	0
196524	54301.34369	78.1889	500.7383	8.3	228.2	155.58	207.8	94.7	−0.99538	36.0	328.0	299.1	139.5	−0.95918	2916	1	1	50	0
196524	54307.27750	78.2116	500.0268	5.0	174.9	147.41	147.4	94.3	−0.99803	35.4	267.0	225.8	146.9	−0.95862	3965	1	1	50	0
196524	54308.28913	77.8873	500.3942	7.8	328.6	149.35	282.7	167.6	−0.99852	35.9	449.5	387.2	231.2	−0.98366	1847	1	1	50	0
196524	54320.24118	79.0568	498.6158	5.8	196.0	147.34	165.1	105.9	−0.99790	41.4	290.7	245.8	160.7	−0.95253	3235	0	1	50	0
196524	54341.25708	81.6521	495.3649	4.6	17.6	158.90	16.5	7.7	−0.76593	39.1	141.9	133.1	62.8	−0.74747	3750	0	1	50	0
196524	54348.24998	82.2682	494.3164	3.9	22.9	160.61	21.6	8.4	−0.87375	38.0	143.1	135.6	59.5	−0.73876	6075	0	1	50	0
196524	54356.23181	82.7031	493.3491	3.9	24.2	163.29	23.2	7.9	−0.85949	38.0	143.5	137.9	55.0	−0.69504	4753	0	1	50	0
196524	54363.21162	83.4030	492.4233	17.8	402.7	162.64	384.4	121.3	−0.98811	76.2	541.9	517.7	177.3	−0.89320	1389	0	1	50	0
196524	54377.20906	84.5719	490.3751	4.9	41.6	170.78	41.1	8.2	−0.79676	39.6	150.1	148.3	45.9	−0.48657	4606	0	1	50	0
196524	54384.16336	85.2876	489.4183	7.3	51.2	165.73	49.6	14.5	−0.85221	44.7	155.0	150.6	57.7	−0.60527	4009	0	1	50	0
196524	54385.15314	85.2516	489.2226	6.5	57.8	161.55	54.9	19.3	−0.93502	42.8	158.9	151.3	64.7	−0.71834	4382	0	1	50	0
196524	54627.40783	105.8214	450.9476	10.1	281.6	148.74	240.7	146.4	−0.99672	36.4	391.9	335.6	205.8	−0.97839	2756	1	1	50	0
196524	54629.40264	105.5982	450.8387	6.9	230.4	148.83	197.2	119.4	−0.99773	35.7	330.6	283.5	173.8	−0.97093	3328	1	1	50	0
196524	54653.33660	107.9257	446.4978	8.6	135.0	147.77	114.2	72.3	−0.99007	36.0	224.5	190.9	123.6	−0.93930	2889	1	1	50	0
196524	54678.25808	109.9239	442.0530	7.1	263.9	147.02	221.5	143.8	−0.99826	35.7	370.5	311.4	203.9	−0.97805	3090	1	1	50	0
196524	54685.23690	110.1886	440.9976	6.3	255.9	146.54	213.5	141.2	−0.99857	35.6	360.9	301.7	201.2	−0.97740	2853	1	1	50	0
196524	54695.32872	111.2543	438.7978	14.0	145.7	167.64	142.3	34.0	−0.90750	37.7	235.5	230.2	62.4	−0.78638	1885	1	1	50	0
196524	54696.23641	111.2657	438.8904	9.4	236.4	150.86	206.6	115.4	−0.99567	36.2	337.7	295.5	167.5	−0.96893	2948	1	1	50	0
196524	54707.32334	112.5222	436.7090	12.0	232.5	175.65	231.8	21.3	−0.82495	37.0	333.1	332.2	44.7	−0.55803	1359	1	1	50	0
196524	54713.25461	113.0873	435.5313	5.5	56.7	162.68	54.2	17.7	−0.94600	35.4	158.2	151.4	58.0	−0.76967	4255	1	1	50	0
196524	54740.14335	114.4883	431.0694	10.8	419.4	155.84	382.7	171.9	−0.99763	36.6	562.9	513.8	232.8	−0.98503	1595	1	1	50	0
196524	54742.14085	114.5775	430.6359	21.2	1055.0	156.14	964.9	427.1	−0.99853	40.9	1378.6	1260.9	558.9	−0.99679	1109	1	1	50	0
196524	54749.13151	116.4486	428.8318	37.0	1987.4	158.68	1851.4	723.4	−0.99849	50.9	2587.4	2410.4	941.9	−0.99831	638	1	1	50	0
202275	52896.18633	43.1322	28.3062	7.3	73.4	150.12	63.8	37.1	−0.97374	44.7	169.4	148.6	92.9	−0.83622	854	0	0	100	0
202275	52897.16089	42.9726	29.2560	6.4	99.7	146.48	83.2	55.3	−0.99049	42.6	190.8	160.8	111.2	−0.89058	1698	0	0	100	0
202275	52915.20668	46.9137	41.1243	9.2	122.4	163.69	117.5	35.5	−0.96301	49.5	211.9	203.9	76.1	−0.73744	885	0	0	100	0
202275	52917.18635	46.8907	42.6174	4.0	71.9	160.61	67.8	24.2	−0.98482	38.2	168.3	159.3	66.5	−0.79500	2197	0	0	100	0

Table 4
(Continued)

HD Number	HJD 2400000.5	δR.A. (mas)	δDecl. (mas)	σ_{min} (μas)	σ_{maj} (μas)	ϕ_e (deg)	$\sigma_{R.A.}$ (μas)	$\sigma_{Decl.}$ (μas)	$\frac{\sigma^2_{R.A.,decl.}}{\sigma_{R.A.}\sigma_{decl.}}$	$\sigma_{min,c}$ (μas)	$\sigma_{maj,c}$ (μas)	$\sigma_{R.A.,c}$ (μas)	$\sigma_{Decl.,c}$ (μas)	$\frac{\sigma^2_{R.A.,decl.,c}}{\sigma_{R.A.,c}\sigma_{decl.,c}}$	N	LDC	Align	Rate (Hz)	Outlier
202275	52918.17605	46.9123	43.3930	6.9	80.3	158.50	74.7	30.1	−0.96946	43.7	174.6	163.3	75.8	−0.78716	1181	0	0	100	0
202275	52920.20175	46.8784	44.7321	9.7	403.8	166.02	391.9	98.0	−0.99474	50.8	543.3	527.3	140.2	−0.92764	970	0	0	100	0
202275	52929.16173	49.5693	50.3719	4.7	87.8	162.42	83.7	26.9	−0.98301	39.3	180.6	172.6	66.2	−0.78352	1846	0	0	100	0
202275	52930.16500	49.3717	51.1594	14.0	353.4	163.85	339.5	99.2	−0.98921	63.7	480.3	461.7	146.9	−0.89258	584	0	0	100	0
202275	52951.10502	53.1315	64.3282	31.5	890.9	163.63	854.8	252.9	−0.99154	124.7	1166.6	1119.9	349.9	−0.92851	232	0	0	100	0
202275	53172.44864	30.9086	105.4061	7.1	223.4	153.00	199.0	101.6	−0.99695	44.2	322.4	288.0	151.6	−0.94522	1142	0	0	100	0
202275	53173.40524	30.6928	104.8851	9.1	165.6	17.94	157.5	51.7	0.98293	49.2	256.8	244.8	91.9	0.82742	1322	0	0	100	0
202275	53181.40299	28.0314	101.4540	9.5	413.7	149.29	355.7	211.4	−0.99865	50.3	555.7	478.5	287.1	−0.97909	679	0	0	100	0
202275	53182.40362	27.4784	101.1195	7.7	352.2	149.87	304.6	176.9	−0.99874	45.6	478.8	414.7	243.6	−0.97634	1391	0	0	100	0
202275	53186.40418	25.5096	99.5865	18.2	733.9	151.54	645.2	350.1	−0.99825	77.5	964.3	848.6	464.6	−0.98186	250	0	0	100	0
202275	53187.40064	26.2103	98.5359	6.0	214.8	151.72	189.2	101.9	−0.99778	41.8	312.4	275.8	152.5	−0.95066	2087	0	0	100	0
202275	53197.39934	21.9937	93.8954	4.1	33.4	155.89	30.5	14.1	−0.94769	38.3	146.6	134.7	69.3	−0.79908	2668	0	0	100	0
202275	53198.37488	21.8510	93.2834	3.9	36.0	152.64	32.0	16.9	−0.96512	38.0	147.6	132.3	75.8	−0.82861	3203	0	0	100	0
202275	53199.39640	22.2859	92.4201	17.5	782.0	156.61	717.8	310.8	−0.99812	75.1	1026.2	942.3	413.2	−0.98019	515	0	0	100	0
202275	53208.32346	17.7858	87.9997	5.2	51.9	20.76	48.6	19.0	0.95683	40.2	155.4	146.0	66.7	0.76712	3244	0	0	100	0
202275	53214.34527	15.9121	84.5147	5.9	55.4	154.04	49.9	24.8	−0.96434	41.6	157.4	142.7	78.4	−0.81113	2792	0	0	100	0
202275	53215.34493	15.4419	83.9798	3.6	34.8	153.85	31.3	15.7	−0.96757	37.6	147.1	133.1	73.1	−0.82282	3947	0	0	100	0
202275	53221.26852	14.0157	80.9109	3.3	63.3	15.60	61.0	17.3	0.98013	37.2	162.4	156.7	56.5	0.73125	5719	0	0	100	2
202275	53222.34771	12.6374	79.9100	4.3	206.5	159.11	192.9	73.7	−0.99806	38.6	302.8	283.2	113.8	−0.93187	2302	0	0	100	0
202275	53229.30700	10.0093	75.6266	4.4	108.0	154.99	97.9	45.8	−0.99442	38.8	198.3	180.4	90.9	−0.88323	2316	0	0	100	0
202275	53236.24325	8.2332	70.6560	25.8	960.6	147.94	814.3	510.4	−0.99822	104.1	1256.6	1066.4	672.8	−0.98324	66	0	0	100	0
202275	53249.24609	1.7949	62.9850	3.9	50.8	153.48	45.5	22.9	−0.98154	38.0	154.8	139.5	77.0	−0.83691	2234	0	0	100	0
202275	53251.20507	2.4740	60.8709	14.3	1217.5	148.21	1034.9	641.5	−0.99966	64.6	1588.9	1351.0	838.9	−0.99589	794	0	0	100	0
202275	53508.51014	−86.2661	−117.6466	25.7	1872.8	150.49	1630.0	922.7	−0.99949	103.7	2438.7	2122.9	1204.6	−0.99509	263	0	0	100	0
202275	53550.41476	−94.5634	−143.7430	33.6	248.4	151.98	219.8	120.4	−0.94901	132.4	352.0	316.9	202.5	−0.68742	370	0	0	100	0
202275	53552.39070	−95.1314	−144.7394	10.0	85.5	150.13	74.3	43.5	−0.96433	51.7	178.8	157.1	99.7	−0.80762	1352	0	0	100	0
202275	53571.33708	−99.1014	−155.5406	9.8	68.1	149.71	59.0	35.4	−0.94763	51.1	165.6	145.3	94.5	−0.78738	1089	0	0	100	0
202275	53584.32209	−101.4808	−162.5820	10.4	104.4	151.49	91.9	50.7	−0.97257	52.8	195.0	173.2	104.0	−0.82056	774	0	0	100	0
202275	53586.30551	−102.0699	−163.5724	13.2	831.4	150.94	726.8	404.0	−0.99930	61.2	1089.8	953.1	532.1	−0.99132	639	0	0	100	0
202275	53607.23153	−105.7110	−174.9132	3.2	80.6	148.50	68.8	42.2	−0.99616	37.1	174.9	150.4	96.7	−0.89515	4856	0	0	100	0
202275	53613.22656	−107.1689	−177.7122	6.7	243.9	150.28	211.8	121.0	−0.99794	43.3	346.6	301.8	175.9	−0.95923	1601	0	0	100	0
202275	53614.22404	−106.8640	−178.5237	5.9	174.7	150.30	151.8	86.7	−0.99697	41.6	266.8	232.7	137.0	−0.93755	1597	0	0	100	0
202275	53637.20260	−111.2011	−189.7810	12.3	357.4	157.38	330.0	137.9	−0.99532	58.4	485.3	448.5	194.3	−0.94564	570	0	0	100	0
202275	53656.13119	−114.1212	−198.7176	16.3	215.2	154.15	193.8	95.0	−0.98163	71.1	312.8	283.2	150.7	−0.85325	526	0	0	100	0
202275	53874.48740	−133.8872	−275.5346	12.3	424.1	147.53	357.9	227.9	−0.99794	58.4	568.8	480.9	309.3	−0.97476	264	0	1	100	0
202275	53909.42929	−133.9992	−283.9042	6.1	58.2	152.62	51.8	27.3	−0.96784	42.0	159.1	142.6	82.1	−0.82143	2646	0	1	50	0
202275	53957.31225	−133.5951	−293.0314	9.0	405.4	154.61	366.3	174.0	−0.99836	36.1	545.3	492.9	236.1	−0.98555	1127	1	1	50	0
202275	53970.25687	−133.8277	−294.8670	5.7	50.6	153.56	45.3	23.1	−0.96133	35.5	154.7	139.4	75.8	−0.85488	2387	1	1	50	0
202275	53971.25697	−133.8720	−294.9994	7.3	62.3	152.11	55.1	29.8	−0.96094	35.8	161.7	143.9	82.0	−0.87171	1682	1	1	50	0
202275	53977.26568	−133.7452	−295.9258	5.3	39.3	157.55	36.4	15.8	−0.93150	35.4	149.0	138.4	65.6	−0.81413	3320	1	1	50	0
202275	54003.21436	−132.9971	−299.3500	16.7	206.3	161.12	195.3	68.6	−0.96619	38.8	302.5	286.5	104.5	−0.92011	835	1	1	50	0
202275	54005.19256	−133.0756	−299.4872	11.6	115.3	157.22	106.4	45.9	−0.96173	36.9	205.1	189.6	86.4	−0.88707	1614	1	1	50	0
202275	54028.10997	−132.3819	−301.8684	13.3	406.8	153.38	363.7	182.7	−0.99667	37.4	547.1	489.4	247.4	−0.98558	632	1	1	50	0
202275	54037.11371	−132.9331	−302.3088	11.0	319.6	159.14	298.7	114.3	−0.99468	36.7	438.4	409.9	159.8	−0.96940	556	1	1	100	0
202275	54230.50430	−116.0750	−301.5447	13.1	508.3	146.70	424.9	279.3	−0.99843	37.4	675.5	564.9	372.2	−0.99277	933	1	1	50	0

Table 4
(Continued)

HD Number	HJD 2400000.5	δR.A. (mas)	δDecl. (mas)	σ_{min} (μas)	σ_{maj} (μas)	ϕ_e (deg)	$\sigma_{R.A.}$ (μas)	$\sigma_{Decl.}$ (μas)	$\frac{\sigma^2_{R.A.,decl.}}{\sigma_{R.A.}\sigma_{decl.}}$	$\sigma_{min,c}$ (μas)	$\sigma_{maj,c}$ (μas)	$\sigma_{R.A.,c}$ (μas)	$\sigma_{Decl.,c}$ (μas)	$\frac{\sigma^2_{R.A.,decl.,c}}{\sigma_{R.A.,c}\sigma_{decl.,c}}$	N	LDC	Align	Rate (Hz)	Outlier
202275	54266.47312	−111.8958	−297.2173	13.2	112.0	158.12	104.1	43.5	−0.94549	37.4	202.0	188.0	82.9	−0.87454	1315	1	1	50	0
202275	54273.44060	−111.3234	−296.1236	10.4	448.6	153.94	403.0	197.3	−0.99828	36.5	599.7	539.0	265.5	−0.98822	1172	1	1	50	0
202275	54286.44916	−109.0169	−294.5057	17.0	830.5	162.69	792.9	247.6	−0.99741	38.9	1088.7	1039.4	326.1	−0.99216	502	1	1	50	0
202275	54287.45890	−107.4535	−294.6102	39.0	1181.8	165.87	1146.1	291.0	−0.99042	52.4	1542.7	1496.1	380.0	−0.98984	208	1	1	50	0
202275	54321.35282	−104.6007	−288.5396	7.9	290.0	162.36	276.3	88.2	−0.99560	46.1	402.2	383.5	129.5	−0.92773	1872	0	1	50	0
202275	54343.21174	−100.9267	−284.4750	5.3	216.8	147.85	183.5	115.5	−0.99852	40.4	314.7	267.3	170.9	−0.96054	2094	0	1	50	0
202275	54350.27098	−100.0982	−282.7950	9.1	241.6	161.91	229.7	75.5	−0.99192	49.2	343.9	327.2	116.6	−0.89625	1344	0	1	50	0
202275	54383.17856	−95.1820	−275.3360	12.0	337.7	161.87	321.0	105.7	−0.99284	57.5	460.8	438.3	153.4	−0.91917	1237	0	1	50	0
202275	54389.15740	−93.5380	−274.1005	26.4	260.9	161.04	246.9	88.4	−0.94900	106.3	366.9	348.7	155.9	−0.69707	475	0	1	50	0
202275	54627.48303	−43.9409	−188.7326	8.4	227.8	156.57	209.0	90.9	−0.99497	36.0	327.6	300.9	134.4	−0.95654	2290	1	1	50	0
202275	54629.47795	−43.8838	−187.6002	31.0	797.2	156.50	731.2	319.2	−0.99439	46.8	1045.8	959.2	419.2	−0.99258	339	1	1	50	0
202275	54670.36488	−33.8286	−167.4185	16.9	198.7	156.05	181.7	82.1	−0.97445	38.9	293.8	269.0	124.4	−0.94001	513	1	1	50	0
202275	54678.29381	−32.6938	−162.8598	15.7	1030.4	147.67	870.7	551.2	−0.99943	38.4	1346.8	1138.2	721.0	−0.99802	674	1	1	50	0
202275	54695.22568	−26.8923	−154.9510	17.4	1442.8	144.99	1181.8	827.8	−0.99967	39.1	1880.9	1540.7	1079.6	−0.99902	896	1	1	50	0
202275	54698.21273	−27.6502	−152.2701	20.1	1342.1	144.43	1091.8	780.8	−0.99950	40.4	1750.3	1423.9	1018.7	−0.99881	503	1	1	50	0
202275	54706.19610	−26.6969	−147.2190	11.1	853.0	145.08	699.4	488.4	−0.99962	36.7	1117.7	916.7	640.5	−0.99755	1346	1	1	50	0
202275	54707.19017	−25.8258	−147.1529	10.3	663.8	144.75	542.1	383.2	−0.99946	36.5	874.2	714.2	505.4	−0.99609	1413	1	1	50	0
202275	54741.22082	−15.9349	−128.7799	20.8	2031.7	166.92	1979.0	460.2	−0.99892	40.7	2644.9	2576.3	599.9	−0.99757	624	1	1	50	0
202275	54748.19278	−14.0966	−124.6952	9.9	315.6	164.78	304.6	83.4	−0.99238	36.4	433.5	418.4	119.1	−0.94862	1723	1	1	50	0
202275	54762.15379	−8.3398	−117.0524	29.0	1281.7	164.98	1237.9	333.5	−0.99593	45.5	1672.1	1615.0	435.5	−0.99415	514	1	1	50	0
202444	53234.35595	−753.9975	31.7802	12.3	588.3	170.69	580.5	96.0	−0.99147	58.4	777.5	767.3	138.4	−0.90394	1859	0	0	100	0
202444	53243.26521	−754.0677	29.5872	33.0	1259.1	26.66	1125.4	565.7	0.99786	130.2	1642.8	1469.3	746.2	0.98079	1292	0	0	100	0
202444	53250.31241	−753.8386	27.5376	9.5	59.1	165.11	57.2	17.7	−0.83399	50.3	159.7	154.9	63.6	−0.57921	2646	0	0	100	0
202444	53270.26350	−754.7529	22.3568	14.6	556.6	172.09	551.3	77.9	−0.98183	65.6	737.0	730.0	120.5	−0.83530	2556	0	0	100	0
202444	53272.24593	−753.7950	21.7361	27.4	1011.7	169.23	993.9	190.9	−0.98926	109.8	1322.6	1299.5	269.7	−0.91002	1737	0	0	100	0
202444	53285.14592	−753.7582	19.1240	8.4	96.3	25.96	86.6	42.8	0.97592	47.4	187.8	170.1	92.6	0.82524	3090	0	0	100	0
202444	53291.15886	−753.7914	16.7714	10.6	82.2	159.82	77.3	30.1	−0.92649	53.4	176.1	166.3	78.7	−0.69648	2807	0	0	100	0
202444	53312.11074	−753.8118	11.3891	6.3	137.8	164.09	132.6	38.3	−0.98535	42.4	227.4	219.0	74.5	−0.80654	4165	0	0	100	0
202444	53551.46586	−750.7528	−50.6872	11.0	70.7	165.49	68.5	20.7	−0.83534	54.5	167.5	162.7	67.4	−0.55440	2729	0	0	100	0
202444	53571.40917	−750.2907	−56.0105	8.8	70.1	171.09	69.3	13.9	−0.76967	48.4	167.0	165.2	54.4	−0.43543	3704	0	0	100	0
202444	53583.41831	−749.7614	−58.9536	13.6	134.6	175.82	134.3	16.7	−0.58190	62.4	224.1	223.5	64.4	−0.23406	2325	0	0	100	0
202444	53600.31206	−749.6416	−63.3621	15.3	97.0	162.16	92.4	33.1	−0.87508	67.9	188.4	180.6	86.6	−0.57602	2059	0	0	100	0
202444	53606.34868	−749.3081	−64.9009	8.0	59.9	171.55	59.3	11.8	−0.73237	46.4	160.2	158.6	51.5	−0.41807	4745	0	0	100	0
202444	53607.32867	−749.1312	−65.1141	12.6	123.2	167.84	120.5	28.7	−0.89315	59.3	212.7	208.3	73.3	−0.56296	2015	0	0	100	0
202444	53613.34066	−748.7877	−66.6577	9.3	80.6	175.46	80.4	11.3	−0.55833	49.7	174.9	174.4	51.5	−0.24707	2722	0	0	100	0
202444	53614.32504	−749.2825	−67.1063	10.7	82.5	171.36	81.6	16.3	−0.74708	53.6	176.4	174.5	59.3	−0.40507	3107	0	0	100	0
202444	53621.20519	−748.6727	−68.8551	21.0	156.3	18.03	148.8	52.3	0.90666	87.1	246.8	236.2	112.7	0.58934	3038	0	0	100	0
202444	53639.26290	−748.5259	−73.6027	11.7	108.9	172.25	107.9	18.7	−0.77459	56.6	199.1	197.4	62.2	−0.39673	2994	0	0	100	0
202444	53649.23303	−748.0584	−76.2148	13.2	123.3	172.68	122.3	20.4	−0.76012	61.2	212.8	211.2	66.4	−0.37410	2348	0	0	100	0
202444	53656.17565	−748.0981	−77.9192	22.5	144.2	164.51	139.1	44.2	−0.84924	92.4	234.0	226.8	108.8	−0.48203	1728	0	0	100	0
202444	53670.19052	−749.2667	−81.3797	14.3	655.5	177.12	654.7	35.9	−0.91688	64.6	863.6	862.5	77.8	−0.55471	1935	0	0	100	0
202444	53676.17822	−747.4412	−83.1706	14.4	177.5	179.35	177.5	14.6	−0.13800	65.0	269.9	269.9	65.0	−0.04436	2978	0	0	100	0
202444	53965.36823	−738.0858	−157.9427	12.0	155.3	171.90	153.8	24.9	−0.87269	37.0	245.7	243.3	50.4	−0.67111	2407	1	1	50	0
202444	53992.32268	−736.9830	−164.7958	22.8	243.0	178.61	242.9	23.5	−0.24912	41.8	345.5	345.4	42.6	−0.19392	2227	1	1	50	0
202444	54003.28908	−736.6610	−167.7696	11.3	124.8	176.37	124.5	13.8	−0.56853	36.8	214.3	213.9	39.1	−0.33648	3157	1	1	50	0

Table 4
(Continued)

HD Number	HJD 2400000.5	δR.A. (mas)	δDecl. (mas)	σ_{min} (μas)	σ_{maj} (μas)	ϕ_e (deg)	$\sigma_{R.A.}$ (μas)	$\sigma_{Decl.}$ (μas)	$\frac{\sigma^2_{R.A.,decl.}}{\sigma_{R.A.}\sigma_{decl.}}$	$\sigma_{min,c}$ (μas)	$\sigma_{maj,c}$ (μas)	$\sigma_{R.A.,c}$ (μas)	$\sigma_{Decl.,c}$ (μas)	$\frac{\sigma^2_{R.A.,decl.,c}}{\sigma_{R.A.,c}\sigma_{decl.,c}}$	N	LDC	Align	Rate (Hz)	Outlier
202444	54005.28445	−736.4926	−168.3373	22.4	200.9	175.26	200.2	27.8	−0.58950	41.6	296.3	295.3	48.1	−0.49893	3404	1	1	50	0
202444	54007.24802	−737.9458	−168.5377	25.6	713.1	172.02	706.2	102.2	−0.96750	43.4	937.5	928.5	137.1	−0.94760	1175	1	1	50	0
202444	54292.47998	−721.5522	−241.3831	17.8	247.0	174.08	245.7	31.0	−0.81763	39.3	350.3	348.4	53.2	−0.67048	2908	1	1	50	0
202444	54294.48070	−721.1221	−241.8132	19.2	196.6	174.28	195.7	27.3	−0.70958	39.9	291.4	290.0	49.2	−0.57911	3448	1	1	50	0
202444	54308.47445	−720.7922	−245.4270	19.4	508.3	3.32	507.4	35.3	0.83420	40.0	675.5	674.3	55.9	0.69716	1949	1	1	50	0
202444	54320.44499	−719.6565	−248.4346	8.9	207.2	4.73	206.5	19.2	0.88543	48.7	303.6	302.6	54.6	0.44679	3478	0	1	50	0
202444	54336.38361	−718.4807	−252.4435	9.5	206.3	0.39	206.3	9.6	0.14705	50.3	302.5	302.5	50.3	0.03979	2915	0	1	50	0
202444	54343.39071	−720.3947	−254.5731	20.6	1194.3	6.81	1185.9	143.1	0.98948	85.7	1558.9	1547.9	203.5	0.90551	1494	0	1	50	0
202444	54348.35784	−717.7994	−255.5873	12.7	133.4	1.40	133.4	13.1	0.24680	59.6	222.9	222.8	59.8	0.08448	2878	0	1	50	0
202444	54356.34408	−716.9435	−257.4669	10.8	229.5	3.71	229.0	18.3	0.80799	53.9	329.6	328.9	57.9	0.35845	3474	0	1	50	0
202444	54370.30092	−716.1909	−260.9870	9.3	172.8	2.93	172.6	12.8	0.68784	49.7	264.7	264.4	51.5	0.25351	3812	0	1	50	0
202444	54389.24995	−715.2299	−265.7632	13.3	243.4	2.83	243.1	17.9	0.66939	61.5	346.0	345.6	63.7	0.25957	2907	0	1	50	0
202444	54685.40356	−693.9389	−338.7618	12.2	270.4	174.93	269.4	26.8	−0.88884	37.1	378.4	376.9	49.8	−0.66482	2269	1	1	50	0
202444	54748.27591	−690.0880	−354.5028	24.5	731.1	6.05	727.1	80.8	0.95232	42.7	960.7	955.3	109.8	0.92028	1432	1	1	50	0
206901	52591.15779	139.4206	−68.9506	22.4	338.6	174.63	337.1	38.7	−0.81429	92.0	461.9	460.0	101.3	−0.40966	149	0	0	100	0
206901	52809.42396	176.3281	−52.8096	8.6	357.0	148.20	303.5	188.3	−0.99855	47.9	484.8	412.8	258.7	−0.97608	835	0	0	100	0
206901	52834.42978	178.7631	−49.4983	8.3	38.1	158.25	35.5	16.1	−0.83208	47.1	148.5	139.0	70.3	−0.69834	1756	0	0	100	0
206901	52836.48099	178.2378	−48.6333	13.4	379.5	173.84	377.4	42.8	−0.94915	61.8	512.8	509.9	82.5	−0.65748	736	0	0	100	0
206901	52862.26859	179.1249	−46.6475	5.2	49.4	144.90	40.5	28.7	−0.97540	40.2	154.0	128.1	94.5	−0.85930	3015	0	0	100	0
206901	52864.44008	180.0358	−45.8584	4.9	95.7	1.42	95.7	5.4	0.43467	39.6	187.3	187.2	39.9	0.11110	1536	0	0	100	0
206901	52865.26284	180.3062	−45.0074	7.5	116.2	146.66	97.2	64.2	−0.99022	45.1	206.0	173.8	119.3	−0.89394	2067	0	0	100	0
206901	52868.43221	179.3846	−45.8721	3.5	89.2	2.24	89.1	5.0	0.70400	37.4	181.8	181.7	38.1	0.17866	2573	0	0	100	0
206901	52891.31479	180.2397	−42.5409	5.0	18.6	172.30	18.5	5.6	−0.41389	39.8	142.1	140.9	43.8	−0.40002	1935	0	0	100	0
206901	52893.35685	180.8687	−42.7415	9.0	313.4	0.77	313.4	9.9	0.42163	48.9	430.8	430.8	49.3	0.11598	939	0	0	100	0
206901	52894.34291	181.2303	−42.0470	4.3	37.8	0.66	37.8	4.3	0.10017	38.6	148.4	148.4	38.7	0.04121	2171	0	0	100	0
206901	52895.31557	181.5077	−41.4499	5.8	21.5	173.23	21.4	6.3	−0.37133	41.4	142.8	141.9	44.4	−0.34712	1568	0	0	100	0
206901	52896.29588	180.7689	−41.3583	3.3	11.5	172.05	11.4	3.7	−0.39838	37.2	140.8	139.5	41.7	−0.43461	3320	0	0	100	0
206901	52897.29256	180.3940	−41.7392	2.9	9.7	171.46	9.6	3.2	−0.41204	36.7	140.6	139.1	41.9	−0.46430	4804	0	0	100	0
206901	52915.28773	180.4714	−39.4499	5.7	26.1	179.52	26.1	5.7	−0.03695	41.2	144.1	144.0	41.2	−0.02692	1315	0	0	100	0
206901	52916.29801	179.8881	−39.7949	8.1	329.1	1.79	329.0	13.1	0.78564	46.6	450.2	449.9	48.7	0.28586	1054	0	0	100	0
206901	52918.12279	181.2809	−38.7867	9.6	569.7	147.06	478.1	309.9	−0.99931	50.6	753.7	633.2	412.0	−0.98928	765	0	0	100	0
206901	52919.29319	181.3655	−38.3084	3.6	91.3	2.52	91.2	5.4	0.74137	37.6	183.5	183.4	38.4	0.20134	2859	0	0	100	0
206901	52920.12509	180.8836	−38.2825	11.0	768.0	148.32	653.6	403.4	−0.99949	54.5	1008.2	858.4	531.5	−0.99272	936	0	0	100	0
206901	52929.27392	181.2991	−37.9988	9.8	198.4	4.54	197.8	18.5	0.84767	51.1	293.5	292.6	56.0	0.40225	707	0	0	100	0
206901	52930.26391	181.2731	−37.3092	11.9	287.8	2.96	287.4	19.0	0.77841	57.2	399.5	399.0	60.7	0.33277	855	0	0	100	0
206901	52950.22395	179.7824	−34.3871	14.2	845.7	7.01	839.3	104.2	0.99047	64.3	1108.3	1100.0	149.6	0.90127	480	0	0	100	0
206901	52952.20412	180.7615	−35.0045	14.1	511.9	3.52	510.9	34.5	0.91183	64.0	680.0	678.8	76.3	0.54227	562	0	0	100	0
206901	52983.12407	179.3424	−30.6826	11.5	355.3	5.09	353.9	33.5	0.93894	56.0	482.6	480.8	70.3	0.60079	452	0	0	100	0
206901	53130.50531	168.6205	−9.8425	13.0	575.3	143.15	460.4	345.1	−0.99890	60.5	760.9	609.9	458.9	−0.98636	1027	0	0	100	0
206901	53145.46573	168.9519	−7.4875	29.9	2133.0	143.09	1705.5	1281.3	−0.99958	118.9	2776.4	2221.1	1670.1	−0.99603	312	0	0	100	0
206901	53152.47126	166.1403	−4.9520	7.3	136.4	146.80	114.2	74.9	−0.99313	44.7	225.9	190.6	129.2	−0.91227	2389	0	0	100	0
206901	53168.42498	164.7522	−3.8657	14.3	637.2	145.84	527.3	358.0	−0.99884	64.6	840.1	696.1	474.7	−0.98641	709	0	0	100	0
206901	53172.46956	162.4897	−2.9051	2.8	27.6	155.52	25.2	11.7	−0.96478	36.6	144.5	132.4	68.5	−0.81264	3600	0	0	100	0
206901	53173.44613	162.7452	−3.3452	4.3	108.4	21.10	101.1	39.2	0.99311	38.6	198.6	185.8	80.1	0.85684	2831	0	0	100	0
206901	53181.41429	162.9372	−0.9773	4.4	55.9	150.65	48.7	27.6	−0.98325	38.8	157.7	138.8	84.4	−0.85270	2322	0	0	100	0

Table 4
(Continued)

HD Number	HJD 2400000.5	δR.A. (mas)	δDecl. (mas)	σ_{min} (μas)	σ_{maj} (μas)	ϕ_e (deg)	$\sigma_{R.A.}$ (μas)	$\sigma_{Decl.}$ (μas)	$\frac{\sigma^2_{R.A.,decl.}}{\sigma_{R.A.}\sigma_{decl.}}$	$\sigma_{min,c}$ (μas)	$\sigma_{maj,c}$ (μas)	$\sigma_{R.A.,c}$ (μas)	$\sigma_{Decl.,c}$ (μas)	$\frac{\sigma^2_{R.A.,decl.,c}}{\sigma_{R.A.,c}\sigma_{decl.,c}}$	N	LDC	Align	Rate (Hz)	Outlier
206901	53182.41243	162.5235	−0.6682	5.5	73.1	150.81	63.9	36.0	−0.98450	40.8	169.2	149.1	89.9	−0.85722	2407	0	0	100	0
206901	53186.42249	161.7314	−0.6717	6.8	88.9	153.55	79.6	40.1	−0.98173	43.5	181.5	163.7	89.8	−0.84321	835	0	0	100	0
206901	53187.40438	162.1818	−0.1174	5.2	75.5	154.17	68.0	33.2	−0.98451	40.2	171.0	154.9	82.8	−0.84438	3234	0	0	100	0
206901	53197.36675	159.6345	0.5089	3.0	29.9	149.29	25.7	15.5	−0.97505	36.8	145.3	126.3	80.7	−0.85121	4372	0	0	100	0
206901	53198.39543	160.0522	1.0916	2.4	21.2	156.02	19.4	8.9	−0.95641	36.2	142.7	131.2	66.7	−0.80788	5139	0	0	100	0
206901	53199.40686	160.6159	1.6193	9.4	177.6	157.43	164.0	68.7	−0.98902	50.0	270.0	250.1	113.5	−0.87948	1046	0	0	100	0
206901	53200.41612	159.4855	1.7590	7.0	439.9	29.74	382.0	218.3	0.99931	44.0	588.8	511.7	294.5	0.98514	1414	0	0	100	0
206901	53207.41539	157.6357	2.4066	7.4	101.4	33.07	85.1	55.7	0.98740	44.9	192.3	163.0	111.5	0.87989	2391	0	0	100	0
206901	53208.36952	157.5620	2.1611	5.7	248.5	24.63	225.9	103.7	0.99817	41.2	352.1	320.5	151.4	0.95438	2253	0	0	100	0
206901	53215.32976	156.9976	3.2389	3.0	32.1	151.09	28.1	15.7	−0.97571	36.8	146.1	129.1	77.6	−0.84389	4811	0	0	100	0
206901	53221.39324	156.3876	3.9671	3.2	46.3	35.67	37.7	27.1	0.98965	37.1	152.4	125.7	93.8	0.87788	6197	0	0	100	0
206901	53228.30457	155.6000	5.6295	2.7	17.1	155.62	15.6	7.5	−0.91724	36.5	141.8	130.0	67.3	−0.80659	3450	0	0	100	0
206901	53229.29698	156.0966	6.1881	3.1	22.7	152.91	20.3	10.7	−0.94425	36.9	143.1	128.5	73.0	−0.82613	3851	0	0	100	0
206901	53233.24583	154.8587	5.5452	9.5	804.5	145.13	660.0	460.0	−0.99969	50.3	1055.2	866.2	604.7	−0.99486	691	0	0	100	0
206901	53234.27318	154.9429	6.3996	3.1	20.8	152.93	18.6	9.9	−0.93637	36.9	142.6	128.1	72.7	−0.82497	4093	0	0	100	0
206901	53235.28320	155.2381	7.0259	3.1	23.5	154.23	21.2	10.6	−0.94743	36.9	143.3	130.0	70.6	−0.81728	2679	0	0	100	0
206901	53236.24527	154.6529	7.2612	6.2	42.6	150.03	37.1	22.0	−0.94661	42.2	150.6	132.1	83.6	−0.81817	1184	0	0	100	0
206901	53249.22827	151.8697	8.8392	2.9	42.4	148.88	36.4	22.1	−0.98827	36.7	150.5	130.2	83.9	−0.86276	4247	0	0	100	0
206901	53270.23356	148.9027	11.8985	7.5	254.2	160.31	239.3	86.0	−0.99575	45.1	358.9	338.2	128.2	−0.92757	1474	0	0	100	0
206901	53285.23902	145.3551	13.9452	5.0	79.9	37.54	63.4	48.8	0.99161	39.8	174.3	140.3	110.8	0.89483	3656	0	0	100	0
206901	53313.11002	142.2376	18.5970	4.1	96.9	159.77	91.0	33.7	−0.99156	38.3	188.3	177.2	74.4	−0.83690	3846	0	0	100	0
206901	53494.50860	104.6070	43.3686	13.6	645.9	143.23	517.4	386.8	−0.99904	62.4	851.3	682.9	512.0	−0.98839	702	0	0	100	0
206901	53586.36546	83.9661	55.9065	2.2	11.5	166.51	11.2	3.4	−0.75101	36.0	140.8	137.2	48.0	−0.63848	5532	0	0	100	0
206901	53637.29660	71.2325	62.9288	6.3	53.5	173.82	53.2	8.5	−0.66479	42.4	156.3	155.5	45.4	−0.34331	1639	0	0	100	0
206901	53921.45247	24.8756	86.0577	43.2	10260.1	160.72	9684.6	3388.1	−0.99991	167.8	13338.9	12590.9	4407.1	−0.99919	615	0	1	50	0
206901	53963.35933	−9.1868	98.3657	6.2	79.3	165.54	76.8	20.7	−0.95158	35.5	173.9	168.6	55.4	−0.74981	2244	1	1	100	0
206901	53978.32784	−14.0826	99.4668	2.7	17.6	162.84	16.8	5.8	−0.87053	35.1	141.9	135.9	53.6	−0.73042	5863	1	1	50	0
206901	53995.24459	−17.0642	101.1075	11.5	514.3	159.38	481.4	181.5	−0.99770	36.8	683.1	639.5	243.0	−0.98680	389	1	1	100	0
206901	54003.32693	−22.4853	101.1584	10.9	849.6	3.09	848.3	47.1	0.97274	36.7	1113.3	1111.7	70.3	0.85280	1590	1	1	50	0
206901	54008.31169	−21.6045	102.0985	4.6	114.0	2.48	113.9	6.7	0.73343	35.3	203.9	203.7	36.4	0.23537	2850	1	1	50	0
206901	54075.12742	−38.5877	107.2121	7.0	183.8	3.06	183.5	12.0	0.81544	35.7	276.9	276.5	38.6	0.37675	1756	1	1	50	0
206901	54265.40042	−84.8151	119.9655	8.2	390.0	142.94	311.2	235.1	−0.99904	35.9	526.0	420.3	318.3	−0.98996	3661	1	1	50	0
206901	54300.44689	−92.7572	122.5645	6.4	195.8	167.80	191.4	41.9	−0.98783	35.6	290.5	284.0	70.6	−0.85674	3456	1	1	50	0
206901	54350.31082	−104.3619	124.6444	4.1	121.5	167.58	118.7	26.5	−0.98705	38.3	211.1	206.3	58.8	−0.74566	5489	0	1	50	0
206901	54357.29056	−106.1244	125.6022	6.5	163.6	167.26	159.5	36.6	−0.98337	42.8	254.6	248.5	70.0	−0.77899	5452	0	1	50	0
206901	54383.21418	−111.9102	126.9752	4.6	113.3	166.17	110.0	27.4	−0.98521	39.1	203.2	197.5	61.7	−0.75768	5858	0	1	50	0
206901	54679.41161	−172.8035	133.2679	11.4	57.9	168.80	56.8	15.9	−0.68026	36.8	159.0	156.1	47.5	−0.61437	1589	1	1	50	0
206901	54696.35516	−176.7584	132.9610	11.1	244.3	165.65	236.7	61.5	−0.98236	36.7	347.1	336.4	93.1	−0.91343	1878	1	1	50	0
206901	54741.24018	−184.2790	134.0046	8.5	307.9	167.71	300.8	66.1	−0.99128	36.0	424.0	414.4	96.9	−0.92481	2678	1	1	50	0
206901	54748.22201	−186.2535	133.4596	8.3	333.1	168.07	325.9	69.3	−0.99255	36.0	455.1	445.3	100.4	−0.93063	2579	1	1	50	0
206901	54762.18297	−187.3707	132.5954	15.6	576.8	168.19	564.6	119.1	−0.99100	38.3	762.8	746.7	160.6	−0.96982	1121	1	1	50	0
207652	53197.45645	−133.8768	81.2102	8.5	381.2	164.04	366.5	105.1	−0.99644	47.6	515.0	495.3	148.8	−0.94301	1007	0	0	100	0
207652	53208.37830	−132.0981	82.5773	14.0	78.5	25.57	71.0	36.2	0.90366	63.7	173.2	158.7	94.3	0.67550	1352	0	0	100	0
207652	53221.37388	−130.3666	84.1157	8.0	123.3	32.79	103.8	67.1	0.99003	46.4	212.8	180.7	121.7	0.89360	2875	0	0	100	0
207652	53222.43753	−130.3333	84.2283	6.8	213.4	175.50	212.7	18.1	−0.92544	43.5	310.7	309.8	49.8	−0.48039	1990	0	0	100	0

Table 4
(Continued)

HD Number	HJD 2400000.5	δR.A. (mas)	δDecl. (mas)	σ_{min} (μas)	σ_{maj} (μas)	ϕ_e (deg)	$\sigma_{R.A.}$ (μas)	$\sigma_{Decl.}$ (μas)	$\frac{\sigma^2_{R.A.,decl.}}{\sigma_{R.A.}\sigma_{decl.}}$	$\sigma_{min,c}$ (μas)	$\sigma_{maj,c}$ (μas)	$\sigma_{R.A.,c}$ (μas)	$\sigma_{Decl.,c}$ (μas)	$\frac{\sigma^2_{R.A.,decl.,c}}{\sigma_{R.A.,c}\sigma_{decl.,c}}$	N	LDC	Align	Rate (Hz)	Outlier
207652	53235.38748	−128.1930	85.8001	12.1	241.3	171.68	238.7	36.9	−0.94315	57.8	343.5	340.0	75.8	−0.63733	685	0	0	100	0
207652	53242.29037	−127.3840	86.6003	22.3	130.9	24.69	119.3	58.3	0.90756	91.7	220.4	203.8	124.1	0.60218	553	0	0	100	0
207652	53249.33920	−125.9704	87.4362	8.2	198.0	169.28	194.5	37.7	−0.97529	46.9	293.0	288.0	71.3	−0.74402	1427	0	0	100	0
207652	53263.30482	−124.0721	89.1354	4.1	87.0	170.16	85.8	15.4	−0.96361	38.3	180.0	177.4	48.7	−0.60264	4312	0	0	100	0
207652	53271.28256	−123.2069	90.1595	8.0	177.9	170.13	175.3	31.5	−0.96623	46.4	270.3	266.5	65.1	−0.69097	2051	0	0	100	0
207652	53272.27909	−122.4090	90.1623	20.7	479.4	170.13	472.3	84.7	−0.96884	86.1	638.8	629.5	138.5	−0.77596	639	0	0	100	0
207652	53284.17716	−121.1109	91.7648	16.9	142.3	26.99	127.0	66.3	0.95840	73.1	232.0	209.4	123.8	0.75609	1007	0	0	100	0
207652	53285.17291	−120.8239	91.9257	10.7	117.8	27.12	104.9	54.5	0.97529	53.6	207.5	186.3	106.0	0.82580	1818	0	0	100	0
207652	53312.18733	−116.7492	95.0140	4.4	73.2	174.05	72.8	8.8	−0.86435	38.8	169.3	168.4	42.4	−0.39217	3685	0	0	100	0
207652	53313.18134	−116.8817	95.1509	11.5	220.6	174.15	219.4	25.2	−0.88879	56.0	319.1	317.5	64.5	−0.48870	1295	0	0	100	0
207652	53340.10789	−113.0726	98.4038	8.9	312.1	174.65	310.7	30.4	−0.95618	48.7	429.2	427.4	62.8	−0.62855	1458	0	0	100	0
207652	53544.49033	−81.9289	122.1372	9.1	170.7	161.30	161.7	55.4	−0.98479	49.2	262.4	249.0	96.2	−0.84228	1309	0	0	100	0
207652	53552.42931	−80.9221	123.1689	12.2	72.5	152.49	64.6	35.2	−0.92074	58.1	168.8	152.1	93.4	−0.72390	1269	0	0	100	0
207652	53578.44813	−77.2454	126.1175	22.5	466.7	171.70	461.8	71.0	−0.94719	92.4	622.7	616.3	128.2	−0.68550	372	0	0	100	0
207652	53586.41630	−75.7361	126.9855	6.5	73.2	167.25	71.4	17.4	−0.92283	42.8	169.3	165.4	56.0	−0.62285	1642	0	0	100	0
207652	53606.31027	−72.4123	129.1602	5.8	39.9	155.80	36.4	17.2	−0.92833	41.4	149.3	137.2	71.9	−0.77991	2522	0	0	100	0
207652	53607.34935	−72.3787	129.3258	9.9	46.8	164.01	45.1	16.0	−0.76585	51.4	152.6	147.4	64.9	−0.57212	1069	0	0	100	0
207652	53613.28991	−71.5268	129.9927	15.6	89.2	156.91	82.3	37.8	−0.89401	68.8	181.8	169.4	95.4	−0.63224	433	0	0	100	0
207652	53614.27712	−71.1540	130.0019	10.2	87.0	154.18	78.4	39.0	−0.95665	52.2	180.0	163.6	91.4	−0.77776	760	0	0	100	0
207652	53620.24356	−70.6217	130.8757	16.1	189.3	153.20	169.2	86.6	−0.97802	70.5	283.1	254.7	142.3	−0.83482	578	0	0	100	0
207652	53639.31674	−69.8895	132.7556	20.8	549.8	0.26	549.7	20.9	0.12128	86.4	728.3	728.3	86.5	0.03767	1078	0	0	100	0
207652	53909.47841	−25.1811	161.4653	7.9	82.8	158.93	77.3	30.7	−0.96081	46.1	176.6	165.6	76.7	−0.76749	2894	0	1	50	0
207652	53915.41682	−24.1394	162.0001	15.8	146.1	150.18	127.0	73.9	−0.96911	69.5	236.0	207.6	131.9	−0.80094	748	0	1	50	0
207652	53916.50872	−23.9195	162.1643	13.5	556.9	169.15	547.0	105.6	−0.99151	62.1	737.4	724.3	151.6	−0.90890	868	0	1	50	0
207652	53958.34819	−17.3136	166.2722	13.5	110.6	159.82	103.9	40.2	−0.93369	37.5	200.7	188.8	77.7	−0.85817	1083	1	1	50	0
207652	53964.28411	−16.7308	167.0270	33.7	541.3	150.87	473.1	265.2	−0.98936	48.6	717.5	627.2	351.8	−0.98744	382	1	1	50	0
207652	53965.26136	−16.5547	167.1254	5.6	74.4	147.81	63.0	39.9	−0.98621	35.4	170.2	145.2	95.5	−0.90047	3910	1	1	50	0
207652	53970.28910	−15.7220	167.5639	6.7	60.0	155.38	54.6	25.7	−0.95825	35.6	160.3	146.4	74.2	−0.85079	2897	1	1	50	0
207652	53971.27626	−15.6794	167.7189	12.1	101.1	153.62	90.7	46.2	−0.95635	37.0	192.0	172.8	91.5	−0.89328	1462	1	1	50	0
207652	53977.27336	−14.5286	168.2311	8.7	427.1	154.19	384.5	186.1	−0.99866	36.1	572.6	515.7	251.4	−0.98723	2242	1	1	50	0
207652	53979.26824	−13.8536	168.2328	22.9	269.6	153.21	240.9	123.2	−0.97814	41.8	377.4	337.4	174.2	−0.96325	453	1	1	50	0
207652	54004.25001	−9.9478	170.7274	16.5	97.8	162.39	93.4	33.5	−0.85688	38.7	189.1	180.6	68.1	−0.80363	1317	1	1	50	0
207652	54006.21622	−9.3107	170.7578	8.7	242.5	158.12	225.1	90.7	−0.99459	36.1	344.9	320.4	132.8	−0.95632	1872	1	1	50	0
207652	54055.10631	−2.4938	175.7309	34.6	656.3	164.26	631.7	181.1	−0.98007	49.2	864.6	832.3	239.3	−0.97691	500	1	1	50	0
207652	54250.48384	28.5977	193.1474	19.0	563.7	148.52	480.8	294.8	−0.99715	39.8	746.1	636.6	391.1	−0.99285	733	1	1	50	0
207652	54273.48711	32.2170	195.0610	14.2	239.3	159.58	224.4	84.6	−0.98380	37.8	341.1	320.0	124.2	−0.94596	1030	1	1	50	0
207652	54285.42022	33.8562	196.2516	25.5	191.3	153.97	172.3	87.0	−0.94539	43.3	285.4	257.1	131.1	−0.93043	374	1	1	50	0
207652	54320.37597	39.5862	198.8974	11.8	282.0	162.62	269.2	85.0	−0.98930	56.9	392.4	374.9	129.2	−0.88744	1115	0	1	50	0
207652	54321.35550	40.0575	198.8870	8.9	93.2	159.03	87.1	34.4	−0.96069	48.7	185.1	173.8	80.3	−0.76381	1947	0	1	50	0
207652	54336.36273	42.3585	200.1153	12.0	133.4	167.80	130.5	30.5	−0.91564	57.5	222.9	218.2	73.3	−0.59876	919	0	1	50	0
207652	54341.27437	42.9497	200.5359	17.4	133.0	154.87	120.7	58.7	−0.94493	74.8	222.5	203.9	116.2	−0.71202	562	0	1	50	0
207652	54349.26104	44.1403	201.2312	16.3	193.1	156.63	177.4	78.0	−0.97378	71.1	287.4	265.4	131.4	−0.80995	690	0	1	50	0
207652	54356.27856	45.6029	201.6078	12.8	113.6	162.34	108.3	36.5	−0.93059	59.9	203.5	194.8	84.1	−0.66753	951	0	1	50	0
207652	54370.24774	47.9721	202.6525	32.0	824.9	164.25	793.9	226.0	−0.98912	126.5	1081.5	1041.4	317.8	−0.91053	334	0	1	50	0
207652	54763.15991	107.5791	228.2302	27.8	212.8	161.68	202.2	71.9	−0.91341	44.7	310.0	294.7	106.3	−0.89679	234	1	1	50	0

Table 4
(Continued)

HD Number	HJD 2400000.5	δR.A. (mas)	δDecl. (mas)	σ_{min} (μas)	σ_{maj} (μas)	ϕ_e (deg)	$\sigma_{R.A.}$ (μas)	$\sigma_{Decl.}$ (μas)	$\frac{\sigma^2_{R.A.,decl.}}{\sigma_{R.A.}\sigma_{decl.}}$	$\sigma_{min,c}$ (μas)	$\sigma_{maj,c}$ (μas)	$\sigma_{R.A.,c}$ (μas)	$\sigma_{Decl.,c}$ (μas)	$\frac{\sigma^2_{R.A.,decl.,c}}{\sigma_{R.A.,c}\sigma_{decl.,c}}$	N	LDC	Align	Rate (Hz)	Outlier
207652	54769.15275	108.1681	228.6971	11.0	101.6	163.39	97.4	30.9	−0.92795	36.7	192.5	184.7	65.3	−0.81073	875	1	1	50	0
214850	52929.30989	−85.7984	40.6140	14.1	313.2	4.20	312.3	26.9	0.85015	64.0	430.6	429.4	71.2	0.43312	1210	0	0	100	0
214850	53199.43265	−34.1236	−60.9225	18.3	1390.8	152.99	1239.2	631.8	−0.99947	77.9	1813.5	1616.0	826.5	−0.99440	1066	0	0	100	0
214850	53214.45293	−28.1837	−63.4211	18.2	87.0	167.02	84.8	26.4	−0.70618	77.5	180.0	176.2	85.7	−0.38247	1022	0	0	100	0
214850	53222.34762	−26.2844	−68.8409	5.5	74.3	149.26	63.9	38.3	−0.98572	40.8	170.1	147.7	93.7	−0.86548	3649	0	0	100	1
214850	53228.38604	−21.7678	−65.8955	7.4	36.1	158.04	33.6	15.1	−0.85052	44.9	147.7	138.0	69.2	−0.71922	2912	0	0	100	0
214850	53234.28734	−18.8760	−66.9964	13.2	441.4	145.20	362.6	252.2	−0.99797	61.2	590.7	486.3	340.8	−0.97595	1175	0	0	100	0
214850	53249.34575	−11.1521	−69.3863	4.9	28.3	161.40	26.8	10.1	−0.86155	39.6	144.8	137.8	59.5	−0.71441	3439	0	0	100	0
214850	53251.36251	−9.1149	−65.3152	21.0	417.5	166.81	406.5	97.4	−0.97516	87.1	560.5	546.1	153.5	−0.81265	753	0	0	100	1
214850	53263.28708	−4.6554	−70.9525	3.3	18.7	158.58	17.4	7.5	−0.88220	37.2	142.1	133.0	62.4	−0.77093	6541	0	0	100	0
214850	53271.28405	0.1596	−67.3104	5.0	29.0	162.41	27.7	10.0	−0.85313	39.8	145.0	138.7	58.0	−0.69613	4719	0	0	100	1
214850	53272.33767	−1.5094	−67.2046	27.1	1013.9	175.25	1010.4	88.2	−0.95126	108.8	1325.5	1321.0	154.3	−0.70672	745	0	0	100	1
214850	53284.25772	4.5993	−67.2050	8.7	102.7	36.94	82.3	62.1	0.98459	48.1	193.5	157.3	122.5	0.87536	3128	0	0	100	1
214850	53291.23760	9.3687	−73.4842	12.5	103.0	162.27	98.2	33.6	−0.92004	59.0	193.7	185.4	81.5	−0.65380	1552	0	0	100	0
214850	53313.17667	19.9534	−74.7293	5.7	43.9	163.11	42.1	13.9	−0.90357	41.2	151.2	145.2	59.0	−0.68701	4510	0	0	100	0
214850	53558.47353	124.7631	−63.1929	30.2	204.3	31.24	175.4	109.1	0.94663	120.0	300.2	264.1	186.5	0.68196	510	0	0	100	0
214850	53572.47237	129.4358	−62.0761	13.5	405.5	37.43	322.1	246.7	0.99762	62.1	545.4	434.8	335.2	0.97261	1543	0	0	100	0
214850	53699.12563	171.5710	−47.4356	36.3	1209.6	36.35	974.5	717.5	0.99802	142.3	1578.7	1274.3	942.7	0.98236	375	0	0	100	0
214850	53915.46401	230.5831	−19.3065	8.3	90.2	152.95	80.5	41.7	−0.97488	47.1	182.6	164.0	93.0	−0.82600	3857	0	1	50	0
214850	53921.47505	231.3387	−18.2154	14.1	142.2	160.22	133.9	49.9	−0.95419	64.0	231.9	219.3	98.9	−0.72931	3103	0	1	50	0
214850	53922.45053	231.9841	−18.1996	7.8	68.8	154.68	62.3	30.3	−0.95840	45.9	166.1	151.4	82.3	−0.79116	4345	0	1	50	0
214850	53923.45395	232.2589	−18.0692	14.1	127.2	155.28	115.7	54.7	−0.95888	37.7	216.7	197.4	96.9	−0.90404	2319	1	1	50	0
214850	53928.45512	234.2969	−17.7839	35.4	428.4	157.15	395.0	169.5	−0.97397	49.8	574.2	529.5	227.7	−0.97148	700	1	1	50	0
214850	53972.29694	243.6457	−11.5526	6.4	89.4	150.49	77.8	44.4	−0.98604	35.6	182.0	159.3	94.8	−0.90352	5227	1	1	50	0
214850	53977.29227	244.6056	−10.7498	4.7	43.1	151.56	37.9	20.9	−0.96752	35.3	150.8	133.7	78.2	−0.86064	7603	1	1	50	0
214850	53986.25515	246.4636	−9.4808	11.1	218.5	149.77	188.9	110.4	−0.99322	36.7	316.7	274.2	162.6	−0.96539	2392	1	1	50	0
214850	53991.23821	247.7312	−8.9313	22.0	243.8	150.06	211.6	123.2	−0.97861	41.3	346.5	301.0	176.6	−0.96300	1562	1	1	50	0
214850	53992.23683	248.4780	−9.1510	33.0	529.7	147.74	448.3	284.1	−0.99056	48.1	702.7	594.8	377.3	−0.98859	1089	1	1	50	0
214850	53996.23681	248.6310	−8.1911	6.7	233.9	150.67	203.9	114.7	−0.99777	35.6	334.8	292.4	166.9	−0.96965	5448	1	1	50	0
214850	54004.25476	250.8699	−7.2371	11.0	162.8	157.93	150.9	62.0	−0.98141	36.7	253.8	235.6	101.2	−0.92064	2940	1	1	50	0
214850	54006.24651	251.4713	−7.0401	6.4	212.7	156.90	195.6	83.6	−0.99650	35.6	309.9	285.4	125.9	−0.95177	5311	1	1	50	0
214850	54008.22793	251.2939	−6.4971	4.6	60.2	154.51	54.3	26.2	−0.98062	35.3	160.4	145.6	76.0	−0.85922	6996	1	1	50	0
214850	54009.24001	250.7240	−6.0639	9.6	398.2	157.25	367.3	154.3	−0.99774	36.3	536.3	494.7	210.1	−0.98231	3927	1	1	50	0
214850	54272.47261	301.4287	29.1132	17.7	474.6	149.76	410.1	239.5	−0.99634	39.2	632.7	546.9	320.4	−0.98993	1897	1	1	50	0
214850	54278.46198	302.2981	30.0087	30.9	1252.5	150.91	1094.6	609.6	−0.99831	46.7	1634.3	1428.3	795.6	−0.99774	796	1	1	50	0
214850	54280.45627	302.5046	30.3333	20.3	870.7	150.78	760.0	425.4	−0.99850	40.5	1140.5	995.6	557.9	−0.99654	1176	1	1	50	0
214850	54286.48156	303.8200	30.9290	9.3	90.9	157.57	84.1	35.8	−0.95951	36.2	183.2	169.9	77.5	−0.86381	3756	1	1	50	0
214850	54287.49296	304.8060	30.7331	23.0	359.3	162.08	342.0	112.7	−0.97671	41.9	487.6	464.1	155.2	−0.95899	1562	1	1	50	0
214850	54299.43856	306.0079	32.5123	27.8	400.2	156.73	367.8	160.1	−0.98201	44.7	538.8	495.3	216.8	−0.97452	885	1	1	50	0
214850	54301.41509	306.0451	32.9879	20.3	208.5	153.13	186.2	96.0	−0.97140	40.5	305.1	272.7	142.5	−0.94825	1152	1	1	50	0
214850	54308.40973	307.0107	34.0340	13.7	244.9	155.35	222.7	102.9	−0.98928	37.6	347.8	316.5	149.0	−0.96082	1694	1	1	50	0
214850	54315.38540	308.4879	34.7380	15.6	157.0	154.61	142.0	68.8	−0.96822	68.8	247.5	225.5	123.0	−0.78917	1778	0	1	50	0
214850	54320.38497	309.2132	35.4745	7.1	62.3	156.94	57.4	25.3	−0.95222	44.2	161.7	149.8	75.3	−0.77353	4109	0	1	50	0
214850	54341.35276	312.6661	38.1674	9.4	86.8	162.07	82.6	28.2	−0.93639	50.0	179.8	171.8	73.0	−0.69689	3141	0	1	50	0
214850	54349.34561	313.8073	39.2502	7.7	42.1	166.16	40.9	12.5	−0.77680	45.6	150.3	146.4	57.1	−0.57061	4479	0	1	50	0

Table 4
(Continued)

HD Number	HJD 2400000.5	δR.A. (mas)	δDecl. (mas)	σ_{min} (μas)	σ_{maj} (μas)	ϕ_e (deg)	$\sigma_{R.A.}$ (μas)	$\sigma_{Decl.}$ (μas)	$\frac{\sigma^2_{R.A.,decl.}}{\sigma_{R.A.}\sigma_{decl.}}$	$\sigma_{min,c}$ (μas)	$\sigma_{maj,c}$ (μas)	$\sigma_{R.A.,c}$ (μas)	$\sigma_{Decl.,c}$ (μas)	$\frac{\sigma^2_{R.A.,decl.,c}}{\sigma_{R.A.,c}\sigma_{decl.,c}}$	N	LDC	Align	Rate (Hz)	Outlier
214850	54357.29628	315.1705	40.2712	10.0	80.8	159.10	75.6	30.3	−0.93593	51.7	175.0	164.5	78.9	−0.71771	3785	0	1	50	0
214850	54376.25470	318.2691	42.6486	11.0	85.8	160.95	81.2	29.9	−0.92161	54.5	179.0	170.1	77.9	−0.67666	3054	0	1	50	0
214850	54385.20924	319.2450	43.9520	18.7	287.0	155.37	261.0	120.8	−0.98546	79.2	398.5	363.7	181.0	−0.87759	1806	0	1	50	0
214850	54426.10562	324.5429	49.5298	29.4	1245.5	159.16	1164.1	443.9	−0.99748	117.1	1625.2	1519.4	588.4	−0.97709	754	0	1	50	0
214850	54713.31324	360.3687	85.7081	29.3	714.0	156.75	656.1	283.2	−0.99366	45.6	938.7	862.7	372.9	−0.99109	705	1	1	50	0
214850	54740.27892	362.9611	89.1431	26.8	238.9	167.11	233.0	59.3	−0.88665	44.1	340.7	332.2	87.3	−0.85553	688	1	1	50	0
214850	54763.18334	365.2987	91.9101	12.4	89.2	158.63	83.2	34.5	−0.92288	37.1	181.8	169.8	74.7	−0.84680	1374	1	1	50	0
214850	54769.18268	365.8592	92.7334	5.4	40.7	161.91	38.7	13.7	−0.90838	35.4	149.7	142.7	57.4	−0.76223	5155	1	1	50	0
214850	54794.12643	368.3490	95.6714	32.9	432.6	165.55	418.9	112.6	−0.95335	48.0	579.5	561.3	151.9	−0.94521	722	1	1	50	0
215182	53199.47142	−14.3227	−50.7725	30.0	1320.8	161.31	1251.2	424.1	−0.99721	119.3	1722.7	1632.3	563.5	−0.97474	2307	0	0	100	0
215182	53235.39101	−8.6744	−53.1595	12.3	70.1	176.49	70.0	13.0	−0.32050	58.4	167.0	166.8	59.2	−0.15168	4739	0	0	100	0
215182	53250.35168	−9.5047	−47.4531	33.6	1689.1	165.00	1631.7	438.3	−0.99684	132.4	2200.3	2125.6	583.7	−0.97204	1632	0	0	100	0
215182	53341.13206	−18.3176	−45.3506	14.4	171.1	165.46	165.6	45.2	−0.94423	65.0	262.8	254.9	91.1	−0.67833	6749	0	0	100	0
221673	52862.41340	549.4289	−59.1585	12.9	714.5	158.14	663.2	266.3	−0.99864	60.2	939.3	872.1	354.2	−0.98308	782	0	0	100	0
221673	52863.47102	549.2919	−59.1185	8.6	62.9	169.96	62.0	13.8	−0.77782	47.9	162.1	159.9	55.0	−0.46866	708	0	0	100	0
221673	52864.44442	549.2326	−59.0766	2.9	11.3	166.02	11.0	3.9	−0.65394	36.7	140.8	136.9	49.2	−0.64239	6123	0	0	100	0
221673	52865.38748	548.9158	−58.9585	14.1	147.0	155.01	133.4	63.4	−0.96962	64.0	236.9	216.4	115.7	−0.79575	968	0	0	100	0
221673	52867.46329	549.6920	−60.0242	28.4	729.9	120.82	374.7	627.0	−0.99611	113.5	959.1	501.0	825.7	−0.96478	834	0	0	100	0
221673	52868.50300	549.1984	−59.2133	4.3	99.4	1.65	99.3	5.1	0.55474	38.6	190.5	190.4	39.0	0.13488	1333	0	0	100	0
221673	52891.30989	549.5545	−59.7791	10.7	125.4	154.89	113.6	54.1	−0.97577	53.6	214.9	195.9	103.3	−0.82195	970	0	0	100	0
221673	52893.38611	549.5980	−59.6624	5.3	19.6	172.98	19.4	5.8	−0.38275	40.4	142.3	141.3	43.7	−0.36579	2323	0	0	100	0
221673	52894.33540	548.9453	−59.6509	8.3	29.2	160.27	27.7	12.6	−0.71937	47.1	145.1	137.5	66.1	−0.65856	1541	0	0	100	0
221673	52895.35912	549.2563	−59.6784	7.6	25.4	173.18	25.2	8.1	−0.33554	45.4	143.8	142.9	48.2	−0.31899	1518	0	0	100	0
221673	52896.38533	549.3331	−59.6550	3.6	16.6	174.46	16.5	3.9	−0.38760	37.6	141.7	141.0	39.8	−0.31912	3555	0	0	100	0
221673	52897.34630	549.3711	−59.6767	6.4	23.2	167.02	22.7	8.1	−0.59109	42.6	143.2	139.9	52.5	−0.55680	2267	0	0	100	0
221673	52915.26425	549.0868	−59.9704	8.0	121.2	157.33	111.9	47.3	−0.98303	46.4	210.8	195.3	91.8	−0.83849	1922	0	0	100	0
221673	52916.28479	549.2595	−60.0644	4.5	20.7	159.65	19.5	8.3	−0.82134	39.0	142.6	134.3	61.6	−0.74121	5027	0	0	100	0
221673	52918.35122	549.2852	−60.1093	2.7	17.6	178.08	17.6	2.7	−0.21085	36.5	141.9	141.8	36.8	−0.12074	4616	0	0	100	0
221673	52919.27980	549.3843	−60.0741	3.6	17.7	162.79	16.9	6.3	−0.79874	37.6	141.9	136.0	55.2	−0.70434	4140	0	0	100	0
221673	52929.30328	549.3110	−60.3371	5.8	23.7	172.35	23.5	6.6	−0.45239	41.4	143.4	142.2	45.2	−0.38660	1503	0	0	100	0
221673	52930.29591	549.5447	−60.1763	4.3	21.8	174.57	21.7	4.8	−0.41521	38.6	142.8	142.2	40.8	−0.30727	3473	0	0	100	0
221673	52951.29151	549.5450	−60.7551	9.4	513.2	4.93	511.3	45.1	0.97768	50.0	681.7	679.2	76.9	0.75764	688	0	0	100	0
221673	52952.18546	549.6621	−60.9652	9.3	351.4	161.84	333.9	109.9	−0.99598	49.7	477.8	454.3	156.2	−0.94227	858	0	0	100	0
221673	52979.20973	549.3397	−61.3501	7.1	253.4	4.62	252.6	21.6	0.94347	44.2	357.9	356.8	52.6	0.53927	1596	0	0	100	0
221673	52983.09470	549.0704	−61.2782	12.5	352.7	160.94	333.4	115.8	−0.99344	59.0	479.4	453.5	166.2	−0.92691	1157	0	0	100	0
221673	53173.48472	550.0843	−65.6975	5.1	104.1	12.56	101.6	23.2	0.97442	40.0	194.7	190.3	57.6	0.70335	2425	0	0	100	2
221673	53181.47785	550.4844	−65.2139	4.2	92.8	148.47	79.1	48.7	−0.99477	38.5	184.8	158.8	102.1	−0.89866	2091	0	0	100	0
221673	53182.47712	550.1318	−65.0467	9.8	226.9	148.55	193.6	118.7	−0.99527	51.1	326.5	279.8	175.8	−0.94074	2260	0	0	100	0
221673	53186.46492	550.5223	−65.2587	11.0	296.4	147.39	249.8	160.0	−0.99669	54.5	410.0	346.6	225.7	−0.95830	378	0	0	100	0
221673	53187.47920	550.5175	−65.4077	8.3	171.2	150.63	149.2	84.3	−0.99355	47.1	262.9	230.3	135.3	−0.91762	2126	0	0	100	0
221673	53197.49019	550.1753	−65.3980	2.0	44.9	157.62	41.6	17.2	−0.99174	35.8	151.7	140.9	66.6	−0.81528	5990	0	0	100	0
221673	53198.50084	550.1909	−65.4282	2.4	49.6	159.84	46.5	17.2	−0.98895	36.2	154.1	145.2	63.0	−0.79326	6530	0	0	100	0
221673	53200.43538	550.1017	−66.0207	2.7	11.4	24.06	10.5	5.2	0.83198	36.5	140.8	129.4	66.4	0.80154	7666	0	0	100	0
221673	53207.47422	549.9007	−66.2948	6.4	67.2	33.40	56.2	37.4	0.97868	42.6	165.0	139.8	97.6	0.85668	3228	0	0	100	0
221673	53208.42692	550.1943	−66.0788	5.4	38.9	22.72	35.9	15.8	0.92842	40.6	148.9	138.2	68.6	0.77082	3512	0	0	100	0

Table 4
(Continued)

HD Number	HJD 2400000.5	δR.A. (mas)	δDecl. (mas)	σ_{min} (μas)	σ_{maj} (μas)	ϕ_e (deg)	$\sigma_{R.A.}$ (μas)	$\sigma_{Decl.}$ (μas)	$\frac{\sigma^2_{R.A.,decl.}}{\sigma_{R.A.}\sigma_{decl.}}$	$\sigma_{min,c}$ (μas)	$\sigma_{maj,c}$ (μas)	$\sigma_{R.A.,c}$ (μas)	$\sigma_{Decl.,c}$ (μas)	$\frac{\sigma^2_{R.A.,decl.,c}}{\sigma_{R.A.,c}\sigma_{decl.,c}}$	N	LDC	Align	Rate (Hz)	Outlier
221673	53214.47246	550.4298	−65.6234	9.2	290.6	162.94	277.8	85.7	−0.99370	49.5	402.9	385.4	127.3	−0.91379	1433	0	0	100	0
221673	53215.44040	550.1716	−65.6325	4.2	42.7	157.36	39.5	16.9	−0.96245	38.5	150.6	139.8	68.0	−0.79267	3208	0	0	100	0
221673	53221.48070	550.0917	−66.5736	5.8	227.5	38.06	179.1	140.3	0.99863	41.4	327.2	258.9	204.3	0.96672	1722	0	0	100	0
221673	53228.38579	550.6584	−66.1699	4.6	224.7	152.99	200.2	102.1	−0.99875	39.1	323.9	289.1	151.2	−0.95705	1590	0	0	100	0
221673	53229.42358	550.2706	−65.9502	3.9	70.7	162.59	67.5	21.5	−0.98183	38.0	167.5	160.2	61.9	−0.76642	2676	0	0	100	0
221673	53234.46422	550.6167	−66.1891	3.2	14.9	179.37	14.9	3.2	−0.04800	37.1	141.3	141.3	37.1	−0.03903	3304	0	0	100	0
221673	53235.42219	550.3449	−66.1579	3.8	13.1	161.46	12.4	5.5	−0.68764	37.9	141.0	134.3	57.4	−0.72150	1997	0	0	100	0
221673	53236.43069	550.4971	−66.2728	6.4	23.9	169.38	23.5	7.7	−0.53396	42.6	143.4	141.2	49.5	−0.48571	2366	0	0	100	0
221673	53242.31297	550.0230	−66.6882	4.8	23.4	14.35	22.7	7.5	0.74431	39.5	143.3	139.1	52.2	0.62728	4848	0	0	100	0
221673	53243.31094	549.7876	−66.7023	6.3	45.9	13.02	44.8	12.0	0.84520	42.4	152.2	148.6	53.7	0.58782	3605	0	0	100	0
221673	53249.42642	550.4547	−66.4007	2.2	10.7	171.04	10.6	2.7	−0.58625	36.0	140.7	139.1	41.8	−0.49002	4940	0	0	100	0
221673	53250.38253	550.5730	−66.5028	4.5	15.3	167.50	14.9	5.5	−0.55162	39.0	141.4	138.3	48.8	−0.57830	3012	0	0	100	0
221673	53251.45045	549.1802	−66.5891	18.7	812.1	0.52	812.1	20.1	0.36563	79.2	1065.0	1064.9	79.8	0.12045	531	0	0	100	0
221673	53263.35701	550.4810	−66.6103	2.4	9.0	167.99	8.8	3.0	−0.58360	36.2	140.5	137.6	45.9	−0.59388	4619	0	0	100	0
221673	53270.31676	550.6152	−66.7473	13.8	125.6	157.48	116.2	49.8	−0.95375	63.0	215.1	200.1	100.9	−0.74093	636	0	0	100	0
221673	53271.34096	550.6568	−66.7652	2.4	9.8	171.28	9.7	2.8	−0.49347	36.2	140.6	139.1	41.6	−0.47779	4872	0	0	100	0
221673	53272.35697	550.7969	−66.8644	7.6	55.2	166.25	53.7	15.0	−0.85560	45.4	157.3	153.2	57.8	−0.59163	2815	0	0	100	0
221673	53284.29576	550.0727	−67.6204	7.6	80.6	34.68	66.4	46.3	0.97970	45.4	174.9	146.1	106.3	0.85953	1246	0	0	100	0
221673	53294.19718	551.3057	−67.7952	15.1	899.1	151.47	789.9	429.7	−0.99919	67.2	1177.2	1034.7	565.3	−0.99081	1164	0	0	100	0
221673	53312.24114	550.4505	−67.4818	1.7	7.9	175.41	7.9	1.8	−0.32459	35.6	140.4	140.0	37.2	−0.28241	6680	0	0	100	0
221673	53341.16609	551.1716	−68.1655	3.2	19.4	170.58	19.2	4.5	−0.68551	37.1	142.3	140.5	43.3	−0.50032	4955	0	0	100	0
221673	53557.50429	548.8653	−70.9760	34.7	2311.5	157.60	2137.1	881.4	−0.99909	136.4	3008.2	2781.7	1153.3	−0.99178	397	0	0	100	0
221673	53571.46204	551.0010	−72.2548	3.8	22.2	162.32	21.1	7.7	−0.85188	37.9	142.9	136.7	56.4	−0.71263	3440	0	0	100	0
221673	53605.48331	550.8475	−73.1599	2.3	60.1	0.80	60.1	2.4	0.34815	36.1	160.3	160.3	36.1	0.05880	4938	0	0	100	0
221673	53606.47795	550.9714	−73.1236	2.5	68.3	0.20	68.3	2.5	0.09257	36.3	165.8	165.8	36.3	0.01519	4234	0	0	100	0
221673	53607.46900	550.7180	−73.1690	2.5	128.8	179.12	128.8	3.2	−0.61707	36.3	218.3	218.2	36.4	−0.08951	3439	0	0	100	0
221673	53613.46276	550.8423	−73.2931	3.2	81.0	1.08	81.0	3.6	0.42838	37.1	175.2	175.2	37.2	0.08481	3235	0	0	100	0
221673	53614.46039	551.1958	−73.2973	4.8	126.8	0.96	126.8	5.3	0.40252	39.5	216.3	216.2	39.6	0.08839	2679	0	0	100	0
221673	53620.41852	551.2319	−73.3194	3.2	27.5	177.10	27.4	3.5	−0.39330	37.1	144.5	144.3	37.7	−0.18105	4006	0	0	100	0
221673	53621.41100	551.3038	−72.9044	29.5	1209.0	41.57	904.7	802.5	0.99879	117.4	1577.9	1183.1	1050.7	0.98883	570	0	0	100	0
221673	53632.28961	551.2917	−73.6416	8.6	155.4	154.09	139.8	68.3	−0.99016	47.9	245.8	222.1	115.7	−0.88894	1813	0	0	100	0
221673	53636.27235	551.1164	−73.6035	2.6	29.0	152.96	25.8	13.4	−0.97649	36.4	145.0	130.2	73.4	−0.83420	4562	0	0	100	0
221673	53637.29322	551.2846	−73.6352	5.4	24.2	163.61	23.3	8.6	−0.75819	40.6	143.5	138.1	56.2	−0.66100	2444	0	0	100	0
221673	53638.33555	551.2646	−73.3866	16.2	808.2	36.98	645.7	486.4	0.99913	70.8	1059.9	847.8	640.1	0.99039	586	0	0	100	0
221673	53648.31722	551.4661	−73.9306	15.7	77.9	171.44	77.0	19.4	−0.57355	69.2	172.8	171.2	73.1	−0.29502	216	0	0	100	0
221673	53655.33875	550.7180	−73.9970	5.0	121.1	178.77	121.0	5.7	−0.45936	39.8	210.7	210.6	40.1	−0.10882	1277	0	0	100	0
221673	53656.33367	552.0201	−74.0009	12.7	386.1	179.79	386.1	12.8	−0.11179	59.6	521.1	521.1	59.6	−0.03160	1192	0	0	100	0
221673	53712.13247	551.9463	−74.2856	32.7	876.9	37.57	695.2	535.3	0.99703	129.1	1148.5	913.7	707.7	0.97336	315	0	0	100	0
221673	53914.48372	551.8130	−78.5447	3.1	59.6	150.39	51.9	29.6	−0.99269	36.9	160.0	140.3	85.3	−0.86971	5235	0	1	100	0
221673	53929.43482	551.8314	−78.8102	6.4	84.9	147.91	72.0	45.4	−0.98626	35.6	178.3	152.2	99.4	−0.90786	2663	1	1	50	0
221673	53930.43636	551.9096	−78.8448	5.5	70.9	149.19	61.0	36.6	−0.98477	40.8	167.6	145.5	92.7	−0.86217	3229	0	1	50	0
221673	53935.43080	553.3732	−79.7331	5.2	79.0	151.00	69.2	38.6	−0.98789	35.4	173.6	152.8	89.7	−0.89391	4371	1	1	50	0
221673	53936.42395	551.9311	−79.0137	4.7	56.3	149.90	48.8	28.5	−0.98204	35.3	158.0	137.8	84.9	−0.87906	4141	1	1	50	0
221673	53937.43272	551.9178	−78.9330	2.4	57.7	151.64	50.8	27.5	−0.99495	36.2	158.8	140.8	81.9	−0.86706	5496	0	1	50	0
221673	53949.39037	551.0453	−78.6201	9.5	275.1	150.30	239.0	136.5	−0.99681	36.3	384.1	334.1	192.9	−0.97636	691	1	1	50 & 100	0

Table 4
(Continued)

HD Number	HJD 2400000.5	δR.A. (mas)	δDecl. (mas)	$\sigma_{\rm min}$ (μas)	$\sigma_{\rm maj}$ (μas)	$\phi_{\rm e}$ (deg)	$\sigma_{\rm R.A.}$ (μas)	$\sigma_{\rm Decl.}$ (μas)	$\frac{\sigma^2_{\rm R.A.,decl.}}{\sigma_{\rm R.A.}\sigma_{\rm decl.}}$	$\sigma_{\rm min,c}$ (μas)	$\sigma_{\rm maj,c}$ (μas)	$\sigma_{\rm R.A.,c}$ (μas)	$\sigma_{\rm Decl.,c}$ (μas)	$\frac{\sigma^2_{\rm R.A.,decl.,c}}{\sigma_{\rm R.A.,c}\sigma_{\rm decl.,c}}$	N	LDC	Align	Rate (Hz)	Outlier
221673	53951.38665	551.7626	−79.1717	4.7	64.3	150.67	56.1	31.7	−0.98519	35.3	163.1	143.2	85.6	−0.88280	3771	1	1	50	0
221673	53956.35084	551.7124	−79.1795	5.6	190.3	146.46	158.7	105.3	−0.99795	35.4	284.3	237.7	159.8	−0.96420	3394	1	1	50	0
221673	53957.34458	551.6692	−79.1902	5.5	254.3	145.98	210.8	142.3	−0.99890	35.4	359.0	298.2	203.0	−0.97768	2587	1	1	50	0
221673	53958.38759	551.8129	−79.2895	3.6	27.8	156.17	25.5	11.7	−0.94184	35.2	144.6	133.0	66.7	−0.81928	3409	1	1	50	0
221673	53964.33245	552.1755	−79.5331	19.2	820.2	146.70	685.6	450.7	−0.99870	39.9	1075.4	899.1	591.4	−0.99673	849	1	1	50	0
221673	53965.32670	551.4894	−79.1123	4.9	201.2	146.25	167.3	111.8	−0.99863	35.3	296.7	247.5	167.4	−0.96745	2373	1	1	50	0
221673	53986.27129	552.1597	−79.8650	6.3	109.4	146.83	91.6	60.1	−0.99205	35.6	199.6	168.2	113.2	−0.92788	2201	1	1	50	0
221673	53991.28888	551.8293	−79.7872	13.9	217.3	151.89	191.7	103.1	−0.98825	37.7	315.3	278.7	152.2	−0.96002	918	1	1	50	0
221673	54005.20826	552.7337	−80.5138	17.9	1173.3	144.70	957.7	678.1	−0.99948	39.3	1531.7	1250.3	885.7	−0.99852	998	1	1	50	0
221673	54007.21609	552.3667	−80.2662	4.8	235.0	146.27	195.5	130.6	−0.99900	35.3	336.1	280.2	188.9	−0.97452	2115	1	1	50	0
221673	54029.19479	552.4126	−80.5909	15.0	131.5	152.99	117.3	61.2	−0.96157	38.1	221.0	197.6	105.9	−0.91567	1045	1	1	50	0
221673	54279.48952	552.4951	−85.0218	3.8	87.2	151.03	76.3	42.4	−0.99471	35.2	180.1	158.5	92.5	−0.90169	5095	1	1	50	0
221673	54285.49505	552.9978	−85.3929	14.1	372.7	154.55	336.6	160.7	−0.99526	37.7	504.3	455.7	219.4	−0.98171	375	1	1	50	0
221673	54300.41432	552.1334	−85.1757	6.4	256.8	147.43	216.4	138.4	−0.99849	35.6	362.0	305.7	197.2	−0.97690	2442	1	1	50	0
221673	54350.34574	552.8836	−86.3918	4.3	131.5	159.08	122.8	47.1	−0.99530	38.6	221.0	206.9	86.8	−0.87967	4633	0	1	50	0
221673	54376.24276	552.5559	−86.5712	5.1	215.2	153.05	191.8	97.6	−0.99828	40.0	312.8	279.5	146.2	−0.95192	2996	0	1	50	0
221673	54653.45217	553.6985	−92.1632	24.0	2079.0	148.10	1765.2	1098.8	−0.99967	42.4	2706.3	2297.7	1430.6	−0.99939	707	1	1	50	0
221673	54678.38762	553.0523	−92.2873	13.4	732.2	148.58	624.9	381.9	−0.99915	37.5	962.1	821.3	502.6	−0.99618	1147	1	1	50	0
221673	54741.26504	553.9814	−93.8159	9.9	539.5	157.03	496.7	210.7	−0.99870	36.4	715.2	658.6	281.1	−0.99008	1599	1	1	50	0
221673	54748.24700	552.7592	−93.2839	19.0	1071.7	157.43	989.6	411.8	−0.99875	39.8	1400.2	1293.1	538.7	−0.99679	933	1	1	50	0
221673	54762.20752	553.1224	−93.7379	25.2	1864.2	156.99	1715.9	729.1	−0.99929	43.1	2427.5	2234.4	949.7	−0.99878	498	1	1	50	0
221673	54776.17063	554.0054	−94.3155	36.5	391.2	157.92	362.8	150.9	−0.96536	50.6	527.5	489.2	203.7	−0.96352	484	1	1	50	0
222842	54343.42036	−770.8249	139.0081	42.7	1642.4	169.94	1617.2	289.9	−0.98874	166.0	2139.7	2107.0	407.9	−0.91063	5312	0	1	50	0
224930	53243.35715	−615.0169	−480.7104	26.0	885.7	21.70	823.0	328.3	0.99637	104.8	1159.9	1078.4	439.8	0.96658	624	0	0	100	0
224930	53687.21451	−732.3355	−366.6561	22.2	130.1	33.37	109.3	73.9	0.93384	91.3	219.6	190.1	142.8	0.67433	1275	0	0	100	0
224930	53699.10666	−745.6906	−368.9391	18.0	224.3	19.70	211.3	77.5	0.96910	76.8	323.5	305.6	130.8	0.78345	1466	0	0	100	0
224930	54376.37317	−840.3871	−218.3862	26.2	419.5	175.80	418.4	40.3	−0.75862	105.5	563.0	561.6	113.0	−0.35194	785	0	1	50	0

Notes. All quantities are in the ICRS 2000.0 reference frame. The uncertainty values presented in Columns 5–10 have not been rescaled, whereas the values in Columns 11–15 have been scaled according to the correction formula presented in Section 4. Column 1 is the star's HD catalog number. Column 2 is the heliocentric modified Julian date. Columns 3 and 4 are the differential right ascension and declination between A and B, in milli-arcseconds. Columns 5 and 6 are the formal 1σ uncertainties in the minor and major axes of the measurement uncertainty ellipse, in microarcseconds. Column 7, $\phi_{\rm e}$, is the angle between the major axis of the uncertainty ellipse and the right ascension axis, measured from increasing differential right ascension through increasing differential declination (the position angle of the uncertainty ellipse's orientation is $90 - \phi_{\rm e}$); this is to be used with either Columns 5 and 6 or Columns 11 and 12—the uncertainty scaling operates on the ellipse major and minor axes, and thus does not change the ellipse's rotation angle. Columns 8 and 9 are the projected formal uncertainties in the right ascension and declination axis, in micro-arcseconds, while Column 10 is the covariance between these. Columns 11 and 12 are the rescaled 1σ uncertainties in the minor and major axes of the measurement uncertainty ellipse, in microarcseconds. Columns 13 and 14 are the projected rescaled uncertainties in the right ascension and declination axis, in microarcseconds, while Column 15 is the covariance between these. Column 16 is the number of scans taken during a given night. Column 17 is 1 if the longitudinal dispersion compensator was in use, 0 otherwise. Column 18 is 1 if the autoaligner was in use, 0 otherwise. Column 19 represents the tracking frequency of the phase-referencing camera. Column 20 is 0 if the measurement is consistent with the other measures, 1 if a fringe ambiguity is suspected (the measurement is in error by ∼4 mas), and 2 if it is a significant outlier but not of the fringe ambiguity variety.

(This table is also available in machine-readable and Virtual Observatory (VO) forms in the online journal.)

Table 5
Keck AO Differential Photometry Measurements

HD	HJD 2453227.5	Filter	Δm	σ
5286	0.49	H_2	0.442	0.002
6811	0.49	H_2	1.426	0.002
13872	0.50	H_2	0.137	0.002
17904	0.51	K_p	1.218	0.003
17904	0.54	H_2	1.206	0.003
40932	0.63	H_2	0.002	0.005
41116	0.64	H_2	2.043	0.008
44926	0.64	H_2	0.215	0.004
137107	0.33	K_p	0.185	0.001
140436	0.35	K_p	0.936	0.001
165908	0.40	H_2	2.063	0.002
165908	0.40	K_p	1.909	0.001
171745	0.40	K_p	0.278	0.001
171745	0.41	H_2	0.272	0.001
171779	0.42	K_p	0.167	0.002
171779	0.42	H_2	0.163	0.003
176051	0.43	H_2	1.308	0.001
176051	0.43	K_p	1.235	0.001
196524	0.46	H_2	1.096	0.002
196867	0.46	H_2	1.587	0.004
202275	0.47	H_2	0.066	0.004
206901	0.44	H_2	0.188	0.001
207652	0.48	K_p	0.740	0.004
213973	0.44	K_p	0.293	0.003
221673	0.45	H_2	0.570	0.003

Notes. Column 1 is the star's HD catalog number. Column 2 is the heliocentric Julian date offset by the day of observations. Column 3 is the filter used during the observation (K_p or H_2). Columns 5 and 6 are the differential photometry and uncertainty measurements in units of magnitudes.

Though it has no impact on the current study, as an astrometry team we could not resist pointing out that—due to precession—PHASES target HD 149630 (σ Her) was the pole star around 8250 BC. PHASES benefits from the efforts of the PTI collaboration members who have each contributed to the development of an extremely reliable observational instrument. Without this outstanding engineering effort to produce a solid foundation, advanced phase-referencing techniques would not have been possible. We thank PTI's night assistant Kevin Rykoski for his efforts to maintain PTI in excellent condition and operating PTI in phase-referencing mode every week. Part of the work described in this paper was performed at the Jet Propulsion Laboratory under contract with the National Aeronautics and Space Administration. Interferometer data were obtained at the Palomar Observatory with the NASA Palomar Testbed Interferometer, supported by NASA contracts to the Jet Propulsion Laboratory. This publication makes use of data products from the Two Micron All Sky Survey, which is a joint project of the University of Massachusetts and the Infrared Processing and Analysis Center/California Institute of Technology, funded by the National Aeronautics and Space Administration and the National Science Foundation. This research has made use of the Simbad database, operated at CDS, Strasbourg, France. M.W.M. acknowledges support from the Townes Fellowship Program, Tennessee State University, and the state of Tennessee through its Centers of Excellence program. Some of the software used for analysis was developed as part of the *SIM* Double Blind Test with support from NASA contract NAS7-03001 (JPL 1336910). PHASES is funded in part by the California Institute of Technology Astronomy Department, and by the National Aeronautics and Space Administration under grant no. NNG05GJ58G issued through the Terrestrial Planet Finder Foundation Science Program. This work was supported in part by the National Science Foundation through grants AST 0300096, AST 0507590, and AST 0505366. M.K. is supported by the Foundation for Polish Science through a FOCUS grant and fellowship, by the Polish Ministry of Science and Higher Education through grant N203 3020 35.

Facilities: PO:PTI, Keck:I

REFERENCES

Carroll, B. W., & Ostlie, D. A. 1996, An Introduction to Modern Astrophysics (Reading, MA: Addison-Wesley)
Colavita, M. M. 2009, NAR, 53, 344
Colavita, M. M., et al. 1999, ApJ, 510, 505
Cox, A. N. (ed.) 2000, Allen's Astrophysical Quantities (4th ed.; New York: AIP)
Kaplan, G. H., Hughes, J. A., Seidelmann, P. K., Smith, C. A., & Yallop, B. D. 1989, AJ, 97, 1197
Lane, B. F., & Colavita, M. M. 2003, AJ, 125, 1623
Lane, B. F., & Muterspaugh, M. W. 2004, ApJ, 601, 1129
Lanza, A. F., De Martino, C., & Rodonò, M. 2008, New Astron., 13, 77
Lawson, P. R. (ed.) 2000, Principles of Long Baseline Stellar Interferometry (Pasadena, CA: NASA)
Lindegren, L. 1980, A&A, 89, 41
Muterspaugh, M. W., Lane, B. F., Konacki, M., Burke, B. F., Colavita, M. M., Kulkarni, S. R., & Shao, M. 2005, AJ, 130, 2866
Muterspaugh, M. W., Lane, B. F., Konacki, M., Burke, B. F., Colavita, M. M., Kulkarni, S. R., & Shao, M. 2006, A&A, 446, 723
Muterspaugh, M. W., Lane, B. F., Kulkarni, S. R., Konacki, M., Burke, B. F., Colavita, M. M., & Shao, M. 2010a, AJ, 140, 1631 (Paper III)
Muterspaugh, M. W., et al. 2008, AJ, 135, 766
Muterspaugh, M. W., et al. 2010b, AJ, 140, 1646 (Paper IV)
Muterspaugh, M. W., et al. 2010c, AJ, 140, 1623 (Paper II)
Muterspaugh, M. W., et al. 2010d, AJ, 140, 1657 (Paper V)
Press, W. H., Teukolsky, S. A., Vetterling, W. T., & Flannery, B. P. 1992, Numerical Recipes in C: The Art of Scientific Computing (2nd ed.; Cambridge: Cambridge Univ. Press)
Scargle, J. D. 1982, ApJ, 263, 835
Shao, M., & Colavita, M. M. 1992, A&A, 262, 353
Shao, M., & Staelin, D. H. 1980, Appl. Opt., 19, 1519
Svensson, F., & Ludwig, H.-G. 2004, in 13th Cambridge Workshop on Cool Stars, Stellar Systems, and the Sun, ed. F. Favata et al. (ESA SP-560; Noordwijk: ESA), 979